Regulation of μ-opioid receptor function by pH

Inaugural-Dissertation
to obtain the academic degree
Doctor rerum naturalium (Dr. rer. nat.)

submitted to the Department of Biology, Chemistry and Pharmacy
of Freie Universität Berlin

by

Johanna Charlotte Meyer

2019

The work presented in the present thesis was performed between July 2015 and September 2019 in the research group of Prof. Dr. Christoph Stein at

Charité – Universitätsmedizin Berlin, corporate member of Freie Universität Berlin, Humboldt-Universität zu Berlin, and Berlin Institute of Health,
Department of Anesthesiology and Intensive Care Medicine, Campus Benjamin Franklin

1. Reviewer: Prof. Dr. Rudolf Tauber
2. Reviewer: Prof. Dr. Oliver Daumke

Date of disputation: July 1st, 2020

Acknowledgements

I would like to express my gratitude to all the people who have supported, motivated and inspired me during my graduate studies.
I owe special thanks to Prof. Stein, who did not only provide me with a fascinating project and workplace, but also continued to take an exceptional interest in the project, and thus my progress as scientist.
I am indebted for eternity to Dr. Giovanna Del Vecchio for her patience, support, guidance, encouragement, honesty and humor. I could not have wished for a better mentor.
Heartfelt thanks also to Dr. Viola Seitz who supported me both scientifically and mentally in some of the worst moments of the project.
Many thanks also to all the other members of the Stein group who have been amazing colleagues, allies, teachers and friends.
Thanks also to the Dahlem Research School for providing all sorts of impulses and a platform for interdisciplinary exchange between graduate students. Without the DRS, I'd never have met the wonderful ladies of "shut up and write", whose support during the past months was priceless.
Last but not least, the sincerest thanks go to Martin, my family and friends. I do not like platitudes, but I truly cannot imagine having finished the present thesis without their constant encouragement, support and understanding for my sometimes-unpredictable moods.

Table of contents

Abbreviations

AC	adenylyl cyclase
ANOVA	analysis of variance
BSA	bovine serum albumin
CTX	cholera toxin
DAMGO	[D-Ala2,N-Me-Phe4,Gly5-ol]-enkephalin
DAPI	4′,6-Diamidin-2-phenylindol
DMEM	Dulbecco's Modified Eagle Medium
DTT	dithiothreitol
EGTA	ethylene glycol-bis(β-aminoethyl ether)-*N*,*N*,*N*′,*N*′-tetraacetic acid
EPPS	4-(2-Hydroxyethyl)-1-piperazinepropanesulfonic acid
GPCR	G protein coupled receptor
HEK MOR-H297A	HEK 293 cells stably transfected with mu-opioid receptor mutant H297A
HEK MOR-WT	HEK 293 cells stably transfected with mu-opioid receptor wildtype
HEM	HEPES, EPS, MES
HEPES	4-(2-hydroxyethyl)-1-piperazineethanesulfonic acid
IBMX	3-isobutyl-1-methylxanthine
MES	2-(N-Morpholino)ethanesulfonic acid
MOR	mu-opioid receptor
NLX	naloxone
PBS	phosphate buffered saline
PGE_2	prostaglandin E_2
PTX	pertussis toxin
RT	reverse transcriptase
WT	wildtype

1 Introduction

In October 2017, the president of the United States of America declared the massive spread of opioid drug addiction in the USA a national Public Health Emergency. In Europe, opioid abuse is on the increase as well (Kimergard et al., 2017). The European Monitoring Centre for Drugs and Drug Addiction recently reminded that "drug overdose deaths remain high in Europe, and opioids are implicated in the majority of cases" (EMCDDA, 2018). Nontheless, opioids represent the most efficient treatment for strong pain. As opioids are indispensable for current medical practice, the World Health Organization lists several such compounds amongst the essential medicines required by any functioning health care system (World Health Organization, 2017). To improve patient safety, novel analgesics that exert reduced side effects, most notably reduced abuse liability, are urgently needed.

This goal may be achievable by selective targeting of peripheral opioid receptors in injured tissue (reviewed in Stein, 2018). In the introduction, I will therefore outline how locally restricted activation of peripheral opioid receptor populations in injured and inflamed tissue (the source of many painful conditions) is able to convey analgesia with reduced side effects.

I will begin by providing a brief overview of pain perception and transmission, and then point out general concepts of pharmacological pain treatment and the special importance of opioids. By including both specific details on opioid function as well as general pharmacological concepts, I will assemble the background knowledge to interpret and contextualize the experiments conducted in this study. At the end of this section, I will portray the studies that motivated the present work and the specific questions posed therein.

1.1 Pain perception and transmission

Pain is a warning sign that directs important protective reflexes and behavior. Notwithstanding, pain-induced suffering frequently compromises the evolutional benefits of pain perception.

According to the International Association for the Study of Pain (IASP), pain is "An unpleasant sensory and emotional experience associated with actual or potential tissue damage, or described in terms of such damage" (Merskey, Bogduk, & International Association for the Study of Pain. Task Force on Taxonomy., 1994). The definition gives

credit to the well-established notion that the perception of pain comprises sensory, cognitive and affective components.

Sensory perception of painful stimuli, termed nociception, is mediated by specialized sensory neurons (nociceptors) (Burgess & Perl, 1967; Sherrington, 1903) (Figure 1). The cell bodies of these nociceptive neurons reside in the trigeminal and dorsal root ganglia (DRG), and their axons innervate peripheral tissues. Painful stimuli cover a wide range of potentially noxious cues, from intense mechanical pressure and extreme temperatures (heat or cold) to chemical stimuli such as capsaicin (the pungent component of hot peppers) or acids (i.e. protons). In vertebrates, nociceptive stimuli are registered by free nerve endings of peripheral sensory neurons, converted into action potentials, and transmitted via thinly myelinated Aδ- or unmyelinated C-fibers to cell bodies in dorsal root and trigeminal ganglia (Julius & Basbaum, 2001). Nociceptors are pseudounipolar, with axons projecting into the dorsal horn of the spinal cord or, in case of the trigeminal neurons, the medulla. From this primary afferent synapse, second and third order neurons project to areas within the brainstem, diencephalon, and the thalamocortical system (Groh, Krieger, Mease, & Henderson, 2018; Willis & Westlund, 1997). Conscious perception of pain arises at this latter stage of information processing. In turn, several brain regions initiate inhibitory or facilitatory descending pathways that modulate spinal nociception. This mechanism is thought to provide behavioral prioritization of sensory inputs, but maladaptive responses in descending pathways can also give rise to chronic pain states (Heinricher, Tavares, Leith, & Lumb, 2009).

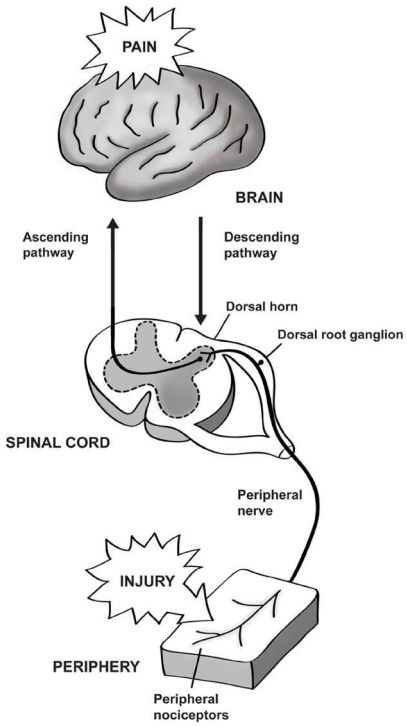

Figure 1. The neural pathway of nociception. Noxious stimuli are registered by primary nociceptors in peripheral tissue and transmitted via the spinal cord towards the brain. Pain results from processing of nociceptive signals in the brain. Figure copied from "Essential Pain Management" by Wayne Morriss and Roger Goucke, ISBN 978-0-9873236-1-3, Creative Commons Attribution-NonCommercial 3.0 Unported License.

Nociceptive neurons respond to noxious stimuli. Tissue injury sensitizes nociceptive neurons, which leads to exaggerated responses to noxious stimuli (hyperalgesia) and nociceptive responses to otherwise innocuous stimuli (allodynia).

Analgesia, the loss of pain perception, can be achieved by blocking transmission of nociceptive cues at several levels of the nociceptive circuit.

1.2 Pharmacological treatment of pain – nonopioid analgesics

The most common nonopioid analgesics inhibit cyclooxygenases (COX-1 and COX-2), the enzymes that synthesize prostanoids from arachidonic acid. Prostanoids, most notably prostaglandin E_2 (PGE_2), elicit nociception and hyperalgesia in inflamed tissue. COX inhibitors produce analgesic, anti-inflammatory and antipyretic (fever-reducing) effects, but also increase the risks of cardiovascular adverse events, renal failure and gastric ulcers (McMahon, 2013, p. 448).

Several medications not primarily developed to treat pain, termed co-analgesics, are additionally used. Anticonvulsant drugs mostly act via inhibition of voltage-gated Ca^{2+} and Na^{+} channels. Adverse effects are elicited in the cardiovascular and central nervous system (CNS) (McMahon, 2013, p. 491). Analgesic effects of antidepressants appear to be

moderate and possibly confined to neuropathic pain (McMahon, 2013, p. 465). The use of cannabinoids may be effective in neuropathic pain and multiple sclerosis, but clinical evidence on efficacy and risks is as yet limited (McMahon, 2013, p. p. 538).

1.3 Opioids

The term 'opioid' is derived from opium, an extract from the opium poppy (*Papaver somniferum*). Medical use of opium can be traced back to 1500 B.C. (Papyrus Ebers, see e.g. Brownstein, 1993). Since the isolation of morphine from opium by Sertürner around 1805, knowledge about the modes of action, naturally occurring variants (opiates and opioid peptides) and efforts to generate synthetic analogs have increased drastically. Initially used to treat diarrhea and coughing, today most opioids are used as pain medication.

1.3.1 The endogenous opioid system

The endogenous opioid system evolved as a crucial mechanism guiding behavior, and its importance is illustrated by a high degree of conservation across species and evolutionary time (Dreborg, Sundstrom, Larsson, & Larhammar, 2008; Pasternak & Pan, 2013). Opioids bind to specific sites, the opioid receptors (Pert & Snyder, 1973a; Simon, Hiller, & Edelman, 1973; Terenius, 1973). Opioid peptides are derived by cleavage of the precursor proteins pre-proenkephalin, pre-proopiomelanocortin and pre-prodynorphin. The origin of a fourth class of opioid peptides, the endomorphins, is unknown to date (Matus-Ortega et al., 2017; Terskiy et al., 2007). Opioid peptides are expressed throughout the nervous system as well as in neuroendocrine cells (pituitary and adrenal glands), the gastrointestinal tract and immune cells and modulate nociception, stress responses, addictive behavior and emotions (Nummenmaa & Tuominen, 2018). The central challenge of opioid drug development lies in dissecting the various roles, anatomical localization and related pathways of opioid signaling, to selectively activate only those that are beneficial.

1.3.2 Opioid receptors

Opioid receptors belong to the class A (rhodopsin) family of guanine nucleotide-binding protein (G-protein) coupled receptors (GPCRs) which are integral membrane proteins and possess seven α-helical transmembrane domains connected by short extra-and intracellular loops. Ligands bind to a specific binding site - termed the binding pocket - that is accessible from the extracellular side and penetrates halfway into the receptors' central seven-helix bundle (McMahon, 2013, p. 415). High-resolution structures of opioid

receptors have been published and enable detailed analysis of the 3D receptor architecture (Figure 2).

Opioid receptor types are classified as δ-, κ- and μ-opioid receptors (DOR, KOR and MOR, respectively). A fourth, more distantly related subtype, the opioid receptor like-1 (ORL-1) or N/OFQ peptide receptor, is not considered a classical opioid receptor (McMahon, 2013, p. 414). Alternative splicing of mRNA, posttranslational modifications and receptor dimerization result in pharmacological appearance of additional receptor subtypes (Pasternak & Pan, 2013; Regan, Langford, & Khalili, 2016). The clinical relevance of receptor oligomers and splice variants is as yet unclear (Davis, LeGrand, & Lagman, 2005; McMahon, 2013; p.418).

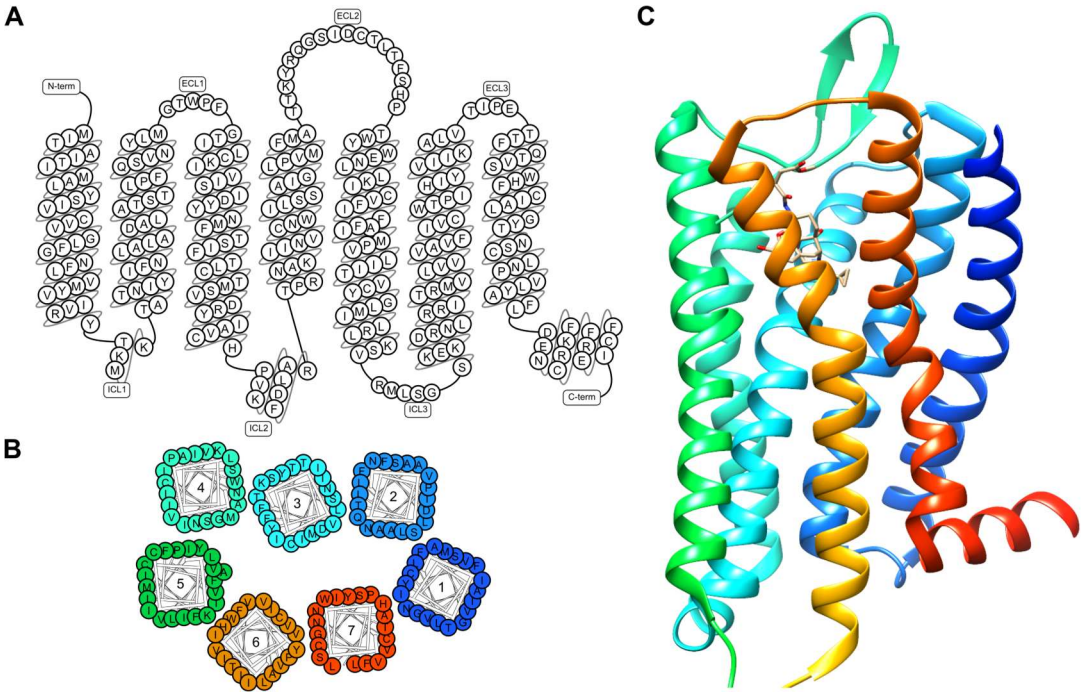

Figure 2. The human MOR. (A) amino acid sequence depicted as snake plot depicting helical domains (packed areas), extracellular and intracellular loops (ECL and ICL, respectively). (B) amino acid sequence depicted as transmembrane helical bundles viewed from the top. Figures A and B were created using tools freely available at gpcrdb.org (Pandy-Szekeres et al., 2018). (C) 3D-structure of the inactive human MOR bound to an antagonist (Manglik et al., 2012). The figure was created using the structure deposited by Manglik et al. as PDB entry 4DKL.

High-resolution structures reveal that the three main opioid receptor types have high sequence and structure similarities (Granier et al., 2012; Manglik et al., 2012; Thompson et al., 2012; Wu et al., 2012). Topologically conserved residues typical of class A GPCRs as well as opioid receptor-specific structure-function relationships have been demonstrated (Huang et al., 2015).

Opioid analgesia is mediated via activation of opioid receptors at all levels of the neuraxis. Under conditions of inflammatory tissue injury, peripheral opioid receptors become particularly relevant to the analgesic effect of systemic opioids (Jagla, Martus, & Stein,

2014; Sun, Chen, Chen, & Pan, 2019). Peripheral opioid receptors are expressed on all primary nociceptive neurons, as well as neurons of the enteric nervous system. In addition, several types of immune cells express opioid receptors and contribute to opioid analgesia (Machelska, 2007).

1.3.3 Expression patterns and effects mediated by opioid receptors

The opioid receptor subtypes differ in side effect profiles, largely due to their anatomical localization patterns within the brain, on peripheral nerves and immune cells (Stein & Machelska, 2011; Valentino & Volkow, 2018). To date, most opioid analgesics target MOR in the CNS. MOR, or OP_3 by nomenclature of the International Union of Pharmacology (IUPHAR, Dhawan et al., 1996), is expressed in cortical areas, hypothalamus, thalamus, cerebellum and the medulla oblongata. In addition, MOR is expressed on DRG and trigeminal neurons, enteric neurons and on immune cells. MOR activity regulates nociceptive responses, the reward system, respiratory, gastrointestinal and immune functions (Le Merrer, Becker, Befort, & Kieffer, 2009; Ninkovic & Roy, 2013; Pattinson, 2008; Sobczak, Salaga, Storr, & Fichna, 2014). MOR activation can induce potent analgesia, but also respiratory depression, constipation and addiction.

Overcoming MOR-dependent adverse effects is a major aim of current pharmacological research, and as I will argue in the following chapters, peripheral opioid receptors may hold the key to achieve that aim.

1.3.4 Molecular mechanisms of opioid analgesia

Neurons transmit signals in the form of action potentials. In the resting state, neurons exhibit an inside-negative electric potential of -60 mV that is established by electrochemical gradients of cations across the membrane (Lodish, 2013, p. 1021). Action potentials are generated by transient depolarization of the resting membrane potential that migrates along the nerve, mediated by voltage-gated Na^+ and K^+ channels (Lodish, 2013, p. 1029). Pre-synaptically, the arriving action potential triggers the release of neurotransmitters into the synaptic cleft. The activation of opioid receptors leads to silencing of neurons by inhibiting depolarization, action potential propagation and/or neurotransmitter release via G-protein mediated pathways (Figure 3).

Following agonist binding, opioids activate mostly inhibitory G-proteins that consist of three subunits termed α, β and γ. In the inactive state, the α subunit is bound to guanosine diphosphate (GDP). Receptor-mediated G-protein activation triggers exchange of GDP for

guanosine triphosphate (GTP), followed by the dissociation into Gα and Gβγ (the latter is a complex of the subunits β and γ that remain associated to one another).

The Gβγ subunits cause opening of inwardly rectifying K^+ channels (GIRK or KIR3), thereby triggering K^+ efflux and hyperpolarization (Ikeda, Kobayashi, Kumanishi, Niki, & Yano, 2000; Logothetis, Kurachi, Galper, Neer, & Clapham, 1987). Furthermore, they inhibit voltage-gated Ca^{2+} channels, thereby blocking depolarization (Dembla et al., 2017).

Meanwhile, the Gα subunits inhibit adenylyl cyclases (AC), leading to reduced production of the second messenger cyclic adenosine monophosphate (cAMP). Reductions in intracellular cAMP indirectly lead to activation of KIR channels and desensitization of pro-nociceptive ion channels such as transient receptor potential vanilloid 1 (TRPV1), hyperpolarization-activated cyclic nucleotide-gated (HCN) channels and acid-gated ion channels (ASIC) (Cai et al., 2014; Ingram & Williams, 1994; Vetter, Wyse, Monteith, Roberts-Thomson, & Cabot, 2006; Wimpey & Chavkin, 1992).

Importantly, opioid receptors are selectively expressed on nociceptive neurons, leaving other sensory perceptions such as innocuous touch unaffected.

Termination of opioid receptor signaling is initiated by phosphorylation of intracellular receptor domains by protein kinases. Subsequently, the regulatory protein β-arrestin binds to the receptor, thereby precluding G-protein binding and inducing internalization of opioid receptors via the clathrin-mediated pathway.

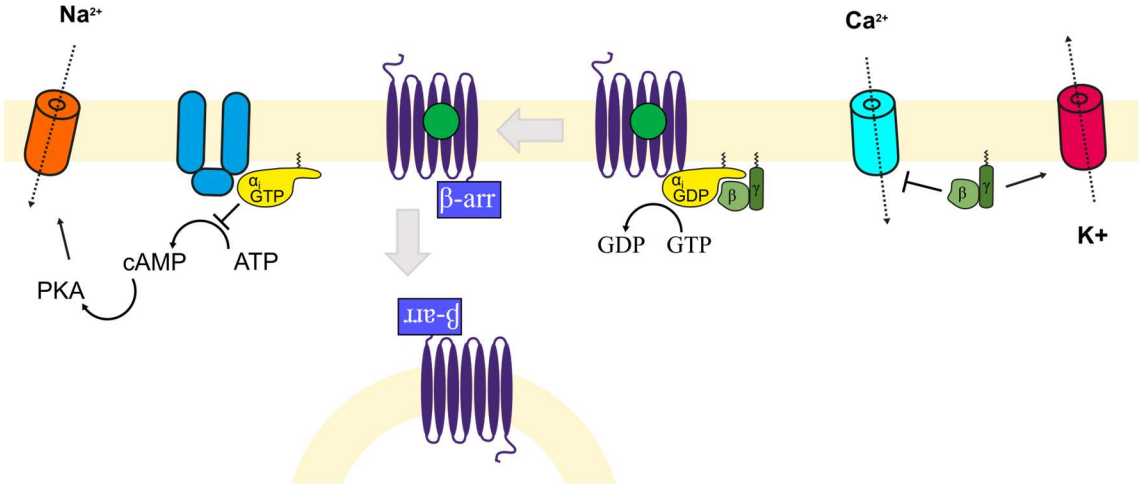

Figure 3. Molecular mechanisms of opioid analgesia. Activation of opioid receptors by ligand binding causes activation of G-proteins. Activated G-protein subunits modulate Ca^{2+}, K^+ and Na^+ channels. β-arrestin binds to activated opioid receptors, mediating removal of receptors from the plasma membrane.

1.3.5 Adverse effects of MOR activation

Most MOR-dependent adverse effects can be traced back to neuronal inhibition at distinct sites. Rewarding effects, triggering addiction and dependence render opioid analgesics

potential drugs of abuse (see also Introduction, p.1). Addiction is defined as "a chronic, relapsing disorder characterized by compulsive drug seeking and use despite adverse consequences", whereas dependence is "a state in which an organism functions normally only in the presence of a drug, manifested as a physical disturbance when the drug is removed (withdrawal)" (NIDA, 2007, 2018). The two pathologies often go hand in hand and are mostly due to opioid-mediated disinhibition of GABAergic neurons in the reward system (McMahon, 2013, p. 420). Sedation and cognitive impairment are caused by inhibition of hypothalamic neurons steering arousal (Y. Li & van den Pol, 2008). Respiratory depression is the major cause of overdose deaths and is primarily caused by neuronal inhibition in the respiratory center of the brainstem. Activation of opioid receptors on intestinal neurons causes constipation by reducing gut motility. Nausea is caused by inhibition of neurons in the medulla, cortex, vestibular apparatus and the gastrointestinal tract.

Alternative mechanisms underlying opioid adverse effects have been suggested. Most prominently, β-arrestin recruitment has been proposed to be a key event (DeWire et al., 2013; Manglik et al., 2016; Raehal & Bohn, 2014). However, opioid analgesics with reduced propensity to trigger β-arrestin recruitment have so far failed to produce significantly improved safety profiles in pre-clinical and clinical trials (Hill et al., 2018; Viscusi et al., 2019).

1.3.6 Targeting peripheral opioid receptors to improve drug safety

Since the most severe opioid side effects are mediated within the CNS, selective targeting of opioid receptors in the peripheral nervous system represents a promising approach. Both preclinical and clinical studies have shown that selective peripheral opioid receptor activation produces analgesia with reduced adverse effects (Gonzalez-Rodriguez et al., 2017; Tiwari et al., 2016; Vanderah et al., 2004; Y. L. Wang et al., 2015; Zeng et al., 2013). Several lines of evidence suggest that such improved selectivity can be achieved by exploiting inherent properties of painful injured and inflamed tissue.

1.4 GPCR pharmacology

1.4.1 The GPCR family

GPCRs constitute the largest family of transmembrane signaling proteins in the human genome, and the most frequent drug targets. They are classified into five main families (Wacker, Stevens, & Roth, 2017). All GPCRs possess an orthosteric binding site for

designated ligands. In addition, allosteric modulators (which bind outside the binding pocket) can affect the receptors' signaling state. GPCR ligands range from neurotransmitters, hormones and metabolites to single ions or, in the case of rhodopsin, photons, reflecting the diverse pivotal roles that GPCRs play. GPCRs represent attractive drug targets because the specificity of receptor-ligand interactions enables the development of efficacious exogenous ligands (Lodish, 2013, p. 687)

1.4.2 Classification of GPCR ligands

Receptor ligands are classified according to their effects on receptor activity: agonists activate receptors, antagonists block and/or reverse receptor activation. Agonists are further divided into "full" or "partial", depending on their inherent ability to induce maximal or submaximal receptor activation. Antagonists are further classified as neutral antagonists if they reduce receptor activity to the baseline level observed for unbound ("free") receptors, or as inverse agonists if they reduce receptor activity below baselines (Figure 4). (Freissmuth, Offermanns, & Böhm, 2016).

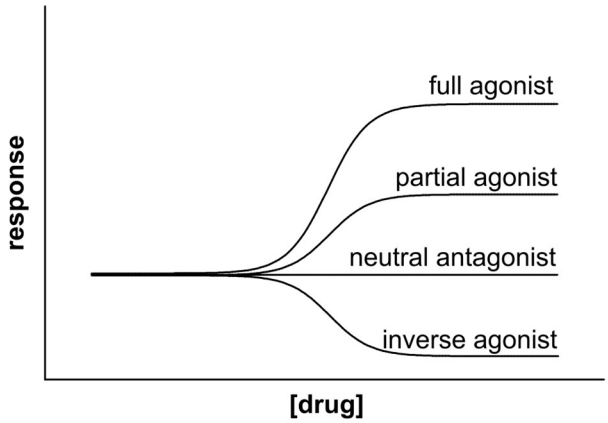

Figure 4. Modes of GPCR modulation

Activation of GPCRs typically modulates several different signaling pathways. Thus, a ligand can be a full agonist regarding G-protein activation, but a partial agonist regarding β-arrestin recruitment. This concept is termed "biased" agonism (Jarpe et al., 1998; Kenakin, 1995).

1.4.3 The driving forces of ligand binding

GPCRs exist in multiple conformations. In the ligand-free (apo) state, most receptors will adopt an inactive state, while some receptors adopt an active state, causing constitutive receptor activity. The distribution of receptor conformations is centered around the

conformation with the lowest Gibbs energy. Agonists stabilize active, inverse agonists inactive states. Neutral antagonists do not influence the equilibrium (Freissmuth et al., 2016). The stabilizing effects of bound ligands are mediated by the various interactions with the receptor as well as by entropic effects. Stronger and more numerous interactions between ligand and receptor will lead to more efficient capturing of the receptor in the energetically preferred state (Warne, Edwards, Dore, Leslie, & Tate, 2019). The affinity of a ligand can thus be improved by introducing chemical moieties that establish additional interactions between ligand and receptor (see e.g. Manglik et al., 2016). Single amino acid exchanges by site-directed mutagenesis offer the possibility to experimentally assess the contribution of individual amino acid side chains to the binding of ligands (Di Cera, 2000, pp. 50 - 53; Munk, Harpsoe, Hauser, Isberg, & Gloriam, 2016). The most common replacement is alanine (A), as its' methyl group side chain induces minimal steric and electrostatic effects (Cunningham & Wells, 1989). Alanine side chains are smaller than those of all other amino acids except for glycine, which induces atypical angles in the protein backbone and is therefore less suitable for such studies. Amino acids that resemble the wildtype residue as closely as possible are typically used to assess the importance of specific side chain properties (Munk et al., 2016). For example, histidine (H) is often replaced by phenylalanine (F) because it approximately resembles histidine in size and possesses an aromatic side chain with delocalized π-electrons (see e.g. Ludwig et al., 2003; Murakami, Yokomizo, Okuno, & Shimizu, 2004; J. Q. Wang et al., 2004).

1.4.4 G-proteins

Heterotrimeric G-proteins are activated by GPCRs as described above (chapter 1.3.4). Humans express numerous α,β and γ subunits. By convention G-proteins are named according to the respective Gα subunits incorporated, as they dictate the major functional differences between G-proteins (Lodish, 2013, p. 691). Most prominently, $G\alpha_s$ subunits stimulate, and $G\alpha_i$ subunits inhibit AC activity. Activated $G\alpha_o$ and $G\alpha_q$ subunits stimulate Phospholipase C (Lodish, 2013, pp. 707-709). Gα subunits that interact with neither of the two well-established pathways have been discovered (Syrovatkina, Alegre, Dey, & Huang, 2016).

The separated subunits of activated G-proteins (see chapter 1.3.4) remain anchored to the plasma membrane and initiate various signaling cascades (Lodish, 2013, p. 691). The intrinsic GTPase function of G-proteins hydrolyzes the bound GTP to GDP, thereby inactivating the $G\alpha_i$ subunits within a few seconds to minutes. Experimentally, the

longevity of active, GTP-bound states is often prolonged by using stable GTP analogs (Lodish, 2013, pp. 689-690). Moreover, toxins of bacterial origin are commonly used to block G-protein activity: while pertussis toxin (PTX) blocks $G_{i/o}$-proteins in the inactive, GDP-bound form, cholera toxin (CTX) blocks GTP hydrolysis at activated $G\alpha_s$-subunits, arresting them in the active form. Both types of G-protein arrest inhibit subsequent stimulus-dependent signaling, thus the toxins can be utilized to identify the G-protein subtypes involved in specific processes (Mangmool & Kurose, 2011). Binding of GTP to the Gα-subunits can be monitored using labeled GTP analogs, for example [^{35}S]-GTPγS (Strange, 2010).

Further downstream, G-protein modulation of AC activity can be monitored via quantification of cAMP levels.

1.5 Inflammation and tissue injury: pain and opioid analgesia

1.5.1 General concepts

Inflammation is an organism's response to tissue injury or infection (reviewed by Chovatiya and Medzhitov (2014)). Inflammation is part of the innate immune system and almost always accompanied by pain. In inflamed tissue, resident macrophages and mast cells produce and release inflammatory mediators that trigger the extravasation of leukocytes and plasma proteins from blood vessels, recruitment of other immune cells, formation of an inflammatory exudate and the production of (further) cytokines (Chavan, Pavlov, & Tracey, 2017). Cytokines and other inflammatory mediators such as prostaglandins, nerve growth factor and protons activate and/or sensitize nociceptors (McMahon, 2013, p. 14). Thus, inflammation leads to spontaneous pain, hyperalgesia and allodynia (Mason, 2011).

1.5.2 Opioid analgesia in inflammation

Inflammation and injury rapidly enhance opioid effects (McMahon, 2013, p. 425). Crucially, activation of peripheral μ-, κ- and δ-receptors reduces inflammatory pain, while it has little to no effect on noxious stimuli in naïve animals (Kayser & Guilbaud, 1983; Stein, Millan, Shippenberg, Peter, & Herz, 1989; Stein, Millan, Yassouridis, & Herz, 1988). In humans, peripherally restricted opioids likewise produce only mild effects in the absence of tissue injury, but convey effective analgesia in inflammatory pain (Gupta, Bodin, Holmstrom, & Berggren, 2001). In a clinical study, the peripherally restricted MOR antagonist methylnaltrexone significantly increased patients' postoperative demand for

morphine, demonstrating that under inflammatory conditions, peripheral opioid receptors significantly contribute to the analgesia conveyed by systemically acting opioids. (Jagla et al., 2014). In line with these findings, conditional knockout mice lacking MOR in a subpopulation of primary nociceptive neurons experienced diminished analgesia of inflammatory pain in response to MOR agonists (Weibel et al., 2013).

It has further been demonstrated that enhanced peripheral opioid responsiveness is locally restricted to the area of inflammation (Labuz & Machelska, 2013; Mousa et al., 2017; Schafer, Imai, Uhl, & Stein, 1995; Spahn et al., 2018).

Numerous studies illustrate mechanisms that may underlie these *in vivo* findings. At the molecular level, it was demonstrated that hindpaw inflammation in rats enhanced MOR binding sites and DAMGO-induced G-protein coupling in DRG neurons (Zollner et al., 2003). The increase in MOR signaling was restricted to neurons innervating the injured side, and MOR binding sites in the CNS were not altered by peripheral inflammation (Shaqura, Zollner, Mousa, Stein, & Schafer, 2004). Hindpaw inflammation also increased axonal MOR transport towards peripheral nerve terminals (Hassan, Ableitner, Stein, & Herz, 1993; Mousa et al., 2007). In addition, increased permeability of nerve-blood barrier and therefore access to opioid receptors is enhanced in inflamed tissue (Abram, Yi, Fuchs, & Hogan, 2006). It was further suggested that under physiological conditions, opioid receptors in peripheral nociceptors are constitutively desensitized. In support of this hypothesis, the antagonist naloxone (NLX) induced functional competence in cultured primary neurons (Sullivan, Chavera, Jamshidi, Berg, & Clarke, 2016). Bradykinin, a vasoactive peptide abundant in inflamed tissue, seems to be an important stimulus to initiate this process (Patwardhan et al., 2005; Sullivan et al., 2016). However, many of these phenomena were only observed after several days of persistent tissue injury. Therefore, the present thesis sought to clarify whether additional features of inflammation may contribute to the rapid enhancement of peripheral opioid receptor function observed in some models.

1.5.3 Tissue injury, inflammation and acidification

Inflammation is accompanied by tissue acidosis. In humans, interstitial pH values as low as 6.0 have been measured under inflammatory conditions; in animal studies and human tumors even stronger acidification has been observed (reviewed in Stein, 2018).

In inflamed tissue, insufficient oxygen supply and heightened metabolic activity forces glycolysis along the anaerobic pathway, leading to accumulation of lactic acid that

dissociates into lactate and protons (Deetjen, Speckmann, Benndorf, & Alzheimer, 2005, p. 565; Karhausen, Haase, & Colgan, 2005). In addition, damaged cells release protons from mitochondria and lysosomes (McMahon, 2013, p. 14; see also chapter 1.6.2). Immune cells further contribute to acidosis by release of protons, and some immune cells are themselves regulated by pH (Capasso, 2014; Erra Diaz, Dantas, & Geffner, 2018). Protons also activate and sensitize nociceptors via acid-sensing ion channels (ASICs) and TRPV1. Overall, protons produce pro-inflammatory and pro-nociceptive effects.

However, previous work from our group has demonstrated that tissue acidosis can also modulate the analgesic potency of ligands at peripheral opioid receptors (Gonzalez-Rodriguez et al., 2017; Spahn et al., 2017). The possible effects of acidic pH on opioid receptors, their interaction with ligands and resulting downstream signaling pathways were not comprehensively studied so far.

1.6 pH: from general concepts to its potential role in MOR function

1.6.1 pH, pK_a and protonation: general concepts

The negative decadic logarithm of the proton activity within a homogeneous solution is termed pH. The proton activity is directly proportional to the proton concentration. For practical purposes, the proton activity is usually approximated as the proton concentration in solution (Nelson, Cox, & Lehninger, 2017).

$$pH = -\log [H^+] \tag{1}$$

The association and dissociation of protons to and from a weak acid (A) follows the law of mass action and is described by

$$[A^-] + [H^+] \rightleftharpoons [\mathrm{AH}] \tag{2}$$

The equilibrium constant K_a for this reaction is defined as

$$K_a = \frac{[H^+][A^-]}{[HA]} \tag{3}$$

The negative decadic logarithm of K_a, the pK_a, is commonly used to characterize the propensity of a weak acid (that can be either a molecule or a functional group) to release a proton, ergo the respective acidity.

Applying equation (*1*) to equation (*3*) and solving for pH yields the Henderson-Hasselbalch equation

$$pH = pK_a + log\frac{[A^-]}{[HA]} \tag{4}$$

The Henderson-Hasselbalch equation thus describes the quantitative relation of a weak acid's pK_a, the surrounding pH, and the resulting ratio of deprotonated to protonated species. In aqueous solution, free protons are quickly taken up by surrounding water molecules to form hydronium ions (H_3O^+). The quick transfer of protons between hydronium ions enables fast net movement of protons within aqueous solutions.

Small deviations in the proton concentration can be offset by buffers, mixtures of weak acids and their conjugate bases that bind or release protons depending on the pK_a of the acidic component in relation to the pH (equation 4). The buffering capacity of such systems is limited; if pK_a of the buffering substance and the surrounding pH differ by more than ± 1 units, changes in the proton concentration will cause significant changes in pH (J. M. Berg, Gatto, Stryer, & Tymoczko, 2003, p. 81). Protonation and deprotonation in aqueous solutions occur fast, providing almost immediate responses to deviations from homeostasis. This renders protons potentially useful "signaling molecules". However, cells have specific requirements concerning the proton concentration of their environment and intracellular fluids.

1.6.2 pH: general role in physiological processes

pH homeostasis is crucial to all living organisms; deviations from standard pH values indicate malfunction and mediate adaptive or defensive reactions (Pocock, Richards, & Richards, 2017). In humans, typical extracellular tissue pH lies at 7.4, and intracellular pH close to 7.2 (Lodish, 2013, p. 47). Several intracellular compartments maintain pH values that deviate from the cytosolic pH. In late endosomes and lysosomes, acidic pH is required to support the functionality of enzymes that are quickly inactivated at cytosolic pH (Lodish, 2013, p. 490). In mitochondria on the other hand, a proton gradient between the intermembrane space and the lumen creates the proton motive force that is required for synthesis of ATP (Lodish, 2013, p. 527). Despite these specific pH requirements, pH regulation *in vivo* displays a wide dynamic range (Cockerill & Reed, 2011, pp. 228 - 231).

1.6.3 pH: role in GPCR signaling

Several class A GPCRs are regulated by extracellular pH variations in the patho-physiological range (Ghanouni et al., 2000; Lans, Dalton, & Giraldo, 2015a; Ludwig et al., 2003). The OGR1 family of GPCRs is directly activated by extracellular protonation, triggering activation of G_s, G_q or G_i proteins and the respective downstream signaling cascades (Dai et al., 2017; Kawabata, 2011; Ludwig et al., 2003).

In rhodopsin, protonation of several acidic residues was demonstrated to stabilizes the active receptor conformation (Arnis, Fahmy, Hofmann, & Sakmar, 1994; Lans et al., 2015a). A similar role of these highly conserved residues was confirmed in the α_{1B}-adrenergic receptor (Scheer, Fanelli, Costa, De Benedetti, & Cotecchia, 1996). In membrane fractions expressing the β_2-adrenergic receptor fused with $G\alpha_s$, acidic pH increased constitutive receptor activity by destabilizing the inactive receptor conformation, but also reduced agonist affinity and induced receptor denaturation (Ghanouni et al., 2000). Based on *in silico* analysis of high-resolution crystal structures, protonation of a highly conserved aspartate was later suggested to trigger pH-dependent activity (Ranganathan, Dror, & Carlsson, 2014).

Several amino acids that were demonstrated to convey proton-sensing functions in various GPCRs are topologically conserved in the MOR (Table 1-1).

Table 1-1.Conserved proton-sensing GPCR residues

residue	domain	MOR	H+-activated GPCRs	Rho-dopsin	α_{1B}-adrenergic receptor	β_2-adrenergic receptor
D2.50	TM2	D114		D83 [1]		D79 [2]
D3.49	TM3	D164		E134 [3]	[4]	D130 not involved [5]
H6.52	TM6	H297	[6, 7, 8]			
H7.36	TM7	H319	[6, 9]			

1 > (Lans, Dalton, & Giraldo, 2015b); 2 > (Ranganathan et al., 2014); 3 >(Arnis et al., 1994); 4 > (Scheer et al., 1996) 5 >(Ghanouni et al., 2000); 6 > (Ludwig et al., 2003); 7 > (J. Q. Wang et al., 2004); 8 > (Murakami et al., 2004); 9 > (Liu et al., 2010)

Considering both the enhanced opioid efficacy in inflamed tissue and the potentially proton-sensing residues conserved in the MOR tertiary structure, it is reasonable to hypothesize that opioid receptor activation is pH-dependent.

1.6.4 Acidic pH and opioid signaling

A small number of studies has assessed the influence of pH on MOR. In Ca^{2+}-imaging experiments on cultured rat DRG neurons, acidic extracellular pH enhanced inhibition of capsaicin- and high potassium-induced Ca^{2+}-currents by morphine and β-endorphin (Vetter, Kapitzke et al. 2006). The authors concluded that acidic pH might thus contribute to the enhanced analgesic efficacy of opioids in injured tissue. The underlying mechanisms, however, remained unclear.

Previously, it was found that transient pre-incubation of membrane fractions from rat brain homogenates at pH 4.5 irreversibly enhanced the opioid inhibition of basal AC activity (Childers & LaRiviere, 1984). Interestingly, the low pH pre-incubation altered neither the binding of [^{3}H]-agonists to the receptor nor the affinity of GTP to G-proteins at pH 7.4 (Lambert & Childers, 1984; Selley, Breivogel, & Childers, 1993). It was then concluded that in these experiments, an irreversible reduction of GTPase activity had potentiated the downstream effects of G-protein activation (Selley et al., 1993). Unfortunately, these studies did not assess immediate effects of acidic pH on opioid signaling.

Some early studies on opioid receptors included assessments of the pH range for optimal radioligand binding and found that acidic pH impaired binding of [^{3}H]-NLX, ^{3}H-dihydromorphine and N-methylmorphine to rat brain membranes (Pert & Snyder, 1973a, 1973b; Smith, 1977). The mechanism underlying this effect has to date not been illuminated.

1.6.5 Acidic pH: putative protonation of MOR residues

To fully characterize effects of low pH on opioid receptor-ligand interactions, it is important to also consider plausible pH-sensitive moieties within the MOR binding pocket. In order to be able to discriminate between normal and inflamed conditions, a pH-sensing moiety must show a pK_a value in the neutral to acidic range (for an overview of pH values in injured and inflamed tissue see Stein, 2018). In folded proteins, pK_a values of amino acid side chains may vary significantly around the pK_a of the isolated species and are difficult to predict. According to a meta-analysis of pK_a measurements in folded proteins, the mean amino acid side chain pKa values of the protonatable side chains show considerable variation: aspartate (D; pK_a 3.5 ± 1.2), glutamate (E; pKa 4.2 ± 0.9), histidine (H; pK_a 6.6 ± 1.0) and cysteine (C; pKa 6.8 ± 2.7). (Grimsley, Scholtz, & Pace, 2009). Among these candidate amino acids were repeatedly demonstrated to serve important functions in ligand binding and receptor activity at physiological pH.

An ionic bond between **D147$^{3.32}$** and MOR ligands has been observed in all high-resolution structures, and ample evidence suggests that this interaction is necessary for receptor binding (Dosen-Micovic, Ivanovic, & Micovic, 2006; J. G. Li et al., 1999). Protonation of D side chains neutralizes their charge. Thus, D$^{3.32}$ in the protonated form is incapable of forming ionic bonds. **D114$^{2.50}$** serves as binding site for an allosteric Na^+ that stabilizes the receptor in an inactive conformation, a role that is widely conserved across class A GPCRs (Huang et al., 2015; Katritch et al., 2014; Mirzadegan, Benko, Filipek, & Palczewski,

2003). Another highly conserved interaction that stabilizes the receptor in an inactive conformation is the intramolecular salt bridge between **D164$^{3.49}$ and R165$^{3.50}$**. Protonation of either D$^{2.50}$ or D$^{3.49}$ has been experimentally connected to receptor activation in several pH-sensitive class A GPCRs (Arnis et al., 1994; Lans et al., 2015a; Ranganathan et al., 2014; Scheer et al., 1996). Protonation of either residue abolishes the intramolecular salt bridge that consists of ionic and hydrogen bonds.

H297$^{6.52}$ is topologically conserved across species and class A GPCRs (including all three opioid receptors) and conveys proton sensing to several proton-activated receptors (Liu et al., 2010; Ludwig et al., 2003; Murakami et al., 2004; J. Q. Wang et al., 2004). High-resolution structures of all main opioid receptor subtypes have consistently reported hydrogen bonds between H$^{6.52}$ and bound ligands (Granier et al., 2012; Koehl et al., 2018; Manglik et al., 2012; Wu et al., 2012). Introduction of a positive charge by exchange of H297$^{6.52}$ for the glutamine or asparagine renders NLX an agonist of the mutant receptor (Spivak et al., 1997). H side chains, in comparison, carry a positive charge only in the double protonated form that predominates at acidic pH (Figure 5B). Protonation changes H side chains from potential hydrogen bond acceptors into ~ donors (S. Li & Hong, 2011)

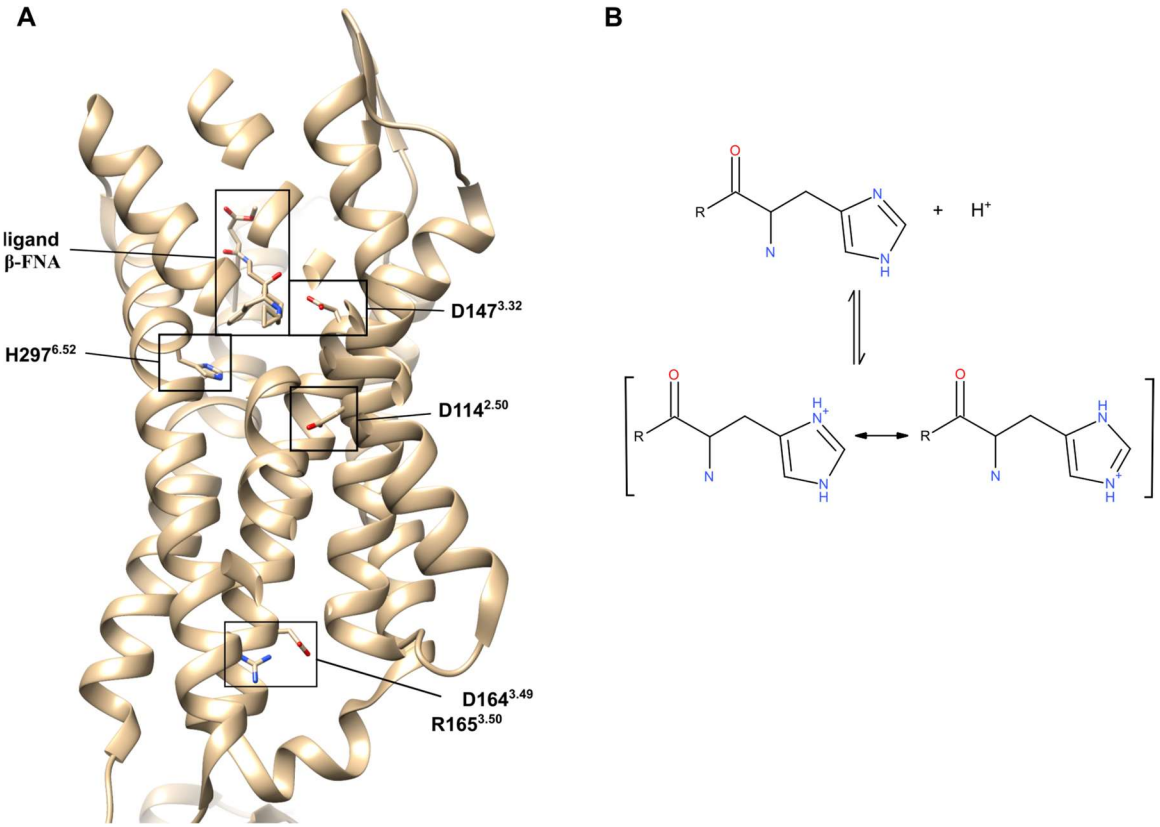

*Figure 5. (**A**) Possible protonation sites among the highly conserved residues of MOR. Structure of the inactive human mu-opioid receptor (MOR) bound to the irreversible antagonist beta-Funaltrexamine (β-FNA) modified from the PDB entry 4DKL (Manglik et al., 2012) with the software USCF Chimera (Pettersen et al., 2004). (**B**) Protonation of a histidine side chain*

1.7 Objectives

In the present studies, I sought to answer two main questions

1. Does acidic pH per se affect MOR binding and signaling of conventional opioids?
2. Does acidic pH alter interaction between ligand and receptor in the MOR binding pocket? If yes, can the effect be exploited for drug targeting?

Based on the pre-existing knowledge presented above, the experiments were designed to test two main hypotheses.

1.7.1 Hypotheses

Hypothesis 1: Acidic pH regulates MOR function

The immediate effects of acidic pH on MOR function have not been comprehensively studied so far. By studying MOR binding, G-protein activation and modulation of intracellular cAMP accumulation, I sought to establish modes and mechanisms of pH-dependent alterations in MOR function.

Hypothesis 2: Protonation of MOR H297$^{6.52}$ regulates MOR function at acidic pH

Data from our group that were published during the course of this study revealed that binding of fentanyl is not impaired at acidic pH (Rodriguez-Gaztelumendi, Spahn, Labuz, Machelska, & Stein, 2018; Spahn et al., 2017). A general incapacity of opioids to bind MOR could therefore be excluded. An *in silico* study suggested that, in contrast to the morphinan-based ligands present in MOR crystal structures, fentanyl does not form hydrogen bonds to H297$^{6.52}$ (Dosen-Micovic et al., 2006; Huang et al., 2015; Manglik et al., 2012). Therefore, it was reasonable to assume that H297$^{6.52}$ could discriminate between fentanyl and NLX in a pH-dependent manner. In contrast, formation of an ionic bond between ligand and D$^{3.32}$ of MOR is a prerequisite for the binding of fentanyl, as for MOR ligands in general (Dosen-Micovic et al., 2006; J. G. Li et al., 1999). Destabilization of inactive receptor conformations generally reduces the binding of antagonists, but not of agonists (De Lean, Stadel, & Lefkowitz, 1980). Accordingly, D$^{3.32}$, D$^{2.50}$, D$^{3.49}$ and R$^{3.50}$ are unlikely to mediate a pH-dependent inhibition of binding that does affect NLX, [^{3}H]-NLX, ^{3}H-di-hydromorphine and N-methylmorphine, but not fentanyl. I hypothesized that pH-dependent protonation of residue H297$^{6.52}$ in the MOR leads to alterations in the hydrogen bond network between receptor and ligand.

2 Materials & Methods

2.1 Materials

2.1.1 Plasmids and constructs

Name	Supplier
pcDNA™3.1 / *myc*-His	Invitrogen, Thermo Fisher Scientific (Hennigsdorf, Germany)
pCMV6-Entry	OriGene Technologies GmbH (Herford, Germany)

The plasmid containing the cDNA encoding the FLAG-epitope-tagged rat mu-opioid receptor (MOR) (oprm1, NM_013071.2) in pcDNA™3.1 vector with geneticin resistance gene was provided by Prof. Christian Zöllner (University Hamburg, Germany) and was used to generate MOR mutants MOR-H297$^{6.52}$A and MOR-H297$^{6.52}$F. Gnai1 (NM_013145) rat tagged ORF clone in pCMV6-Entry vector was purchased from OriGene Technologies.

2.1.2 Bacteria and cell lines

Name	Genotype	Supplier/ generated by
Escherichia coli (E.coli) XL 10-Gold ® Ultracompetent Cells	Tet^rΔ(*mcr*A)183; Δ(*mcr*CB-*hsd*SMR-*mrr*)173 *end*A1 *sup*E44 *thi*-1 *rec*A1*gyr*A96 *rel*A1 *lac* Hte [F′ *pro*AB *lac*I^qZΔ*M*15 Tn*10* (Tet^r) Amy Cam^r]	Agilent Technologies (Waldbronn, Germany)
HEK 293	HEK 293 cells wildtype (human embryonic kidney cells)	DSMZ- German Collection of Microorganisms and Cell Cultures (Braunschweig, Germany)
HEK MOR-WT	HEK 293 cells stably transfected with FLAG-epitope-tagged rat mu-opioid receptor (MOR) (oprm1, NM_013071.2) in pcDNA™3.1 vector	Prof. Christian Zöllner
HEK MOR-$H297^{6.52}$A	HEK 293 cells stably transfected with FLAG-epitope-tagged rat MOR mutated at $H297^{6.52}$ to A in pcDNA™3.1 vector	Dr. Viola Spahn
HEK MOR-$H297^{6.52}$F	HEK 293 cells stably transfected with FLAG-epitope-tagged rat MOR mutated at $H297^{6.52}$ to F in pcDNA™3.1 vector	Johanna Meyer

2.1.3 Antibiotics

Name	Supplier
Ampicillin	Sigma Aldrich (Taufkirchen, Germany)
Geneticin (G418)	Biochrom (Berlin, Germany)
Penicillin / Streptomycin (100 U/ml / 100 µg/ml)	Biochrom

2.1.4 Oligonucleotides

Oligonucleotides were designed as described in the corresponding paragraphs of the chapter "Methods" and ordered from TIB MOLBIOL Sytheselabor GmbH (Berlin, Germany).

Name	5' – 3' sequence	Application
c913t_a914t for	TTgATgATgACgTAgATgAAgATgggggTCCAgCAgAC	mutagenesis MOR H297$^{6.52}$F
c913t_a914t rev	gTCTgCTggACCCCCATCTTCATCTACgTCATCATCAA	mutagenesis MOR H297$^{6.52}$F
ratMOR-01_for	gCgACTgCTCAgACCCCTTA	RT-PCR
ratMOR-01_rev	TCATggTgCAgAgggTgAAT	RT-PCR
ratMOR-flag.1_for:	TACAAggACgACGACGACAA	RT-PCR
ratMOR-flag.1_rev	ggTTCAgACCgCATggAT	RT-PCR
huGAPDH_for	ACATCAAgAAggTggTgAAg	RT-PCR
huGAPDH_rev	AgCTTgACAAAgTggTCgTTg	RT-PCR

2.1.5 Kits

Name	Supplier
Amersham cAMP Biotrak Enzymeimmunoassay kit	GE Healthcare (Solingen, Germany)
$G\alpha_i$ Activation Assay Kit	NewEast Biosciences (Malvern, USA)
High-Capacity-RNA-to-cDNA kit	(Applied Biosystems) Thermo Fisher Scientific
LSBio Mouse/Human/Rat OPRM1/ Mu Opioid Receptor Cell-based ELISA Kit	LifeSpan BioSciences (Seattle, USA)
QIAfilter Plasmid Maxi Kit (25)	QIAGEN (Hilden, Germany)
QIAprep Spin Miniprep Kit	QIAGEN
QuickChange II XL Site-Directed Mutagenesis Kit	(Stratagene) Agilent Technologies
RNeasy Mini Kit	QIAGEN

2.1.6 Enzymes

Enzymes solely purchased as parts of kits are not listed separately.

Name	Supplier
BglII restriction enzyme	New England Biolabs (Frankfurt am Main, Germany)
DreamTaq Green PCR Master Mix	Thermo Fischer Scientific

2.1.7 Antibodies

Antibodies purchased as parts of kits are not listed separately.

Primary antibodies

Name	Specifier	Supplier
Anti-Active $G\alpha_i$ Mouse Monoclonal Antibody	26901	NewEast Biosciences
c-Myc Mouse Monoclonal antibody, FITC conjugate	9E10	Thermo Fisher Scientific
guinea pig anti-MOR-1	AB1774	(Chemicon) Merck (Darmstadt, Germany)

Secondary antibodies

Name	Specifier	Supplier
Alexa Fluor 488 (AF488) goat anti-guinea pig	A11073	(Invitrogen)Thermo Fisher Scientific
HRP-coupled Polyclonal Goat Anti-Mouse Immunoglobulin	P044701-2	(Dako) Agilent Technologies

2.1.8 Pharmacological agents

2.1.8.1 Opioids

Name	Supplier
Fentanyl citrate	Sigma-Aldrich
Naloxone (NLX) hydrochloride	Sigma-Aldrich
[D-Ala2,N-Me-Phe4,Gly5-ol]-enkephalin (DAMGO)	Sigma-Aldrich

2.1.8.2 Radiochemicals

Name	Supplier
[^{3}H]-DAMGO	Perkin Elmer (Waltham, USA)
[^{3}H]-NLX	Perkin Elmer
[^{35}S]-GTPγS	Perkin Elmer

2.1.8.3 Other

Name	Supplier
Cholera toxin (CTX)	Sigma-Aldrich
Forskolin (FSK)	Sigma-Aldrich
Isobutylmethylxanthine (IBMX)	Sigma-Aldrich
Pertussis toxin (PTX)	Sigma-Aldrich
Prostaglandin E_2 (PGE_2)	Sigma-Aldrich

2.1.9 Chemicals, reagents and media

Name	Supplier
4-(2-hydroxyethyl)-1-piperazineethanesulfonic acid (HEPES)	Sigma-Aldrich
4-(2-Hydroxyethyl)-1-piperazinepropanesulfonic acid (EPPS)	Sigma-Aldrich
2-(N-Morpholino)ethanesulfonic acid (MES)	Sigma-Aldrich
Calcium chloride ($CaCl_2$)	Sigma-Aldrich
Complete mini EDTA-free protease inhibitor cocktail	Roche (Mannheim, Germany)
D-(+)-Glucose	Sigma-Aldrich
DAPI (NucBlue^{TM} Fixed Cell Stain)	Sigma-Aldrich
Dulbecco's Modified Eagles Medium (DMEM)	Sigma-Aldrich
ECL	GE healthcare
Ethanol	Carl Roth GmbH + Co. KG (Karlsruhe, Germany)
Etylenediaminetetraacetic acid (EDTA)	Sigma-Aldrich
Ethylene glycol-bis(β-aminoethyl ether)-N,N,N',N'-tetraacetic acid (EGTA)	Sigma-Aldrich
Fetal bovine serum (FBS)	Biochrom
Fluorescent Mounting Medium	(Dako) Agilent Technologies
Hydrochloric acid 37%	Sigma-Aldrich
Isopropyl alcohol	Sigma-Aldrich
LB Agar	(Invitrogen) Thermo Fisher Scientific
LB Broth Base (Lennox)	Carl Roth
Magnesium chloride ($MgCl_2$)	Sigma-Aldrich
Methanol	(J.T. Baker) Thermo Fisher Scientific
Midori Green Advance	Biozym Scientific GmbH (Hessisch Oldendorf, Germany)
Non-fat dry milk powder	Carl Roth
Normal goat serum (NGS)	Jackson Immunoresearch Europe

	Ltd. (Cambridgeshire Business Park, UK)
Optiphase HISAFE 3	Perkin Elmer
Paraformaldehyde (PFA)	Sigma-Aldrich
Phosphate Buffered Saline (PBS) without Ca^{2+}, Mg^{2+}	Biochrom
Potassium chloride (KCl)	Sigma-Aldrich
Polyethyleneimine (PEI)	Sigma-Aldrich
Poly-L-lysine	Sigma-Aldrich
Protein Assay Dye Reagent Concentrate	Bio-Rad, München, Germany
Protein G agarose resin	Pierce Biotechnology (Rockford, USA)
RNAlater	Thermo Fisher Scientific
Sodium Chloride (NaCl)	Carl Roth
Trethylamine (TEA)	Sigma-Aldrich
Tris base	Carl Roth
Tris hydrochloride	Carl Roth
Triton™X-100	Sigma-Aldrich
Trizma® Pre-set crystals, pH 7.4.	Sigma-Aldrich
Tween-20	Sigma-Aldrich
X-tremeGENE HP DNA Transfection Reagent	Roche

2.1.10 Buffers and solutions

Distilled water was used for Tris buffer for wash steps in radioligand and [^{35}S]-GTPγS binding assays. Distilled and deionized water was used for the preparation of all other buffers and solutions.

Name	Composition
Agarose gel	2% agarose, 0.004% Midori Green Advance in TAE
Antibody dilution buffer 1 (primary antibodies ICC)	1% (w/v) BSA, 0.3% (v/v) Triton™ X-100 in PBS
Antibody dilution buffer 2 (secondary antibodies ICC)	0.3% (v/v) Triton™ X-100 in PBS
Assay/ lysis buffer (immunoprecipitation)	50 mM Tris-HCl, 150 mM NaCl, 1 mM EDTA, 1% Triton X-100 in H_2O, pH 7.4
Blocking buffer (immunocytochemistry)	5% normal goat serum, 0.3Triton™ X-100 in PBS
Blocking buffer (immunoblot)	5% (w/v) non-fat dry milk powder in TBST
Blotting buffer (immunoblot)	25 mM Tris base, 190 mM glycine, 20% (v/v) methanol in H_2O, pH 8.3
Extracellular solution	140 mM NaCl, 5 mM KCl, 2 mM $MgCl_2$, 2 mM $CaCl_2$, 10 mM HEPES, 10 mM D-(+)-Glucose in H_2O
Formaldehyde solution	4% formaldehyde in PBS
HEM buffer	8 mM HEPES, 8 mM EPPS, 8 mM MES in H_2O
HEM G protein buffer	8 mM HEPES, 8 mM EPPS, 8 mM MES, 100 mM NaCl, 5 mM $MgCl_2$, 0.2 mM EGTA, 1mM DTT, 0.1% (w/v) BSA in H_2O
LB agar	1.5% (w/v) LB agar (Lennox L Agar)
LB medium	2% (w/v) LB Broth Base in H_2O, autoclaved
sodium dodecyl sulfate polyacrylamide gel electrophoresis (SDS-PAGE) running buffer	25 mM Tris base, 190 mM glycine, 10% SDS in H_2O, pH 8.3
SDS-PAGE sample buffer	250 mM Tris, 8% (w/v) SDS, 40% (v/v) glycerol, 0.04%

(4x)	(w/v) bromphenol blue, 10% (v/v) β-mercaptoethanol in H_2O, pH 6.8
SDS-PAGE separating gel	375 mM Tris, 12% acrylamide/bisacrylamide (Rotiphorese ® Gel), 0.1% (w/v) SDS, 1% (w/v) ammonium persulfate, 0.1% (v/v) TEMED in H_2O, pH 8.8
SDS-PAGE stacking gel	125 mM Tris, 5% (v/v) acrylamide/bisacrylamide, 0.1% (w/v) SDS, 1% (w/v) ammonium persulfate, 0.1% (v/v) TEMED in H_2O, pH 6.8
TAE	40 mM Tris, 20 mM acetic acid, 1 mM EDTA, pH 8.3
TBST	10 mM Tris base, 150 mM NaCl, pH 7.4
TBST	10 mM Tris base, 150 mM NaCl, 0.05 % (v/v) Tween20, pH 7.4
Tris buffer	50 mM Tris

2.1.11 Consumable materials

Name	Supplier
Amersham Hyperfilm™ ECL	GE healthcare
Cell culture bottles	Corning (Wiesbaden, Germany), Sarstedt (Nürmbrecht, Germany)
Cell culture dishes	TPP Techno Plastic Products AG (Trasadingen, Switzerland), Corning (Wiesbaden, Germany)
Cell culture plates	TPP
Cell scrapers	TPP
Coverslips	Carl Roth
Cryo tubes (Nalgene)	Thermo Fisher Scientific
Gel blot paper (Whatman)	GE healthcare
GF/B glass fiber filters (Whatman)	GE healthcare
Microscope slides	R. Langenbrinck (Emmendingen, Germany)
Nail polish	p2 cosmetics, Vienna, Austria
Needles	BD, Becton Dickinson GmbH (Heidelberg,

	Germany)
Parafilm	Bemis packaging (Rheinbach, Germany)
PCR tubes and caps	Thermo Fisher
Pipettes (5-25 ml, single use; Falcon®)	Corning
Pipet tips (1-1000 µl)	Sarstedt; Eppendorf AG (Hamburg, Germany)
Reaction tubes 0.5 ml, 1 ml and 2 ml	Sarstedt
Spatulas, disposable	VWR International GmbH (Darmstadt, Dermany)
Sterile filtration device (single use)	Thermo Fisher Scientific
Syringes	B. Braun (Melsungen, Germany)
Tubes (15 ml and 50 ml, Falcon ®)	Corning
Vacuum pumps	KNF Neugeberger GmbH (Freiburg, Germany)

Glassware

Name	Supplier
Beaker	Schott Ag (Mainz, Germany)
Measuring cylinders	Brand GmbH (Wertheim, Germany)
Microscope slides	Carl Roth
Neubauer counting chambers	Paul Marienfeld GmbH (Lauda-Königshofen, Germany)
SDS-PAGE equipment (Mini PROTEAN® 3 System)	Bio-Rad

2.1.12 Instruments

Name	Supplier
Agarose gel station	Bio-Rad
Avanti JXN-26 ultracentrifuge	Beckmann Coulter (Krefeld, Germany)
Bacterial shaker	GFL Gesellschaft für Labortechnik mbH (Burgwedel, Germany)
Balances (BP1215, BP4100)	Sartorius AG (Göttingen, Germany)
Centrifuge tabletop (Biofuge	Heraeus (Hanau, Germany)

fresco)	
Centrifuge tabletop mini	Biozym
Centrifuge (Multifuge 4KR)	Heraeus
CO_2 incubator	(MMM Group) Heraeus
Confocal microscope;	LSM 510 Meta; EC Plan-Neofluar 40x/1.30 Oil
Objectives	DIC; Objective Plan-Apochromat 63x/1.40 Oil DIC Carl Zeiss AG (Oberkochen, Germany)
Dispenser single channel ("Multipette")	Eppendorf
Dispenser multichannel	Thermo Fischer
Dispergierstation T8.10 (mechanical homogenizer)	IKA-Werke GmbH Co. KG (Staufen, Germany)
DS-11+ spectrophotometer	DeNovix (Wilmington, USA)
GelDoc EZ Imager (	Bio-Rad
Harvester	Brandel (Gaithersburg, USA)
Immunoblot transfer chamber & equipment	Bio-Rad
Laminar airflow (HS18)	Heraeus
Microwave	Galanz (Foshan city, China)
pH-meter MP220	Mettler-Toledo GmbH (Gießen, Germany)
Pipets (Pipetus®-Akku)	Hischmann Laborgeräte (Eberstadt, Germany)
Pipets (1-1000 µl)	B. Braun, Eppendorf, Gilson International B.V. (Limburg, Germany)
Power station electrophoreses	Bio-Rad
Scales (BP1215, BP4100)	Sartorius
Shaker (various models)	VWR, Medgenix (Wevelgem, Belgium)
SDS-PAGE gel chambers % equipment	Bio-Rad
Spectrophotometer plate reader (Spectra Max 340PC)	Molecular Devices (Biberach an der Riss, Germany)
Thermocycler	(Applied Biosystems) Thermo Fisher Scientific

(GeneAmp PCR System 9700)	
Thermomixer	Eppendorf
UV light, detector, camera	Bio-Rad
Vortexmixers	Scientific Industries (Bohemia, USA)
Wallac 1414 Win Spectral Liquid Scintillation Counter	Perkin Elmer
Water bath	Grant Instruments (Shepreth, UK)
Water purification system Direct-Q®	(Millipore) Merck

2.1.13 Software

Name	Supplier
Adobe Illustrator CS5	Adobe systems Software Ireland Limited (Munich, Germany)
BIOVIA Draw version 18.1.NET	Dassault Systèmes (Vélizy-Villacoublay, France)
Endnote X8.2	Clarivate Analytics (London, GB)
ImageJ	National Institutes of Health, USA
Image Lab	Bio-Rad
Microsoft Office	Microsoft Corporation (Munich, Germany)
Primer3: WWW primer tool	Whitehead Institute for Biomedical Research, (Cambridge, USA)
Primer-BLAST	National Center for Biotechnology Information, U.S. National Library of Medicine (NCBI; Bethesda, USA)
Prism	GraphPad (San Diego, USA)
Stratagene QuikChange Primer Design	(Agilent Technologies) Thermo Fisher Scientific
UCSF Chimera	Resource for Biocomputing, Visualization, and Informatics at the University of California (USA)

2.2 Methods

All methods were based on established techniques. Detailed descriptions of the underlying principles can be found in standard textbooks on molecular biology or bio-analytics.

2.2.1 Molecular Biology

2.2.1.1 Amplification and isolation of plasmids from bacteria

Plasmids are strands of extrachromosomal DNA that naturally occur in bacterial, fungal and plant, but not mammalian cells. Engineered plasmids harboring a bacterial replicon and mammalian gene inserts with matching promoters can be amplified in fast growing bacteria, most commonly e.coli, and are used as expression vectors of transgenes in mammalian origin cells such as HEK 293 cells.

Plasmids were either isolated from e.coli glycerol stocks previously used in our group or inserted into and amplified in XL 10-Gold® Ultracompetent cells using QuikChange II XL Site Directed Mutagenesis Kit (Agilent Technologies). Briefly, XL-10 Gold Ultracompetent Cells were permeabilized by incubation with β-mercaptoethanol (2µl per 45 µl cell suspension) for 10 min on ice. After addition of 2µl of the desired plasmid, samples were incubated for further 30 min on ice, followed by a 30 sec heat pulse at 42 °C. Pre-warmed SOC medium was added, samples were transferred to Greiner round-bottom tubes and samples were incubated for 1 h at 37 °C with gentle shaking to allow the bacteria to amplify.

Transformed bacteria were amplified and grown on agar plates containing 50 µg or 100 µg ampicillin per ml overnight. Single colonies were isolated and amplified in LB medium containing 100 µg/ml ampicillin. Plasmids were isolated using "*QIAfilter Plasmid Maxi Kit*" or "*QIAprep Spin Miniprep Kit*" (Qiagen). Briefly, cells were subjected to alkaline lysis, the sample pH was neutralized, and lysates were cleared by centrifugation. Protein-depleted lysate was loaded onto silica DNA purification columns under high-salt conditions, the columns were washed to remove RNA, metabolites, and cellular proteins, and purified DNA was eluted in water.

The resulting DNA concentration was determined via absorption at 260 nm measured with a spectrophotometer. The device's inbuilt software uses the formula

$$A_{260} * 50\ \mu g/ml = c\ (dsDNA)$$

to determine dsDNA concentration.

2.2.1.2 *In vitro site-directed mutagenesis*

In vitro site-directed mutagenesis was performed by DNA polymerase-mediated amplification of whole plasmids using complementary primer pairs with specifically designed mismatches of a few basepairs. Primers, and thereby the desired mutation, were irreversibly incorporated in the newly synthesized DNA strands, and parent DNA was subsequently digested with a DNAse that targets methylated and hemimethylated DNA only, sparing plasmids synthesized in vitro.

Primers for in vitro site-directed mutagenesis were designed using "*Stratagene QuikChange Primer Design*" online software (Agilent Technologies). Mutagenesis and subsequent digestion of parental DNA was conducted using the "*QuickChange II XL Site-Directed Mutagenesis Kit*" (Agilent Technologies). Briefly, template pcDNA™3.1 plasmids with FLAG-epitope-tagged rat MOR were incubated with mutagenesis primers as provided in Table 2-1.

Table 2-1. Mutagenesis master mix per reaction

5 µl	10x reaction buffer
1 µl (10 µg)	pcDNA3.1 MOR (10 mg/ ml)
1µl	dNTP mix
3 µl	Quik Solution
36.5 µl	H_2O

Mutagenesis primers used are listed under "materials" in Table 3.1-3. Reactions were pipetted as provided in Table 2-2.

Table 2-2. Mutagenesis pipetting scheme per reaction

1.25 µl	Forward primer
1.25 µl	Reverse primer
46.5 µl	master mix
1 µl	*PfuUltra* HF DNA polymerase

The expected size of the plasmid containing either wildtype or mutant MOR was ~ 6.6 kb. Accordingly, the duration of the extension step in the thermocycling profile was set to 7 min (1 min per kb of plasmid length). Thermocycling was performed as described in Table 2-3.

Table 2-3. Mutagenesis thermocycling profile

Temperature	Step	Duration	Number of cycles
95 °C	denaturation (initial)	1 min	1
95 °C	denaturation	50 sec	18
60 °C	annealing	50 sec	
68 °C	extension	7 min	
68 °C	extension (final)	7 min	1
4 °C	storages	∞	

Remaining template DNA was removed by incubation with Dpn1 restriction enzyme (10 U/µl, 1 µl per reaction) for 1 h at 27 °C.

Resulting DNA was amplified as described above. Glycerol stocks of all clones were frozen in liquid nitrogen, plasmids were isolated using "*QIAprep Spin Miniprep Kit*" as described above and aliquots of all samples were sequenced by an external service provider (Source BioScience, formerly Berlin, Germany). Plasmids carrying the desired inserts were isolated from glycerol stocks as described above (paragraph 2.2.1.1).

2.2.1.3 mRNA isolation

mRNA encoding MOR and GAPDH (as control) was isolated from HEK 293 cells and analyzed in a semi-quantitative approach.

HEK 293 (untransfected), HEK MOR-WT, and HEK MOR-H297$^{6.52}$F cells were split into aliquots of ~5x10^6 cells, centrifuged, and pellets without supernatant were frozen at -80°C in "RNAlater". Pellets were thawed on ice, resuspended in buffer, and mechanically homogenized for 35 sec with a mechanical disperser. Whole mRNA content was isolated from frozen wildtype and stably transfected HEK 293 cells using "*RNeasy Mini Kit*". Cells were lyzed and homogenized with concomitant inactivation of RNases in a guanidine-thiocyanate-containing lysis buffer provided with the kit. After addition of ethanol, samples were applied to silica membrane spin columns, the columns were washed, incubated with RNA-free DNAse I, washed again, and RNA was eluted in water. Absorption at 260 nm was measured with a spectrophotometer and the RNA concentration was calculated according to the formula A_{260} * 40 µg/ml = c (RNA) by the device's inbuilt software.

2.2.1.4 Reverse-Transcription PCR (RT-PCR)

Reverse transcriptases are enzymes that synthesize cDNA strands complementary to RNA templates. Reverse transcription (RT) enables the indirect quantification of mRNA levels via polymerase chain reaction (PCR) (Mullis & Faloona, 1987).

Reverse transcription was carried out using "*High-Capacity-RNA-to-cDNA Kit*". RT enzyme mix and 1µg mRNA input were incubated in RT buffer for 1 h at 37 °C, followed by enzyme inactivation for 5 min at 95°C. A negative control lacking the RT enzyme mix (no enzyme control, NEC) was included in every experiment.

Resulting cDNA and the NEC were stored overnight at 4 °C or at -20°C for longer periods and analyzed by PCR.

Primers were designed using *"Primer3: WWW primer tool"* and *"Primer-BLAST"*. Two pairs of primers were used: In primer pair 1, both forward and reverse primer target sequences within rat-MOR. In primer pair 2 the forward primer targets the FLAG-tag. The sequences of the primers are provided in the methods section. The pipetting scheme for PCR is provided in Table 2-4 and the thermocycling profile is provided in Table 2-5. A no template control (NTC) was included in every experiment to check for DNA contamination.

Table 2-4. PCR pipetting scheme

Nuclease free H2O	1.5 µl
Forward primer (0.1 µg/ml)	5 µl
Reverse primer (0.1 µg/ml)	5 µl
DreamTaq Green PCR Master Mix (2x)	12.5 µl
DNA template or H_2O	1 µl (1:60)

Table 2-5. Thermocycling profile PCR

Step	Temperature	Time	Number of cycles
Initial denaturation	95°C	3 minutes	1
Denaturation	95°C	30 seconds	28
Annealing	58°C	30 seconds	
Extension	72°C	40 seconds	
Final extension	72°C	15 minutes	1
Hold	4°C	∞	1

Quantitative PCR (qPCR)

qPCR experiments to detect endogenously expressed human MOR-WT in untransfected HEK 293 cells were performed in collaboration with a colleague using the Taqman gene expression assays for MOR (Hs01053957_m1) and GAPDH (Hs02786624_g1).

2.2.1.5 Agarose gel electrophoresis

Gel electrophoresis separates macromolecules based on size and charge. DNA carries negative charges in the backbone phosphate groups, hence migration speed in an electric field of constant strength and direction depends on fragment length.

The method was used to identify stably transfected HEK 293 cells with the highest possible similarity in MOR-1 mRNA expression compared to the HEK MOR-WT cell line. DNA samples were separated in 2% agarose gels with Midori Green Advance intercalating fluorescence dye (4 µl/ 100 ml) to visualize DNA and gels were imaged with GelDoc EZ Imager (BioRad, US). Signal intensities in the resulting images were measured with "*ImageJ*", and FLAG-MOR-1 band intensities were normalized to GAPDH band intensities.

2.2.2 Cell culture

2.2.2.1 Maintenance of cell cultures

HEK 293 cells were maintained in DMEM media supplemented with fetal bovine serum (FBS), penicillin (100 U/ml) and streptomycin (100 µg/ml) with or without geneticin (G418, 100 µg/ml), in 5 % CO_2 at 37 °C. Cells were passaged 1:3–1:20 every second to third day from P8 to P28 depending on confluence.

2.2.2.2 Transfection

24 h after seeding, confluent HEK 293 cells (70–90%) were transfected with 1 µg per 200 µl transfection mix of each plasmid containing the different cDNAs using *"X-tremeGENE HP DNA Transfection Reagent"* following the supplier's recommendations.

For stable transfection, pcDNA^{TM}3.1+ carrying MOR with the desired mutation was linearized with restriction enzyme BglII, and linearization was verified by agarose gel electrophoresis. After 48 hours, the medium containing the transfection reagent was removed and replaced by complete Dulbecco's Modified Eagles Medium (DMEM) with 10% fetal bovine serum (FBS) and penicillin / streptomycin (100 U/ml / 100 µg/ml). G418 at 500µg/ml was added for selection of successfully transfected cells. Medium with 500µg/ml G418 was renewed every 2 to 3 days. 17 days post transfection, single colonies of stably transfected cells were picked using a 100 µl pipet and transferred to poly-L-lysine coated wells of a 96-well plate to create monoclonal cell lines. Cells were grown to confluence and successively moved to larger culture vessels in the continued presence of 500µg/ml G418. Antibiotic concentration was reduced to 100µg/ml when first transferred to 75 cm^2 culture flasks. Monoclonal cell lines were chosen based on immunocytochemistry, MOR mRNA expression, subjective impression of cell growth and overall cell morphology.

2.2.3 Determination of protein concentration

Protein concentrations were determined using the dye Coomassie Brilliant Blue G-250 which shifts its absorption maximum from 465 to 595 nm upon binding to proteins (Bradford, 1976). Because the dye selectively forms complexes with cationic and nonpolar amino acid side chains, binding is dependent on protein sequence. The relation between measured absorbance and protein concentration is established with the help of a standard curve obtained from a fixed protein solution of known composition and concentration. These measurements were determined in duplicates using *"Bio-Rad Protein Assay Dye Reagent Concentrate"* with *"Bio-Rad Protein Assay Standard II"* (BSA) (both Bo-Rad).

Standard or sample and dye reagent concentrate were diluted according to the manufacturer's instructions, thoroughly mixed, and incubated for 5 min at room temperature. Absorption at 595 nM was measured with a spectrophotometer. These measurements were performed in triplicates. Generation of a linear standard curve and interpolation of total protein concentration was performed by the device's inbuilt software. A standard curve was generated for every experiment.

2.2.4 Receptor binding techniques

2.2.4.1 Membrane preparation for radioligand and [^{35}S]-GTPγS binding

Radioligand and [^{35}S]-GTPγS binding were performed on crude membrane fractions of HEK 293 cells. After mechanical homogenization, membranes with embedded and anchored proteins were separated from cytosolic components by centrifugation.

HEK 293 cells, either untransfected, stably expressing MOR-WT, or MOR mutated at specific residues were grown in 175 cm^2 tissue culture flasks to approximately 90 % confluence, rinsed, harvested by centrifugation and resuspended in Tris buffer. Cell suspensions were homogenized using a mechanical disperser at maximum speed for 10 seconds and centrifuged at 42000 g and 4°C for 20 minutes. Supernatants were discarded, and pellets were stored at -80°C. On the day of usage, pellets were thawed on ice in Tris buffer and homogenized. After determination of the total protein concentration homogenates were split according to the number of conditions tested, centrifuged, and pellets were resuspended in the respective assay buffer.

2.2.4.2 Radioligand binding

Radioligand binding was performed in 2 different experimental setups, single-dose and saturation binding. [^{3}H]-naloxone ([^{3}H]-NLX) and [^{3}H]-[D-Ala2,N-Me-Phe4,Gly5-ol]-enkephalin ([^{3}H]-DAMGO) saturation binding was performed on membrane fractions of HEK MOR-WT in *"HEM buffer"* (Ludwig et al., 2003) at pH 7.4, 6.5, and 6.0. Binding experiments on MOR-H297$^{6.52}$A were performed in Tris buffer because it is conventionally used to study MOR radioligand binding. MOR-H297$^{6.52}$A was investigated only at pH 7.4 because alanine side chains cannot be protonated. [^{3}H]-NLX binding to MOR-WT was investigated in HEM buffer to cover a wider pH range. Radioactive concentrations were calculated based on the rate of radiolytic decomposition as provided by the manufacturer. [^{3}H]-NLX or [^{3}H]-DAMGO were serially diluted to yield 10-times concentrated working solutions. Membrane fractions at equivalents of 100 µg protein were incubated in duplicates with [^{3}H]-labeled ligand for 120 min at room temperature (RT) in presence or absence of unlabeled NLX (10 µM) to determine unspecific binding. Free ligands were separated from the membrane fraction by rapid vacuum filtration through Whatman GF/B glass fiber filters soaked in Tris buffer with polyethylenimine (0.1 % w/v), followed by 6 washes with cold *"HEM buffer"* at the respective pH. After overnight incubation of filters in scintillation fluid *"Optiphase HISAFE 3"* bound radioactivity was measured by liquid scintillation spectrometry at 69 % counting efficiency. Specific binding

expressed in counts per minute (cpm) was calculated by subtracting unspecific binding and transformed into fmol of bound radioligand per mg of total protein. Data were fit with nonlinear regression to "One site – specific binding" (paragraph 2.2.11.1). In the pH pre-incubation paradigm, in analogy to (Selley et al., 1993), HEK MOR-WT were incubated in *"extracellular solution"* at pH 7.4, 6.5 or 6.0 ,at 37°C for 20 minutes prior to preparation of membrane fractions. Subsequent [^{3}H]-DAMGO binding was performed in Tris buffer at pH 7.4 as described above. The pharmacological parameters K_d (as measure of affinity) and B_{max} (number of available binding sites) were extrapolated by nonlinear regression as described under "statistical analyses" (paragraph 2.2.11.1).

2.2.4.3 [^{35}S]-GTPγS binding assay

The [^{35}S]-GTPγS binding assay is used to measure G protein activation as reflected in the exchange of GDP for GTP. GTP is replaced by a high concentration of [^{35}S]-GTPγS in the assay solvent, leading to accumulation of [^{35}S]-GTPγS-bound G proteins in the membrane. The agonist dose-response protocol is used to detect changes in a ligands' potency to activate G-proteins (Strange, 2010). [^{35}S]-GTPγS saturation binding, performed with increasing doses of [^{35}S]-GTPγS in the presence of a fixed dose of receptor agonist, is used to measure the G-proteins' affinity towards the guanine nucleotide. [^{35}S]-GTPγS binding to membrane fractions of wildtype or transfected HEK 293 cells was performed as described in (Zollner et al., 2003) with modification. Membrane fractions were prepared as described above. Where stated, pertussis toxin (PTX) (100 ng/ml) and/or cholera toxin (CTX) (500 ng/ml) were added to the cell culture medium and incubated overnight (16 h) before preparation of membrane fractions. Radioactive concentrations were calculated based on the half-life of ^{35}S (87.4 days). In analogy to (Ludwig et al., 2003), 50 µg of membrane fractions in duplicates were incubated with GDP (30 µM), [^{35}S]-GTPγS (0.05 nM) for 90 min at 30°C in *"HEM G protein buffer*" at the indicated pH values. In exploratory experiments, the DTT concentration of the buffer was varied as indicated. Basal [^{35}S]-GTPγS binding was assessed in absence of MOR ligand, and unspecific [^{35}S]-GTPγS binding was assessed by adding unlabeled GTPγS (10 µM) in absence of opioid ligands. Fentanyl (0.1 pM – 100 µM) and NLX (1-100 µM) were applied where stated. Free labeled nucleotides were separated from the membrane fraction by rapid vacuum filtration through Whatman GF/B glass fiber filters, followed by 6 washes with ice-cold Tris buffer. After overnight incubation of filters in scintillation fluid *"Optiphase HISAFE 3"* bound

radioactivity was measured by liquid scintillation spectrometry at 69 % counting efficiency in cpm. Unspecific [^{35}S]-GTPγS binding was subtracted from raw data to yield specific binding. In dose-response experiments, binding curves were fit with nonlinear regression to obtain the EC_{50} and E_{max} of the curve as a measure of fentanyl efficacy and maximum effect on G protein activation, respectively.

2.2.5 Enzyme Immunoassays

2.2.5.1 cAMP EIA

cAMP-enzyme-immune-assay (EIA) was used to quantify fentanyl-induced inhibition of AC.

HEK MOR-WT or MOR-H297$^{6.52}$A cells were seeded into poly-L-lysine-coated 96-well plates the day prior to the experiment to yield 90-100 % confluency. Where stated, PTX (100 ng/ml) was added to the cell culture medium and incubated overnight (16 h) before experiments. On the day of the experiment, the medium was removed, 100 µl solution was added immediately and incubated for 20 min at RT. Co-treatment with isobutylmethylxanthine (IBMX, 2 mM) (to prevent cAMP degradation) and PGE_2 (1 µM) (K. A. Berg et al., 2007) (to stimulate cAMP production) were included in every well unless stated otherwise. Stimuli were diluted in *"extracellular solution"* at pH 7.4, 6.5 and 6.0. Fentanyl was added at various doses (1nM to 50 µM) or a fixed dose of fentanyl (10 µM) was combined with increasing doses of NLX (1 nM to 1 mM). After 20 min incubation at RT, cells were lyzed, and intracellular cAMP levels were detected with *"Amersham cAMP Biotrak Enzymeimmunoassay" (GE Healthcare).* Once lyzed, all samples were handled at the same pH, following the manufacturer's recommendations. cAMP levels were quantified at 450 nM with a spectrophotometer plate reader. Treatments were performed in duplicates or triplicates. Data were normalized by setting PGE_2-stimulated cAMP levels in absence of opioids as 100 % and a value of 0 as 0 % to control for differences in opioid-independent baselines. NLX and fentanyl dose-response curves were fit with nonlinear regression as described in paragraph 2.2.11.1.

2.2.5.2 MOR expression ELISA

Opioid receptor expression in HEK MOR-WT cells was verified with *"LSBio Mouse/Human/Rat OPRM1/ Mu Opioid Receptor Cell-based ELISA Kit"* (LSBio) according to the manufacturer's instructions. HEK 293 cells, either untransfected or stably transfected with MOR-WT, were seeded into 96-well plates and MOR expression was quantified via indirect immune labeling of MOR. GAPDH expression was quantified in matched wells and used for normalization.

2.2.6 Immunocytochemistry

Immunocytochemistry (ICC) is used to visualize expression and localization of proteins via immunodetection and labeling. Specificity of primary antibodies was confirmed by

staining of untransfected HEK 293 cells. Specificity of secondary antibodies was confirmed by omission of primary antibodies.

For immunofluorescence staining, cells were seeded and grown to 90-100% confluence on poly-L-lysin coated glass coverslips. Medium was aspirated and samples were fixed in 4% formaldehyde solution in PBS for 15 min at room temperature. The samples were then washed with ice cold PBS, followed by blocking of unspecific binding sites with 5% (w/v) normal goat serum, 0.3% (v/v) Triton™X-100 in PBS for one h at room temperature. Primary antibody (guinea pig anti-MOR-1, Chemicon AB1774) at a dilution of 1:1000 was allowed to bind overnight at 4°C. The following day, samples were washed with ice cold PBS to then be incubated with secondary antibody Alexa Fluor 488 (AF488) goat anti-guinea pig (Invitrogen A11073, Thermo Fisher Scientific) at a final dilution of 1:2000 for one h at room temperature in the dark. Specimen were again washed with ice cold PBS and mounted on glass slides with "Dako Fluorescent Mounting Medium". Images were acquired with a confocal microscope. Excitation wavelengths were 405 nm (Diode) and 488 nM (Argon laser), emission filters were beam splitter 490 nM, followed by long pass filter 420 nM (DAPI) or 505 nM (AF 488).

2.2.7 Immunoprecipitation

Immunoprecipitation (IP) is a method to isolate specific proteins from a heterogeneous solution such as whole cell lysates. An antibody is used to capture the protein of interest and attach it to an insoluble matrix. Subsequently, the complex of matrix, antibody and target are isolated by centrifugation, and the target is recovered and quantified.

Basal $G\alpha_i$ activation in intact cells was assessed with the *"$G\alpha_i$ Activation Assay Kit"* according to the manufacturer's instructions. HEK MOR-WT cells were cultured in 10 cm culture plates to confluency. One day before the experiment, PTX (100 ng/ml) was added to the cell culture medium and incubated overnight (16 h). On the day of the experiment, the cells were incubated with extracellular solution at pH 7.5, 6.5, or 6.0, for 20 min at room temperature, followed by cell lysis in *"assay/ lysis buffer"* with complete mini EDTA-free protease inhibitor cocktail. Protein concentration was determined in duplicates according to the Bradford method. Immunoprecipitation (IP) of $G\alpha_i$ -GTP was performed on 750 µg of total protein input with Anti-Active $G\alpha_i$ Mouse Monoclonal Antibody (cat. No. 26901, NewEast Biosciences) and protein G agarose resin for 1 h at 4°C, followed by washing steps and elution in SDS-PAGE sample buffer.

2.2.8 Sodium dodecyl sulfate-polyacrylamide gel electrophoresis (SDS-PAGE)

In SDS-PAGE, denatured proteins are subjected to electrophoresis in a polyacrylamide gel. Net negative charge is transferred to the proteins via SDS to induce migration in an electric field. Migration through the gel is slowed down in proportion to protein size by the small diameter of the gel's pores.

Immunoprecipitated and input lysate samples of 20 µg total protein each were subjected to electrophoresis in separate gels. Samples were stacked in 5% polyacrylamide gels at 40 V for 1 h and separated in 12% polyacrylamide gels at 120 V for approximately 2 hours.

2.2.9 Western Blot

Western blot is used to identify and quantify known proteins previously isolated by SDS-PAGE. The proteins are electrically transferred to membranes, and proteins of interest are quantified via antibody detection.

Proteins were transferred to nitrocellulose membranes via migration in an electric field. Membranes were blocked with blocking buffer (TBST [10 mM Tris base, 150 mM NaCl, 0.05 % (v/v) Tween20, pH 7.4] with 5 % (w/v) non-fat dry milk powder) for 1 h at room temperature and incubated with Anti-$G\alpha_i$ Mouse Monoclonal Antibody (cat. No. 26003, NewEast Biosciences, Malvern, USA) 1:500 in blocking buffer at 4°C overnight, followed by incubation with HRP-coupled Polyclonal Goat Anti-Mouse Immunoglobulin (Dako) 1:3000 in TBST for 1 h at room temperature. Membranes were incubated with ECL (GE healthcare, Solingen, Germany), and films (GE healthcare, Solingen, Germany) were exposed for variable times to both membranes in parallel. Resulting bands were quantified by densitometry with Image Lab 6.0 (Bio-Rad Laboratories), and the ratio of IP versus total input lysate band intensity was calculated to control for possible differences in $G\alpha_i$ levels and reduce variability of data between experiments. In pilot experiments, control samples of cells overexpressing $G\alpha_{i1}$ were used to verify the specificity of the quantified bands.

2.2.10 Data handling

Data are represented as means ± SEM (normally distributed data) or median with interquartile range (non-normally distributed data). Experimental layouts were by randomized block design to control for position effects on plates (cAMP assay) or filter apparatus (radioligand and [^{35}S]-GTPγS binding), or unequal sample processing time ($G\alpha_i$ activation assay). Data recording and analysis were not blinded due to obvious effects of pH on most assay baselines. Experimental group size was set to n = 6 for all experiments,

except for pilot experiments and ICC. In [^{35}S]-GTPγS binding experiments, datasets were excluded if applied agonists failed to induce binding in MOR-WT at pH 7.4. In cAMP enzyme-immune-assays, individual measurements were excluded from analysis if normalized values deviated from the overall mean by at least 2 standard deviations (SD). This procedure resulted in exclusion of 11 raw values in fentanyl, and 25 raw values in NLX dose-response curves. Per data point (pH and drug concentration), no more than 2 raw values out of 18 (6 experiments measured in triplicates) were excluded. In single-dose experiments, data were excluded from analysis if PGE_2-induced cAMP levels were outside the assay concentration range, causing a reduced n for MOR-WT and MOR-H297$^{6.52}$F. In $G\alpha_i$ activation assay, experiments were excluded from analysis if at least one band specific for $G\alpha_i$ was too weak for quantification. In all dose-response experiments, concentrations were transformed to log scale, so data could be fit to sigmoidal dose-response curves.

2.2.11 Statistical data analysis

GraphPad Prism5 (GraphPad, San Diego, USA) was used for all curve fitting, statistical analyses, and data graph generation.

2.2.11.1 Nonlinear regression

With nonlinear regression, acquired data are fit to theoretical models in order to derive parameters descriptive of the process analyzed.

In radioligand and [^{35}S]-GTPγS saturation binding, curves were fit to the equation "One site – specific binding"

$$y = Bmax * \frac{x}{Kd + x}$$

With Y = bound ligand in fmol / mg protein and x = concentration of ligand.

In agonist dose-response experiments of [^{35}S]-GTPγS binding and cAMP reduction, curves were either fit to the formula "Log agonist vs response (three parameters):

$$y = Bottom + \frac{Top - Bottom}{(1 + 10^{\log EC50 - x})}$$

With y = [^{35}S]-GTPγS bound or [cAMP], depending on the assay and x = [agonist]

In antagonist dose-response experiments on cAMP reduction, curves were either fit to the formula "Log antagonist vs response (three parameters):

$$y = Bottom + \frac{Top - Bottom}{(1 + 10^{\mathrm{x} - \log EC50})}$$

With y = [cAMP] and x = [antagonist]

2.2.11.2 Hypothesis testing

Hypothesis testing was performed on datasets with a minimum n of 5. Normal distribution of data was assessed using the Kolmogorov-Smirnov test. Bartlett's test was used to test for equal variances of data compared by ANOVA.

The pharmacological parameters and SEM derived from the fit curves were compared by one-way analysis of variance (ANOVA), or one-way ANOVA with Welch's correction if the SD varied significantly. Other data were compared by either one-way or two-way ANOVA. Dunnett's Multiple Comparison post-hoc test was used to compare all conditions to MOR-WT pH 7.4 if the preceding one- or two-way ANOVA revealed a significant

difference. Tukey's Multiple Comparison post-hoc Test was used to compare MOR expression levels amongst all pairs of cell types. *P* values ≤ 0.05 were considered significant and are represented as * or in respective figures and tables.

Non-normally distributed data were analyzed by Kruskal-Wallis Test (independent observations) or Friedman test (dependent observations), followed by Dunn's post hoc test if initial P values were ≤ 0.05.

2.2.12 Protein sequence alignment

Proteins can be compared by aligning amino acid sequences based on structural or functional similarity of sequences and predicted or known secondary structures. In addition to labeling individual residues by amino acid one letter code and position number in the peptide (starting at the amino terminus), the Ballesteros-Weinstein numbering scheme (Ballesteros & Weinstein, 1995) is often used for class A GPCRs.

Protein sequences of known proton-sensing GPCRs (human OGR1, GPR4, TDAG8, G2A, β2-AR, Rhodopsin) were aligned with MOR protein sequences (human, rat) using the freely available alignment program Clustal Omega (Sievers et al., 2011) via the UniProt knowledgebase (UniProt Consortium, 2018) to identify topologically conserved residues in MOR known to mediate proton-sensing in other class A GPCRs.

2.2.13 Molecular graphics

Molecular graphics were created with UCSF Chimera (Pettersen et al., 2004) (Resource for Biocomputing, Visualization, and Informatics at the University of California, San Francisco) using structural information deposited in the Protein Data Bank (www.rcsb.org) (Berman et al., 2000).

2.2.14 Databases

GPCR database	https://gpcrdb.org/ (Pandy-Szekeres et al., 2018)
PubMed	https://www.ncbi.nlm.nih.gov/pubmed NCBI
Protein Data Base	https://www.rcsb.org/ (Berman et al., 2000)
UniProt	https://www.uniprot.org/ (UniProt Consortium, 2018)

3 Results

3.1 Establishing the experimental conditions

3.1.1 Generation of stable cell lines

HEK 293 cells were previously reported to express no endogenous MOR mRNA (Atwood, Lopez, Wager-Miller, Mackie, & Straiker, 2011). Pilot qPCR experiments (n = 2) revealed no MOR mRNA and sub-threshold levels of DOR and KOR mRNA in untransfected HEK 293 cells (Table 3-1).

Table 3-1. Endogenous opioid receptor mRNA expression in HEK 293 cells

Target	Mean CT	Δ CT
GAPDH	18,2	0
MOR	--	--
DOR	30,8	12,6
KOR	32,0	13,8

HEK 293 cells stably expressing the rat MOR-WT and rat MOR-H297$^{6.52}$A had been generated and tested in our group earlier. I qualitatively verified MOR protein expression via immunocytochemistry. Cell lines stably transfected with MOR-WT or mutants displayed stronger labelling by an antibody directed against MOR-1 than untransfected HEK 293 cells (Figure 6).

Figure 6. Immunofluorescence staining of MOR (green) with Hoechst staining of nuclei (blue) in HEK MOR-WT, HEK MOR-H297A, or untransfected HEK 293 cells.

In addition, I generated a cell line stably expressing MOR-H297$^{6.52}$F. Prior to transfection, the appropriate antibiotic dose for selection of stably transfected cells was determined via G418 dose-response curves on untransfected HEK 293 cells (Figure 7). After 10 days cultivation in presence of G418, the estimated confluence was ≤ 5% at concentrations of ≥ 500 µg/ml.

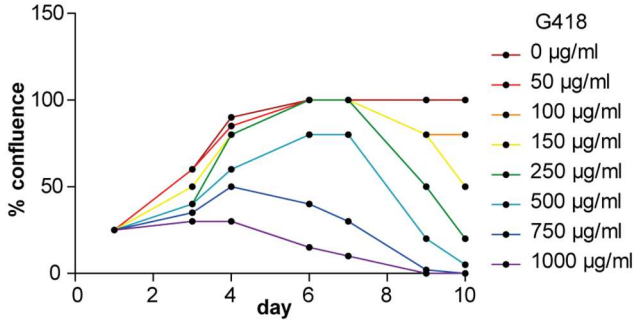

Figure 7. G418 dose-response curve. Estimated confluence of untransfected HEK 293 cells cultivated in the presence of G418 as indicated.

After stable transfection, MOR-H297$^{6.52}$F expression in monoclonal cultures was checked at the mRNA level via RT-PCR (Figure 8 A and B) and at the protein level by immunocytochemistry (Figure 8 C). Clone A2 was chosen for further experiments, since it showed clear membrane expression and MOR protein levels similar to the MOR-WT cell line.

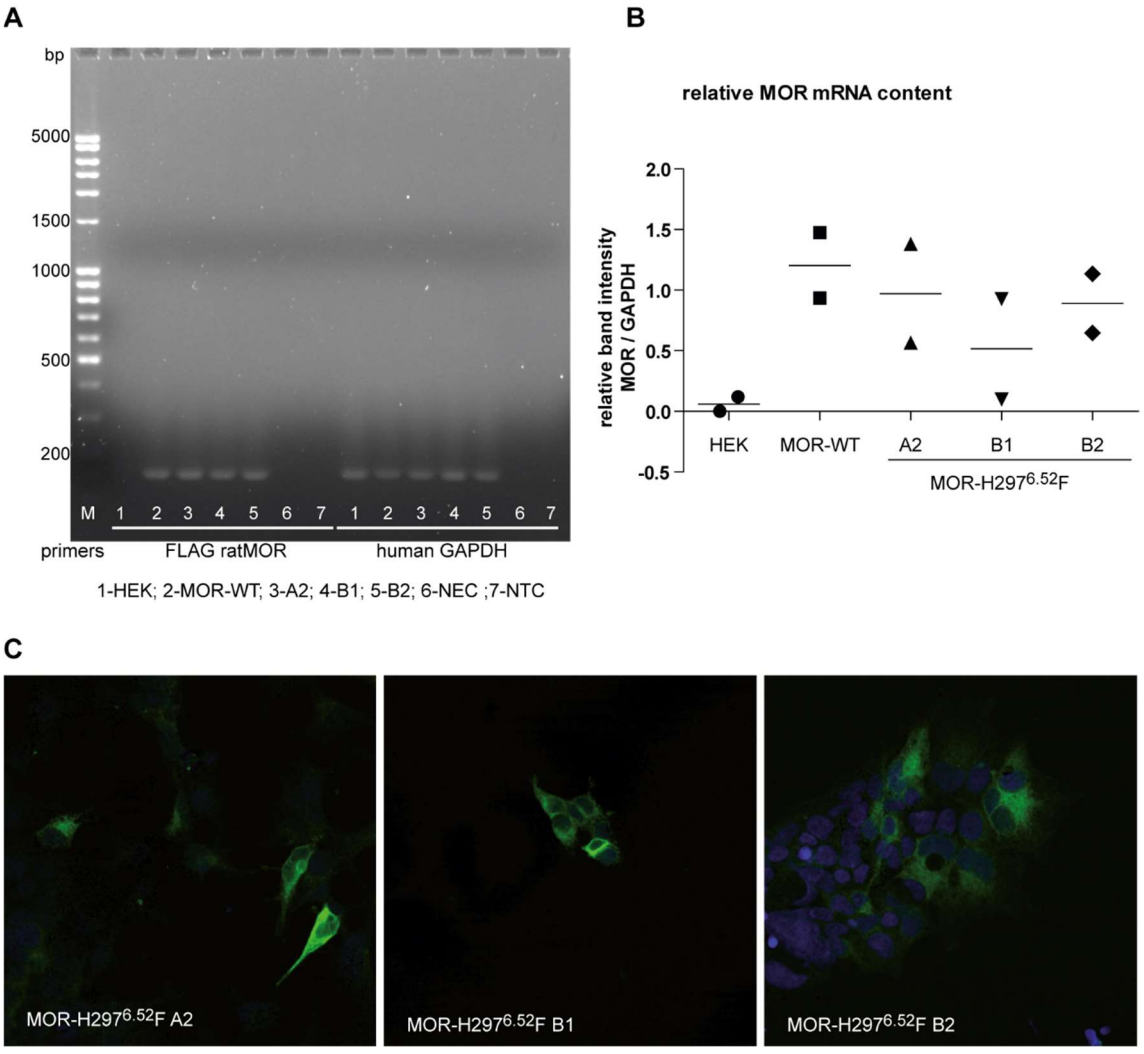

*Figure 8. Selection of monoclonal colony of stably transfected MOR-H297F cells. (**A**) Gelelectrophoresis of PCR products. The image represents one out of two experiments. (**B**) Relative MOR mRNA levels by cell line, n = 2. (**C**) Immunostainings of MOR (green) with Hoechst staining of nuclei (blue) in monoclonal colonies of MOR-H297$^{6.52}$F cells.*

MOR-H297$^{6.52}$A and MOR-H297$^{6.52}$F were both expressed in the plasma membrane of the transfected HEK 293 cells (Figure 9).

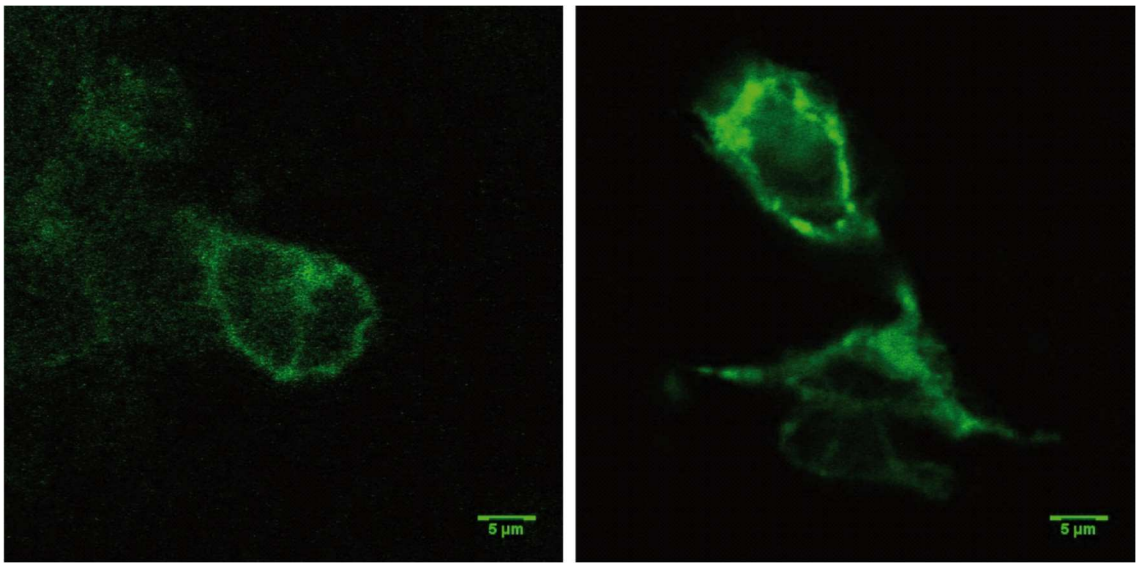

Figure 9. cross section of stably transfected MOR-H297$^{6.52}$A (left) and MOR-H297$^{6.52}$F (right).

Assessment of MOR protein expression by ELISA showed no significant differences, and results for all cell lines except MOR-WT showed a high degree of variability (Figure 10).

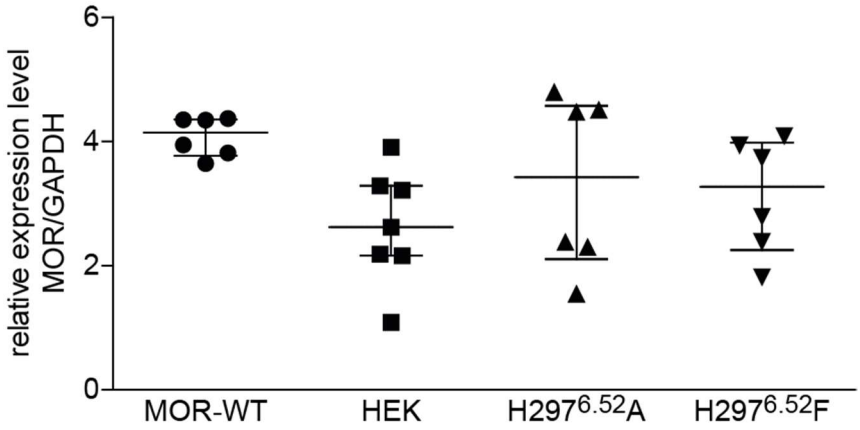

Figure 10. MOR protein expression levels in untransfected and stably transfected HEK 293 cells. No significant differences were found, Kruskal-Wallis test, n = 6.

3.1.2 Buffer optimization

Radioligand and [^{35}S]-GTPγS binding experiments to study MOR are commonly performed in Tris buffers (Pert, Pasternak, & Snyder, 1973; Zollner et al., 2003). In studies of proton-sensing GPCRs, a buffer combining HEPES, EPPS and MES ("HEM buffer") is used to extend the buffered pH range (J. Q. Wang et al., 2004). [^{3}H]-NLX saturation binding and fentanyl-induced [^{35}S]-GTPγS binding to MOR-WT yielded comparable results in HEM and Tris buffers at pH 7.4 (Figure 11 A and B).

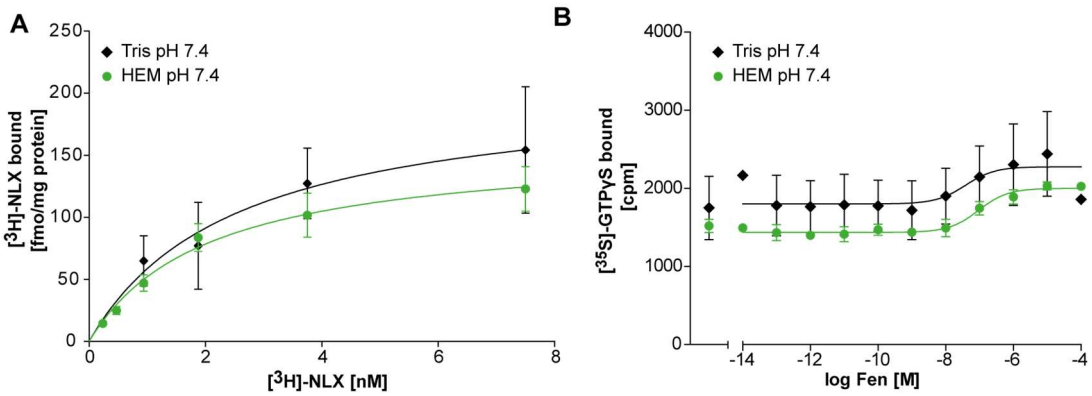

*Figure 11. Assay buffer comparison. (**A**) [^{3}H]-NLX saturation binding and (**B**) fentanyl-induced [^{35}S]-GTPγS binding at pH 7.4 in Tris and HEM buffer each. HEM data in A are duplicates of data depicted in Figure 10 A. No statistical comparisons were performed due to the low sample size of pilot studies (n = 2-3). [^{3}H]-NLX binding data in HEM buffer are duplicates of the data depicted and analyzed in Figure 13. Derived parameters are provided in Tables S1 and S2 of the appendix.*

3.2 MOR stability at acidic pH

In analogy to Selley et al. (1993), the effects of low pH pre-incubation of intact HEK MOR-WT cells at acidic pH had previously been tested in our group. Cell were incubated for 20 min at physiological or acidic pH, followed by preparation of membrane fractions and radioligand or [^{35}S]-GTPγS binding at pH 7.4. Low pH pre-treatment did not alter [^{3}H]-DAMGO binding (Figure 12A), DAMGO-induced [^{35}S]-GTPγS binding (Figure 12B), fentanyl-induced [^{35}S]-GTPγS binding (Figure 12C) or fentanyl-induced [^{35}S]-GTPγS saturation binding (Figure 12D).

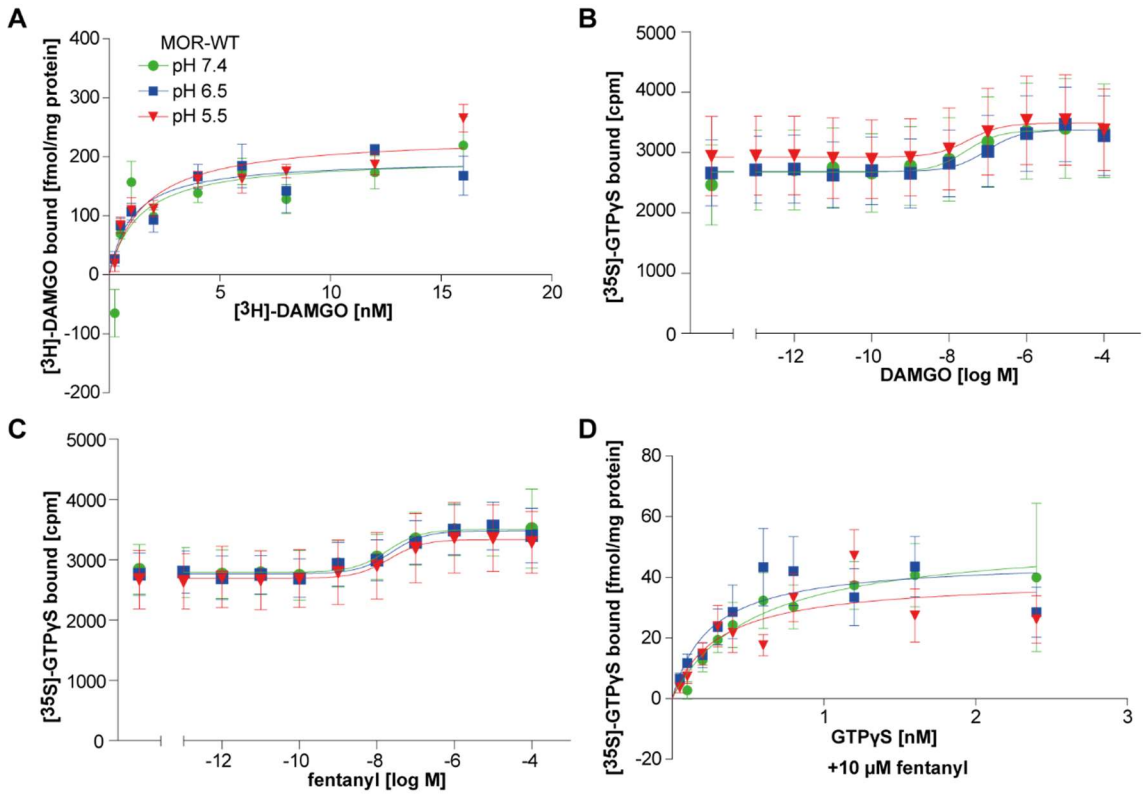

*Figure 12. MOR function at pH 7.4 after pre-incubation at physiological or acidic pH assessed via (**A**) [^{3}H]-DAMGO saturation binding. (**B**) DAMGO-induced [^{35}S]-GTPγS binding. (**C**) fentanyl-induced [^{35}S]-GTPγS binding. (**D**) [^{35}S]-GTPγS saturation binding in constant presence of 10 µM fentanyl. Derived parameters are provided in Table S3 of the appendix.*

3.3 MOR ligand binding at acidic pH

3.3.1 NLX binding – dependence on pH and H297$^{6.52}$

To assess whether binding of [^{3}H]-NLX to MOR-WT is pH-dependent, I performed saturation binding experiments at physiological and acidic pH values. Compared to pH 7.4, pH 6.5 significantly reduced the number of [^{3}H]-NLX binding sites (B_{max}) at MOR-WT. The affinity (K_d) was not different between pH 7.4 and 6.5. At pH 6.0, [^{3}H]-NLX binding

was abolished. (Figure 13 A). To test whether NLX binding depends on H297$^{6.52}$, I performed [^{3}H]-NLX saturation binding experiments on membranes expressing MOR-H297$^{6.52}$A or H297$^{6.52}$F at pH 7.4. Almost no specific binding was detected at either of the two mutant receptors (Figure 13 B).

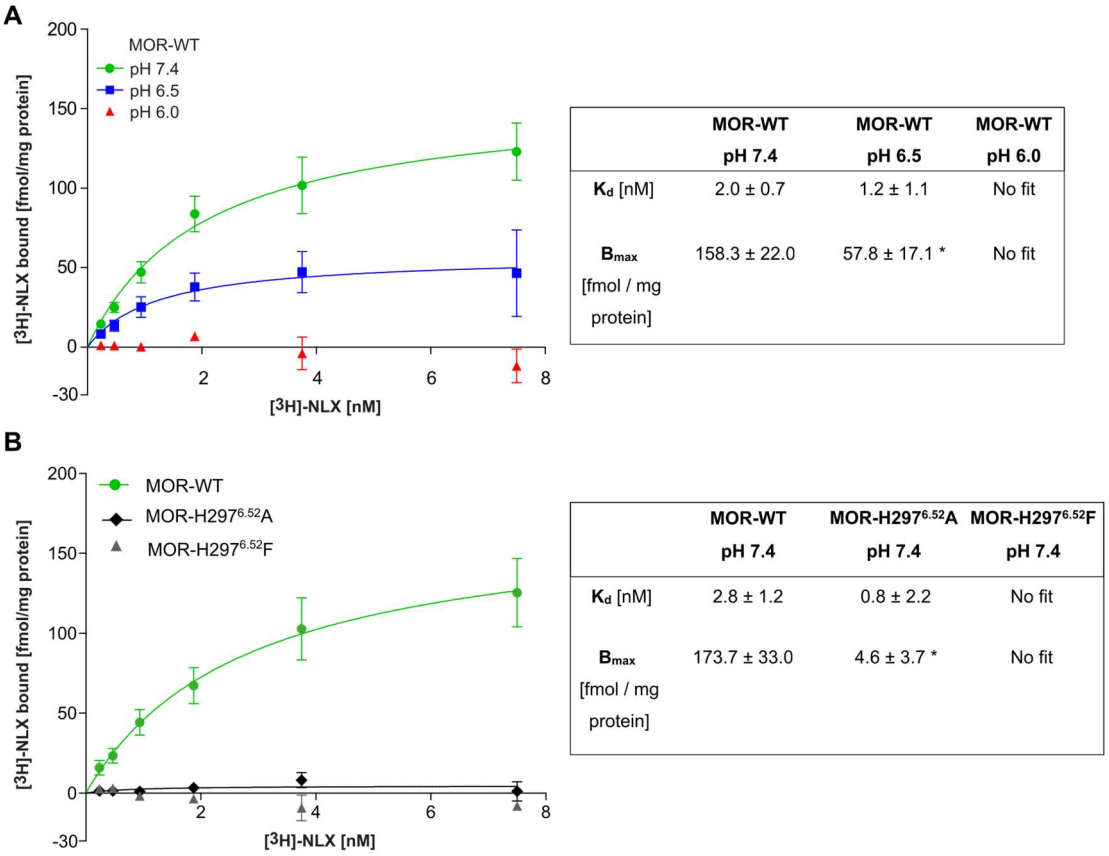

	MOR-WT pH 7.4	MOR-WT pH 6.5	MOR-WT pH 6.0
K_d [nM]	2.0 ± 0.7	1.2 ± 1.1	No fit
B_{max} [fmol / mg protein]	158.3 ± 22.0	57.8 ± 17.1 *	No fit

	MOR-WT pH 7.4	MOR-H297$^{6.52}$A pH 7.4	MOR-H297$^{6.52}$F pH 7.4
K_d [nM]	2.8 ± 1.2	0.8 ± 2.2	No fit
B_{max} [fmol / mg protein]	173.7 ± 33.0	4.6 ± 3.7 *	No fit

*Figure 13. [^{3}H]-NLX saturation binding (**A**) to MOR-WT at pH 7.4, 6.5 and 6.0, and (**B**) to MOR-H297$^{6.52}$A, MOR-H297$^{6.52}$F and MOR-WT at pH 7.4. MOR-WT was included in every experiment. * P < 0.05, K_d and B_{max} were compared by unpaired t-test for each experiment separately, n = 6 per experiment.*

Previous pilot experiments with [^{3}H]-fentanyl had revealed high levels of unspecific binding that prevented data analysis. To qualitatively demonstrate fentanyl binding to MOR H297$^{6.52}$A, I performed single-dose competition binding experiments with fentanyl (10 µM) and a high dose of [^{3}H]-NLX (50 nM). [^{3}H]-NLX binding showed high variability but was suppressed by fentanyl in both MOR-WT and MOR- H297$^{6.52}$A (Figure 14).

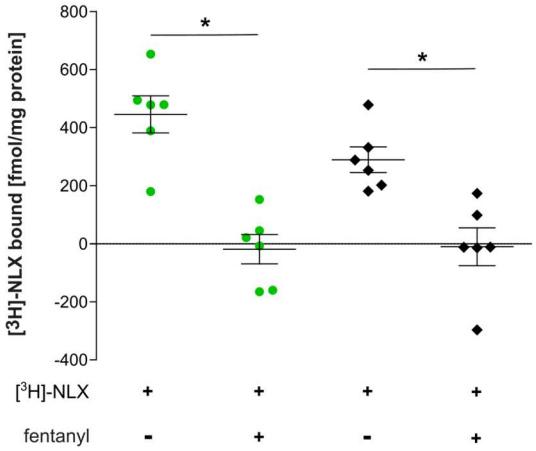

*Figure 14. Single-dose [^{3}H]-NLX competition binding with fentanyl (50 nM) at pH 7.4. * P < 0.05, Kruskal-Wallis Test with Dunn's Multiple Comparison Test, n = 6.*

3.3.2 DAMGO binding – dependence on pH and H297$^{6.52}$

Next, I assessed binding of the MOR peptide agonist DAMGO, which has been demonstrated to form a water-mediated hydrogen bond with H297$^{6.52}$ via a carboxy-terminal hydroxyl group (Koehl et al., 2018). [^{3}H]-DAMGO binding was abolished at pH 6.0. At pH 6.5, [^{3}H]-DAMGO binding showed a tendency towards reduction that was statistically not significant. The K_d was not different between pH 7.4 and 6.5, and could not be obtained at pH 6.0 due to the lack of dose-dependent binding (Figure 15 A, C). MOR-H297$^{6.52}$A did not display specific [^{3}H]-DAMGO binding at pH 7.4 (Figure 15 B).

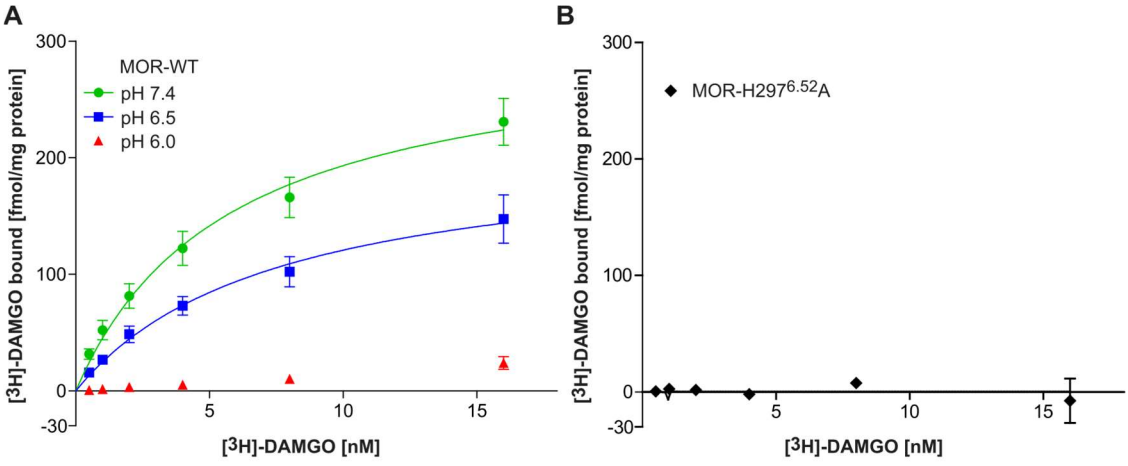

C

	MOR-WT pH 7.4	MOR-WT pH 6.5	MOR-WT pH 6.0	MOR-H297$^{6.52}$A pH 7.4
K_d [nM]	5.7 ± 1.4	7.5 ± 2.5	No fit	No fit
B_{max} [fmol/ mg protein]	304.1 ± 32.6	211.5 ± 33.6	No fit	No fit

*Figure 15. [^{3}H]-DAMGO binding to (**A**) MOR-WT at pH 7.4, 6.5 and 6.0, and (**B**) MOR-H297$^{6.52}$A. (**C**) Pharmacological parameters derived from data depicted in A and B. K_d and B_{max} were each compared by unpaired t-test, no significant differences were found, n = 6 per experiment.*

3.4 G-protein activation at acidic pH

3.4.1 Opioid-independent [^{35}S]-GTPγS binding at acidic pH

Next, I investigated effects of acidic pH and mutation H297$^{6.52}$A on opioid-induced G-protein activation. Acidic pH *per se* enhanced baseline [^{35}S]-GTPγS binding in the absence of opioids both in presence and absence of DTT, ruling out a loss of DTT reactivity as cause (Figure 16 A). Unspecific [^{35}S]-GTPγS binding was independent of acidic pH, and omission of DTT increased the variability in unspecific [^{35}S]-GTPγS binding (Figure 16 B). To examine the identity of opioid-independent [^{35}S]-GTPγS binding sites at each pH, I treated HEK MOR-WT overnight with pertussis toxin (PTX, 100 ng/ml), cholera toxin (CTX, 500 ng/ml), or both. Blocking of $G_{\alpha i}$ subunits alone (PTX) or in combination with $G_{\alpha s}$ (PTX/CTX) abolished the pH-dependent increase in basal [^{35}S]-GTPγS binding, while blocking $G_{\alpha s}$ alone (CTX) did not (Figure 16 C).

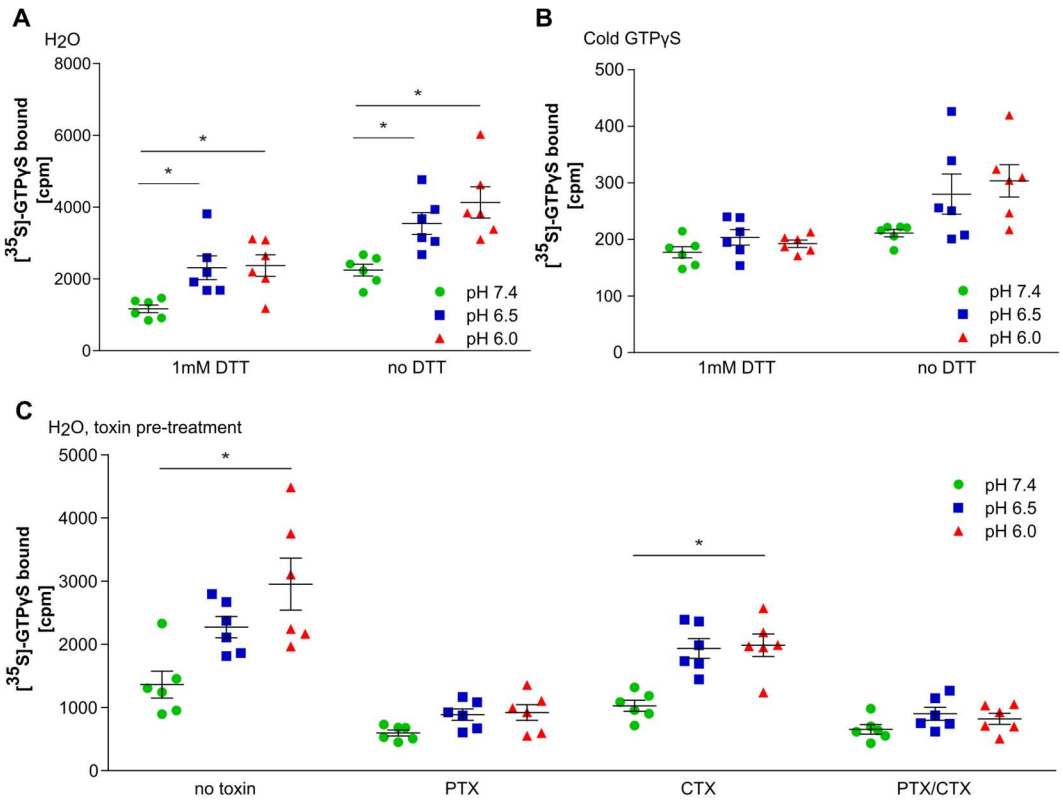

*Figure 16. (**A**) basal [^{35}S]-GTPγS binding in presence or absence of 1 mM DTT. n = 6 per condition, two-way ANOVA with Bonferroni post-hoc tests (within treatment groups), * P < 0.05 (**B**) unspecific [^{35}S]-GTPγS binding in presence of unlabeled ("cold") GTPγS and in presence or absence of DTT. n = 6 per condition, Bartlett's test for unequal variances yielded significant differences for "no DTT". Kruskal-Wallis test yielded no significant differences within treatment groups. (**C**) Basal [^{35}S]-GTPγS binding to MOR-WT, pre-treated (overnight) or not with pertussis toxin (PTX), cholera toxin (CTX), or both (PTX/CTX). n = 6 per condition. one-way ANOVA with Welch's correction for unequal SD with Dunnett's T3 multiple comparison post-hoc test (pH 7.4 vs. pH 6.0 within treatment groups, * P < 0.05). Data in all graphs represent specific [^{35}S]-GTPγS binding in cpm by experiment (dots) with mean ± SEM (line and bars).*

To examine whether acidic extracellular pH affects the activity of intracellular G_i-proteins, I incubated HEK MOR-WT for 20 min at pH 7.4, 6.5 or 6.0, followed by cell lysis and immunoprecipitation of $G\alpha_i$-GTP. Low extracellular pH did not alter basal $G\alpha_i$ activity, and overnight PTX treatment had no effect on the levels of $G\alpha_i$-GTP. Likewise, 20 min incubation with 10 µM fentanyl did not change the apparent quantity of $G\alpha_i$-GTP. Incubation of the input lysate with either GTPγS (to induce the active conformation of G-proteins) or GDP (to induce the inactive conformation of G-proteins) resulted in equal amounts of immunoprecipitated $G\alpha_i$-GTP (Figure 17).

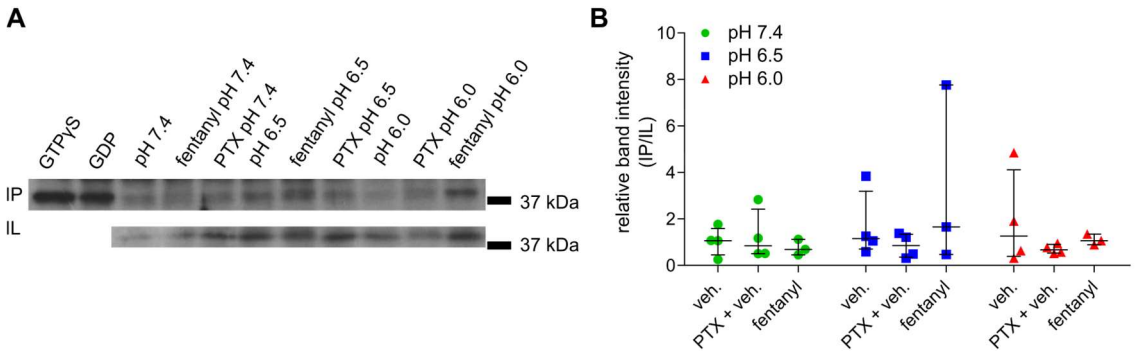

*Figure 17. Immunoprecipitation of active Gαi-GTP. (**A**) representative immunoblot showing immunoprecipitated Gαi-GTP (IP) and total Gαi from input lysate (IL). (**B**) relative band intensities in immunoblots (IP/IL). veh. = ECS buffer*

3.4.2 MOR constitutive activity

Next, I assessed whether acidic pH enhances constitutive MOR activity. NLX at various doses did not antagonize the pH-dependent increase in baseline [^{35}S]-GTPγS binding (Figure 18 A). Baseline [^{35}S]-GTPγS binding appeared comparable between MOR-WT and untransfected HEK 293 cells (Figure 18 B).

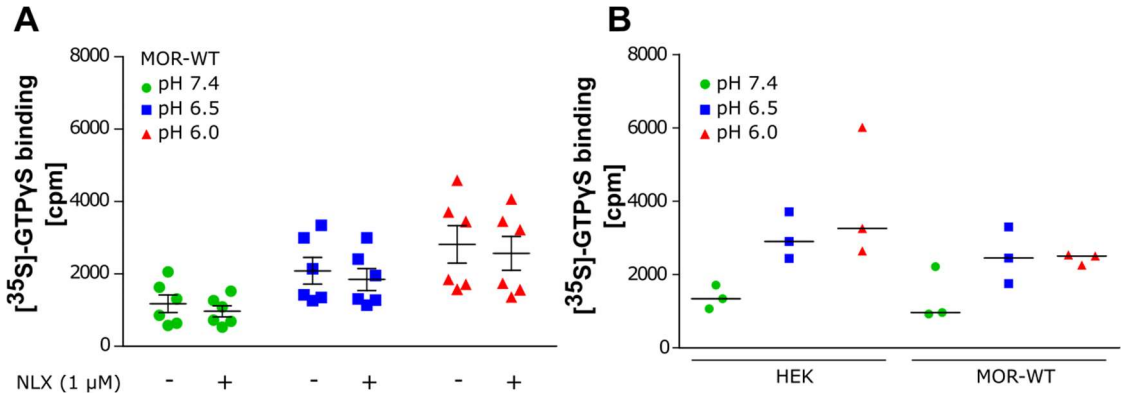

*Figure 18. Agonist-free [^{35}S]-GTPγS binding. (**A**) [^{35}S]-GTPγS binding to MOR-WT, in absence and presence of 1 μM NLX. Data represent specific [^{35}S]-GTPγS binding in cpm by experiment (dots) with median and interquartile range (lines and bars) of [^{35}S]-GTPγS bound in % of pH 7.4 (without NLX). n = 6 per condition, Friedman test with Dunn's Multiple Comparison Test yielded no significant effects of NLX treatment. (**B**) Basal [^{35}S]-GTPγS binding at pH 7.4, 6.5 and 6.0 in membrane fractions of untransfected ("HEK") and HEK MOR-WT cells in absence of opioid ligands. Data represent specific [^{35}S]-GTPγS bound in cpm by experiment (dots) with mean (lines), n = 3 per condition.*

3.4.3 Fentanyl-induced G-protein activation– dependence on pH and H297$^{6.52}$

I then assessed the effects of acidic pH on fentanyl-induced [^{35}S]-GTPγS binding. EC_{50} values and maximum [^{35}S]-GTPγS binding induced by fentanyl did not differ between pH 7.4, 6.5 and 6.0 (Figure 19 A). In membranes expressing MOR-H297$^{6.52}$A, fentanyl induced dose-dependent [^{35}S]-GTPγS binding. Neither EC_{50} nor E_{max} of the dose-response curves were altered by pH (Figure 19 B). [^{35}S]-GTPγS binding data for MOR-H297$^{6.52}$A displayed a higher variability than for MOR-WT; Bartlett's test revealed unequal SD between, but not within the respective groups.

Fentanyl elicited no dose-dependent increase in [^{35}S]-GTPγS binding in cells transfected with MOR-H297$^{6.52}$F (Figure 19 C).

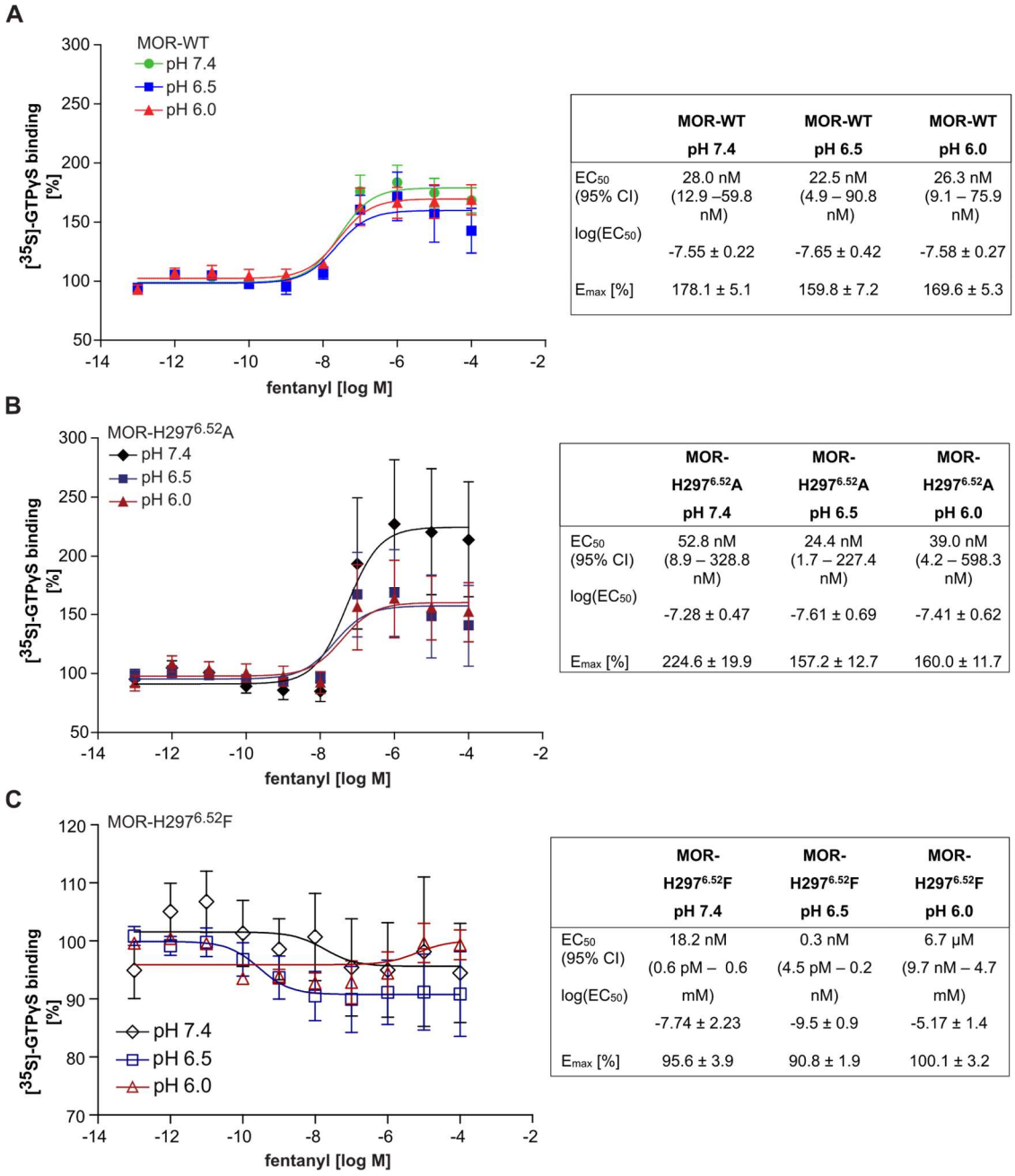

	MOR-WT pH 7.4	MOR-WT pH 6.5	MOR-WT pH 6.0
EC_{50} (95% CI)	28.0 nM (12.9 –59.8 nM)	22.5 nM (4.9 – 90.8 nM)	26.3 nM (9.1 – 75.9 nM)
log(EC_{50})	-7.55 ± 0.22	-7.65 ± 0.42	-7.58 ± 0.27
E_{max} [%]	178.1 ± 5.1	159.8 ± 7.2	169.6 ± 5.3

	MOR-H297$^{6.52}$A pH 7.4	MOR-H297$^{6.52}$A pH 6.5	MOR-H297$^{6.52}$A pH 6.0
EC_{50} (95% CI)	52.8 nM (8.9 – 328.8 nM)	24.4 nM (1.7 – 227.4 nM)	39.0 nM (4.2 – 598.3 nM)
log(EC_{50})	-7.28 ± 0.47	-7.61 ± 0.69	-7.41 ± 0.62
E_{max} [%]	224.6 ± 19.9	157.2 ± 12.7	160.0 ± 11.7

	MOR-H297$^{6.52}$F pH 7.4	MOR-H297$^{6.52}$F pH 6.5	MOR-H297$^{6.52}$F pH 6.0
EC_{50} (95% CI)	18.2 nM (0.6 pM – 0.6 mM)	0.3 nM (4.5 pM – 0.2 nM)	6.7 µM (9.7 nM – 4.7 mM)
log(EC_{50})	-7.74 ± 2.23	-9.5 ± 0.9	-5.17 ± 1.4
E_{max} [%]	95.6 ± 3.9	90.8 ± 1.9	100.1 ± 3.2

*Figure 19. Fentanyl-induced [^{35}S]-GTPγS binding curves with derived parameters at (**A**) MOR-WT, (**B**) MOR-H297$^{6.52}$A. Data represent mean ± SEM of specific [^{35}S]-GTPγS binding in cpm with nonlinear fit. n = 6 per experiment. log (EC_{50}) were compared by one-way ANOVA. E_{max} values were compared by one-way ANOVA with Welch's correction for unequal SD, followed by Dunnett's T3 multiple comparison post-hoc test. No significant differences were found. (**C**) Fentanyl-induced [^{35}S]-GTPγS binding curves with derived parameters at MOR-H297$^{6.52}$F. Experiments were halted after n = 4 because no dose-dependent [^{35}S]-GTPγS binding was observed. No statistics were calculated.*

3.4.4 DAMGO-induced G-protein activation: dependence on pH and H297$^{6.52}$

[^{35}S]-GTPγS binding experiments were then performed with increasing doses of DAMGO at different pH values. At pH 6.5 and 6.0, maximum DAMGO-induced [^{35}S]-GTPγS

binding (E_{max}) was significantly reduced compared to pH 7.4, while the $logEC_{50}$ was not altered. In membranes expressing MOR-H297$^{6.52}$A, the $logEC_{50}$ was markedly shifted rightward irrespective of pH (i.e. to higher DAMGO concentrations), and reliable estimates of the E_{max} could not be obtained.

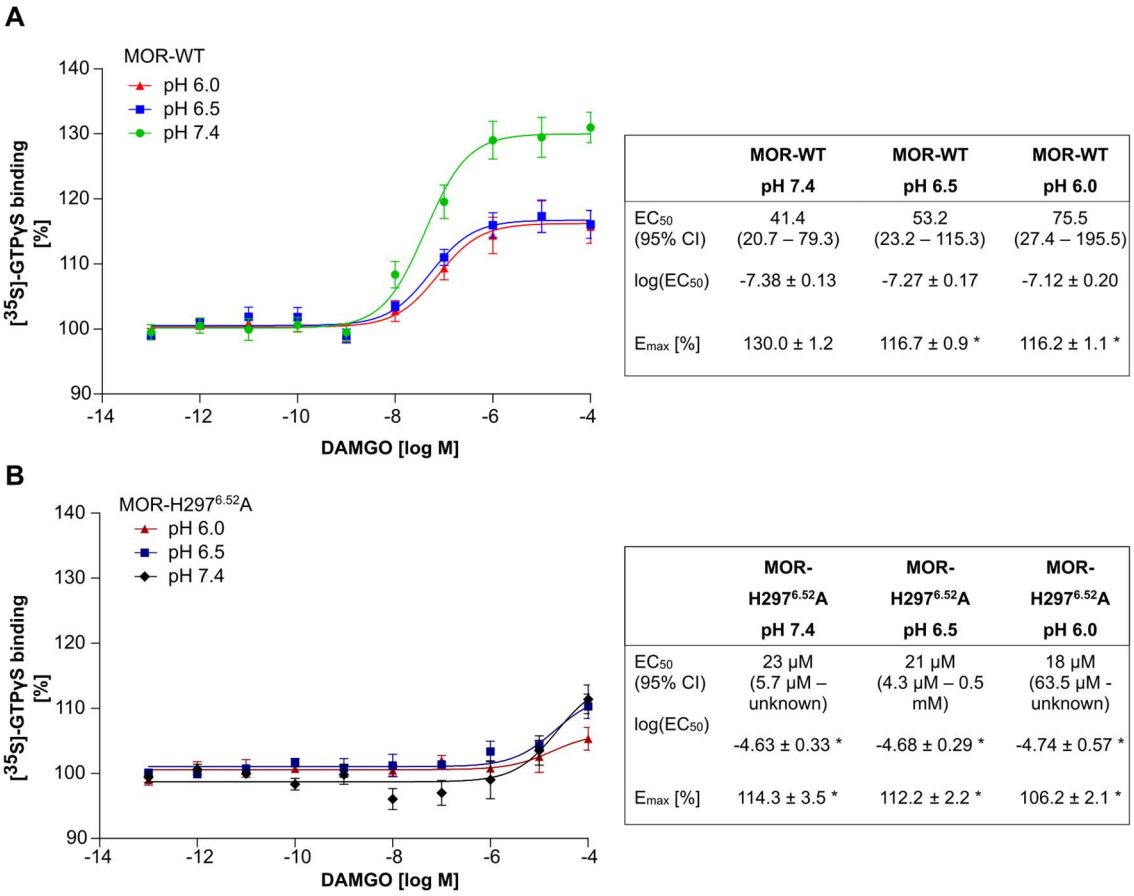

	MOR-WT pH 7.4	MOR-WT pH 6.5	MOR-WT pH 6.0
EC_{50} (95% CI)	41.4 (20.7 – 79.3)	53.2 (23.2 – 115.3)	75.5 (27.4 – 195.5)
log(EC_{50})	-7.38 ± 0.13	-7.27 ± 0.17	-7.12 ± 0.20
E_{max} [%]	130.0 ± 1.2	116.7 ± 0.9 *	116.2 ± 1.1 *

	MOR-H297$^{6.52}$A pH 7.4	MOR-H297$^{6.52}$A pH 6.5	MOR-H297$^{6.52}$A pH 6.0
EC_{50} (95% CI)	23 µM (5.7 µM – unknown)	21 µM (4.3 µM – 0.5 mM)	18 µM (63.5 µM - unknown)
log(EC_{50})	-4.63 ± 0.33 *	-4.68 ± 0.29 *	-4.74 ± 0.57 *
E_{max} [%]	114.3 ± 3.5 *	112.2 ± 2.2 *	106.2 ± 2.1 *

*Figure 20. DAMGO-induced [^{35}S]-GTPγS binding in cells stably transfected with MOR-WT (**A**) and MOR-H297$^{6.52}$A(**B**). log (EC_{50}) values were compared by one-way ANOVA with Dunnet's multiple comparison post-hoc test, control group = MOR-WT pH 7.4. E_{max} values were compared by one-way ANOVA with Welch's correction for unequal SD, followed by Dunnett's T3 multiple comparison post-hoc test. All comparisons were performed within agonist groups, * P < 0.05, n = 6 per experiment.*

3.5 Opioid and pH modulation of cAMP levels

3.5.1 Opioid modulation of cAMP levels

Finally, I investigated the effects of acidic pH and mutation H297$^{6.52}$A on opioid modulation of cAMP levels. In MOR-WT and MOR-H297$^{6.52}$A cells, NLX (10 mM) by itself did not alter PGE_2-induced cAMP levels in either MOR-WT or MOR-H297$^{6.52}$A, regardless of pH (Figure 21 A and B). In MOR-H297$^{6.52}$F, PGE_2 elicited exaggerated cAMP accumulation compared to MOR-WT and MOR-H297$^{6.52}$A (Figure 21 C). The use of this cell line was discontinued.

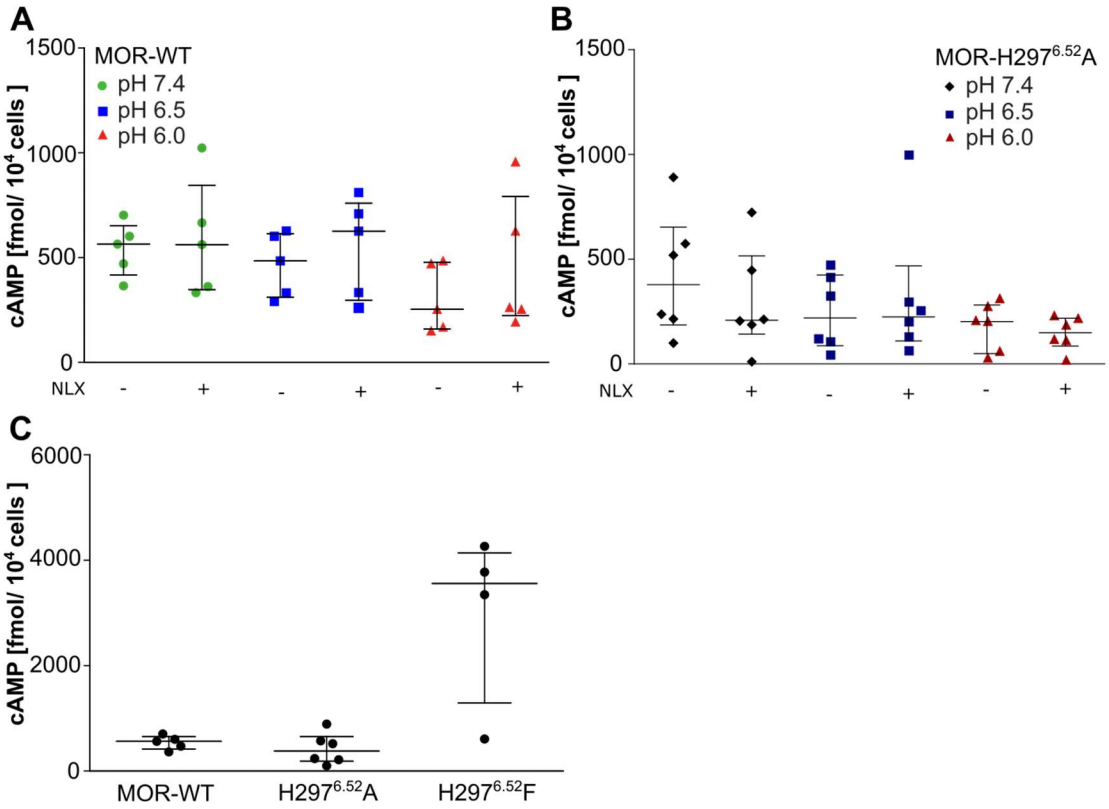

*Figure 21. PGE_2-stimulated cAMP levels. PGE_2-stimulated cAMP levels in absence and presence of NLX (1 mM) in (**A**) HEK MOR-WT and (**B**) HEK MOR-H297$^{6.52}$A. Mean values by cell type were compared by Kruskal-Wallis test with Dunn's multiple comparison post-hoc tests, no significant differences were found. (**C**) PGE_2-stimulated cAMP levels in HEK MOR-WT, MOR- H297$^{6.52}$A and MOR-H297$^{6.52}$F cells. Data represent cAMP levels by experiment (dots) with median and interquartile range (line and bars). MOR-WT, n = 5; MOR-H297$^{6.52}$A n = 6; MOR-H297$^{6.52}$F, n = 4.*

Fentanyl induced dose-dependent cAMP reduction that was not altered by pH. In MOR-H297$^{6.52}$A, fentanyl elicited dose-dependent cAMP reduction that was reduced compared to MOR-WT, both with regard to the IC_{50} and the maximum observed inhibition (Figure 22 A).

NLX antagonism of fentanyl-induced cAMP reduction in MOR-WT was impaired by low pH (Figure 22 B). A strong baseline effect at pH 6.0 on PGE_2-stimulated cAMP levels resulted in an apparent reversal of the pH effect when considering only the normalized data. Due to the significant pH effect on PGE_2-stimulated cAMP levels, the data obtained at pH 6.0 were excluded from analysis.

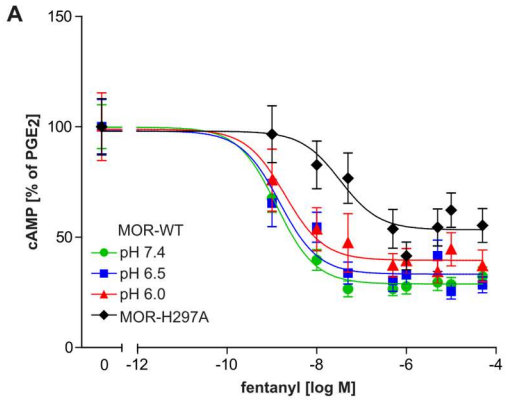

	MOR-WT pH 7.4	MOR-WT pH 6.5	MOR-WT pH 6.0	MOR-H297$^{6.52}$A pH 7.4
IC_{50} [nM] (95% CI)	1.3 (0.7-2.4)	1.4 (0.5-4.0)	1.8 (0.4-8.6)	33.4 (5.6- 198.6)
log(IC_{50})	-8.90 ± 0.14	-8.71 ± 0.33	-8.74 ± 0.34	-7.48 ± 0.40 *
Bottom [%]	28.8 ± 2.1	33.2 ± 2.9	39.5 ± 4.0	53.3 ± 4.7 *

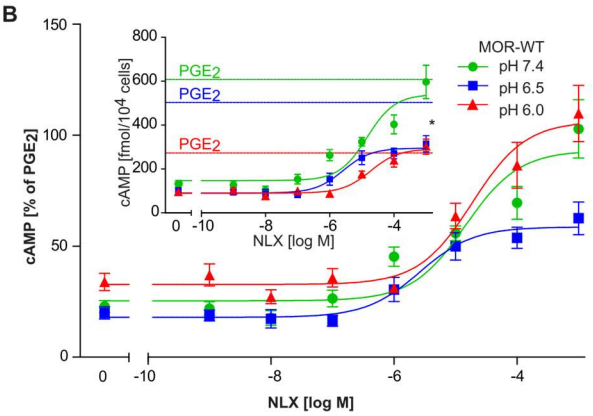

	MOR-WT pH 7.4	MOR-WT pH 6.5	MOR-WT pH 6.0
IC_{50} [µM] (95% CI)	14.4 (5.8 - 35.9)	2.6 (0.9 - 7.7)	18.7 (7.6 - 45.6)
log(IC_{50})	-4.84 ± 0.20	-5.58 ± 0.25 *	-4.73 ± 0.20
Top [%]	93.1 ± 5.7	58.7 ± 3.4 *	106.3 ± 6.3

*Figure 22. Opioid modulation of cAMP levels, dose-response curves. (**A**) Fentanyl-induced cAMP reduction in HEK MOR-WT and in HEK MOR-H297$^{6.52}$A. Data represent mean ± SEM of cAMP accumulation in % of the values obtained with PGE_2 alone at the respective pH, and nonlinear fit; n = 6 per curve. (**B**) NLX antagonism of fentanyl-induced cAMP inhibition in HEK MOR-WT. Data represent mean ± SEM in % of PGE_2-induced baselines at the respective pH (inset: same data before normalization in fmol/10^4 cells with PGE_2-stimulated baselines) with nonlinear fit; n = 6 per curve.*

3.5.2 Opioid-independent cAMP levels at acidic pH

Since pH-dependent alterations of assay baselines in cAMP EIA impeded data interpretation, I enquired into the underlying mechanisms. cAMP levels declined with pH, regardless whether the AC was stimulated indirectly with PGE_2 or with forskolin. The decrease in cAMP accumulation at pH 6.0 persisted when cells were treated with PTX 16 h prior to PGE_2 stimulation (Figure 23 A). In addition, no effect of low pH on basal cAMP content in absence of AC stimulus was observed, and PTX retained its functionality at acidic pH (Figure 23 B and C).

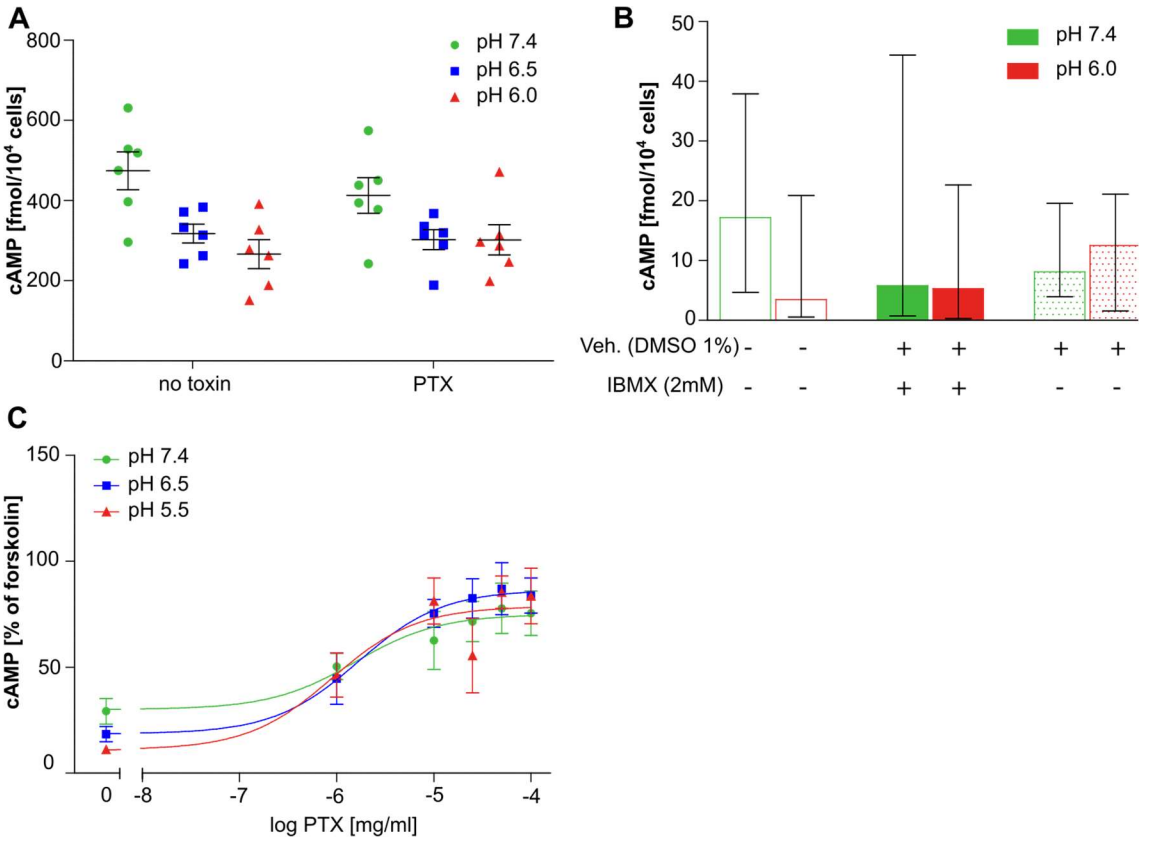

*Figure 23. cAMP baselines. (**A**) cAMP production in HEK MOR-WT pre-treated (overnight) or not with PTX (and then stimulated with PGE_2. Data represent cAMP levels in fmol per 10^4 cells by experiment (dots) with mean ± SEM (lines and bars), n = 6 per condition. Two-way ANOVA, $P < 0.05$, significant source of interaction for pH (not for treatment). (**B**) cAMP accumulation in HEK MOR-WT at extracellular pH 7.4 or 6.0, in absence or presence of dimethyl sulfoxide (DMSO) and/or 3-isobutyl-1-methylxanthine (IBMX). Data represent median with interquartile range of cAMP in fmol/ 10^4 cells, Friedman test, ns, n = 6 per condition. (**C**) Reversal of fentanyl-induced cAMP reduction by PTX in HEK MOR-WT. Data are normalized to cAMP levels in absence of fentanyl and PTX at the respective pH, and represent mean ± SEM with nonlinear fit. Comparison of fits with extra sum of squares F test (Top, $logEC_{50}$), ns, one curve for all datasets, n = 5 per curve.*

4 Discussion and Conclusions

In the present study I demonstrate that acidic pH selectively reduces receptor binding and signaling of opioids that bind to MOR via hydrogen bonds to residue H297$^{6.52}$.
This conclusion was drawn from testing two main hypotheses:

Hypothesis 1: Acidic pH regulates MOR function

In assays examining ligand binding, G-protein activation and modulation of cAMP levels, I demonstrated that acidic pH negatively regulates opioid binding and signaling in a ligand-selective manner. Acidic pH inhibited the morphinan-based MOR antagonist NLX and the peptide agonist DAMGO, but not the phenylpiperidine agonist fentanyl. Hence, pH-modulated opioid binding occurred in different opioid classes, and for agonists as well as antagonists. In addition, a pH-dependency of opioid-independent G-protein activity was observed.

Hypothesis 2: Protonation of MOR H297$^{6.52}$ regulates MOR function at acidic pH

In ligand binding and functional studies, I demonstrated that MOR H297$^{6.52}$ was essential to the binding and signaling of NLX and DAMGO. Both ligands operated poorly at acidic pH. Fentanyl, in contrast, was unaffected by pH and only partially depended on H297$^{6.52}$. I conclude that protonation of H297$^{6.52}$ at acidic pH ligand-selectively impairs opioid binding.
The proposed mechanism is not only in agreement with the observations within this study, but connects early findings on opioid binding with seemingly contradicting findings from our group (Pert & Snyder, 1973b; Smith, 1977; Spahn et al., 2017).

The proposed mechanism reveals an important structure-function relationship for optimal opioid binding and signaling in injured and inflamed tissue.

4.1 MOR stability at acidic pH

As demonstrated in this study, transient exposure of intact HEK MOR-WT to acidic pH altered neither DAMGO binding nor DAMGO-induced G-protein activation at physiological pH. Likewise, neither fentanyl-induced G-protein activation nor G-protein affinity for GTP were altered by this treatment. These results demonstrate that transient exposure of HEK MOR-WT to acidic environments up to a pH of 5.5 does not cause

sustained alteration of opioid binding and signaling at the MOR. Synonymously, these observations confirm that exposure to acidic pH up to 5.5 does not destroy the receptor or its functions, even if the treatment is performed on intact cells. Interestingly, the MOR is thus better equipped to maintain its structural-functional properties at acidic pH than for example the β_2-adrenergic receptor, which is partly denatured by transient treatment at pH 6.5 (Ghanouni et al., 2000). Crucially, these findings demonstrated that further experiments could be performed in the range of pH 7.5 to pH 5.5 without fear of destroying MOR. Further experiments were conducted in the pH range of 7.4 to 6.0.

4.2 MOR ligand binding at acidic pH and to receptor mutants

I assessed the immediate effects of acidic pH on opioid ligand binding. In [^{3}H]-NLX saturation binding experiments, acidic pH progressively reduced the number of measurable binding sites but had no effect on receptor affinity. These findings demonstrated that protonation of the MOR impaired ligand binding, as the protonation state of NLX does not markedly change between pH 7.4 and 6.0 (Mazak, Hosztafi, & Noszal, 2015). In addition, altered protonation of the ligand might alter the apparent ligand affinity, but not the maximum number of available receptor binding sites: If only a fraction of the absolute ligand concentration was able to bind the receptor, full receptor occupancy could still be achieved at higher ligand concentrations.

To test whether NLX binding depends on interaction with H297$^{6.52}$, I used single amino acid exchanges. Exchange of H297$^{6.52}$ for alanine almost, and exchange of H297$^{6.52}$ for F literally abolished NLX binding. These data demonstrate that H297$^{6.52}$ is involved in NLX binding. I next tested whether the presence of a hydrogen bond network between a ligand and MOR residue H297$^{6.52}$ might serve as predictor of pH-sensitivity. The peptide agonist DAMGO is structurally unrelated to NLX but was demonstrated to form a hydrogen network with H297$^{6.52}$ (Koehl et al., 2018). [^{3}H]-DAMGO saturation binding experiments revealed no binding to MOR-H297$^{6.52}$A, confirming that the residue serves an important role in ligand binding. At MOR-WT, acidic pH gradually impaired [^{3}H]-DAMGO binding, but the pH effect appeared slightly less pronounced than observed for NLX binding.

Interestingly, Smith (1977) demonstrated that pH regulation of opioid binding was mediated by functional moiety with a pK_a of 7.0. According to my hypothesis 2, only the unprotonated species of H297$^{6.52}$ should serve as potential NLX binding site, and the Henderson-Hasselbalch equation predicts that a pK_a of 7.0 should result in 71.4 %

unprotonated species at pH 7.4 and 24,2 % unprotonated species at pH 6.5. Consequently, NLX binding at pH 7.4 should be roughly three times that at pH 6.5, which is very close to the observed proportion of 2.7 to 1 at pH 7.4 and 6.5, respectively. For DAMGO, the ratio of binding at pH 7.4 to 6.5 is 1.4. This suggests that hydrogen bonds to H297$^{6.52}$ are less important in binding of DAMGO compared to NLX. As a result, the influence of acidic pH on DAMGO binding is less pronounced than for NLX.

A study that assessed ligand binding at a single dose of [^{3}H]-NLX and [^{3}H]-DAMGO each previously reported [^{3}H]-NLX binding of ~ 10% MOR-WT level to MOR-H297$^{6.52}$A and ~ 30% MOR-WT level to MOR-H297$^{6.52}$F, while [^{3}H]-DAMGO revealed virtually no binding at either of the two mutant receptors (Spivak et al., 1997). As saturation binding experiments on MOR-H297$^{6.52}$A/F were not performed there, it cannot be excluded that unequal receptor expression levels caused the slight discrepancy regarding the level of [^{3}H]-NLX binding reported here.

Unfortunately, direct fentanyl binding studies were prevented by high levels of unspecific [^{3}H]-fentanyl binding to membrane fractions, and competition binding experiments of fentanyl with [^{3}H]-NLX or [^{3}H]-DAMGO were hindered by the low level of high affinity binding to the mutant receptors. Using an unusually high concentration of radiolabelled NLX as radioligand, I observed highly variable [^{3}H]-NLX binding that was fully abolished upon competition by a high dose of unlabelled fentanyl. However, the doses of both labelled and unlabelled ligand used in this experiment were high enough to capture binding to KOR or DOR, which might be expressed in HEK 293 cells (Atwood et al., 2011, preliminary qPCR data presented in this study; Maguire et al., 1992).

4.3 G-protein activation at acidic pH

4.3.1 Basal G-protein activity at acidic pH

In [^{35}S]-GTPγS binding experiments, acidic pH enhanced opioid-independent baseline [^{35}S]-GTPγS binding. A possible cause of this effects could have been the reducing agent dithiothreitol (DTT), which is commonly included in [^{35}S]-GTPγS binding assays of MOR to reduce unspecific binding (Happe, Bylund, & Murrin, 2001). Since the redox potential of DTT is pH-dependent, I compared baseline binding in absence and presence of 1 mM DTT (Han & Han, 1994). Contradicting that hypothesis, 1mM DTT reduced unspecific [^{35}S]-GTPγS binding irrespective of pH, and acidic pH resulted in higher [^{35}S]-GTPγS binding both in absence and presence of DTT. Furthermore, the pH-dependent baseline

effect could be blocked by PTX treatment, but not by the presence of NLX in [^{35}S]-GTPγS binding assays. This suggested that elevated baselines were caused by higher levels of activated $G\alpha_i$ (as opposed to other GTP-bidning proteins, for discussion see Milligan, 2003), but these were not activated by enhanced constitutive MOR activity at acidic pH. Notably, [^{3}H]-NLX binding to MOR was impaired with increasing acidity. Yet, at pH 6.5, I observed significant levels of NLX binding, but no effect of NLX on baseline [^{35}S]-GTPγS binding. Under various experimental conditions, NLX has been reported to act either as MOR neutral antagonist or as inverse agonist, suggesting that its impact on MOR activity is context-dependent (Divin, Bradbury, Carroll, & Traynor, 2009; Masuho et al., 2015; Sirohi, Dighe, Madia, & Yoburn, 2009; D. Wang, Raehal, Bilsky, & Sadee, 2001). In my experiments, a comparatively high concentration of GDP served to suppress constitutive MOR activity, explaining the lack of NLX effects on baseline [^{35}S]-GTPγS binding (Heusler, Tardif, & Cussac, 2016). Yet, if acidic pH had increased constitutive MOR activity to the extent that it caused a significant increase in basal [^{35}S]-GTPγS binding, the presence of NLX should have counteracted this. In addition, pilot experiments with untransfected HEK 293 cells revealed elevated baselines at acidic pH that were comparable to those of MOR-WT. I concluded that the elevated [^{35}S]-GTPγS baselines at acidic pH were caused neither by MOR activation nor by increased MOR constitutive activity.

Elevated baseline [^{35}S]-GTPγS binding at acidic pH has been reported earlier in studies of proton sensing GPCRs (Ludwig et al., 2003; J. Q. Wang et al., 2004). Of the known proton-activated GPCRs, G2A is known to couple to $G\alpha_i$. A large screening study of mRNA expression demonstrated that G2A is not expressed in HEK 293 cells, but no control experiments were conducted in this study, and the existence of other unidentified proton sensing GPCRs cannot be excluded. Notwithstanding, it was reasonable to assume that elevated [^{35}S]-GTPγS binding at acidic pH might be caused by a direct effect of pH on G-proteins: Acidic pH has been demonstrated to increase the thermodynamic stability of the $G\alpha_i$-GTP complex and reduce the GTPase activity of other GTP-binding proteins (Isom et al., 2013; Mendieta et al., 2009). GTPγS, often mislabelled as 'non-hydrolyzable' GTP analogue, is hydrolyzed at a slower rate than the naturally occurring GTP (Ott & Costa, 1989). Acidic pH might slow down the hydrolysis of GTPγS even further, leading to pH-dependent signal strength after two hours of incubation. In other words, it is reasonable to assume that [^{35}S]-GTPγS binding itself is not enhanced at acidic pH, but dissociation of the

labelled probe from the membranes after hydrolysis of the nucleotide leads to reduced measurable signals at pH 7.4 over time. Accordingly, [^{35}S]-GTPγS dose response curves were normalized to baselines at the respective pH to enable comparison of agonists across pH values.

Interestingly, Ghanouni et al. (2000) observed no difference in receptor-independent basal GTPase activity in $G\alpha_s$ expressing membranes at pH 8.0 versus pH 6.5. If acidic pH selectively reduced the GTPase activity of $G\alpha_i$ *in vivo*, it might and enhance $G\alpha_i$ effects (with possible consequence on opioid signaling). To obtain a first hint as to whether the observed effect might be of relevance *in vivo*, I attempted to detect intracellular G-protein activity at different extracellular pH values in intact MOR-WT cells. Unfortunately, the experiments failed due to questionable antibody specificity. Immunoprecipitation with antibodies presumably specific for GTP-bound $G\alpha_i$ did not reveal enhanced G-protein activity after incubation with fentanyl or a high concentration of GTPγS.

4.3.2 Fentanyl-induced G-protein activation at acidic pH and in MOR mutants

Fentanyl equally induced [^{35}S]-GTPγS binding at pH 7.4, 6.5, and 6.0. This finding was reproducible among different experimenters, despite minor differences in assay protocols (Spahn et al., 2018). Additionally, this observation is in agreement with previous work demonstrating that fentanyl binding is independent of acidic pH (Spahn et al., 2017). Importantly, fentanyl elicited dose-dependent G-protein activation in MOR-H297$^{6.52}$A, also regardless of pH. Crucially, these observations also demonstrated that fentanyl binds to MOR-H297$^{6.52}$A. However, agonist-stimulated [^{35}S]-GTPγS binding in MOR-H297$^{6.52}$A revealed a higher variability than in MOR-WT (Bartlett's test yielded unequal SD between the two groups). This might indicate a minor contribution of H297$^{6.52}$ fentanyl either in binding or in G-protein activation (by contributing to the "message", see Huang et al., 2015). Dose-response curves at acidic pH clearly demonstrated that fentanyl-induced G-protein activation in membranes expressing MOR-H297$^{6.52}$A is independent of pH. Examples for a weak, largely pH-insensitive interaction between fentanyl and H297$^{6.52}$ would be aromatic stacking, as suggested by *in silico* studies (Dosen-Micovic et al., 2006; Ellis, Kruhlak, Kim, Hawkins, & Stavitskaya, 2018), or other nonpolar interactions.

Unexpectedly, fentanyl did not elicit G-protein activation in MOR-H297$^{6.52}$F, a mutant that theoretically should allow for stacking interactions with the aromatic ring of phenylalanine, similar to histidine side chains. Given the protrusion of H297$^{6.52}$ into the water-filled binding cavity of MOR however (Manglik et al., 2012), it cannot be excluded that the

exchange of the amphipathic histidine for a fully hydrophobic phenylalanine induced changes in the binding site geometry, and the mutation might thus have produced secondary effects. Based on the observations at MOR-H297$^{6.52}$A, I concluded that H297$^{6.52}$ is not essential to MOR activation by fentanyl.

4.3.3 DAMGO-induced G-protein activation at acidic pH and in MOR mutant

In dose-response experiments, acidic pH reduced the maximum DAMGO-induced [^{35}S]-GTPγS binding. This finding was in agreement with the impairment of [^{3}H]-DAMGO binding by acidic pH. In contrast to fentanyl, DAMGO did not activate G-proteins in membranes expressing MOR-H297$^{6.52}$A, irrespective of pH. Thus, at the level of G-protein activation, DAMGO showed dependence on both pH and H297$^{6.52}$A, mirroring the effects observed on ligand binding and indicating a significant, pH-dependent contribution of H297$^{6.52}$ to DAMGO binding.

The lack of DAMGO-induced G-protein activation in MOR-H297$^{6.52}$A furthermore demonstrates a lack of expression of endogenous MOR-WT at levels sufficient to induce the fentanyl-induced [^{35}S]-GTPγS binding observed in MOR-H297$^{6.52}$A. At concentrations of ≥ 10 µM, DAMGO, however, induced low levels of [^{35}S]-GTPγS binding in MOR-H297$^{6.52}$A membranes. This effect might be due to activation of KOR or DOR, which display a 500-times reduced affinity for DAMGO than MOR (Emmerson, Liu, Woods, & Medzihradsky, 1994). Pilot experiments presented in this work indicate low levels of both DOR and KOR mRNA in untransfected HEK 293 cells, and significant levels of DOR mRNA have previously been detected in HEK 293 cells (Atwood et al., 2011).

4.4 AC activity at acidic pH

4.4.1 Basal AC activity at acidic pH

It is reasonable to assume that changes in ligand binding and G-protein activation are translate into altered downstream signaling. I therefore assessed opioid modulation of AC activity via quantification of cAMP levels in EIA. Unfortunately, strong baseline effects on cAMP stimulation with 1 µM PGE_2 at pH 6.0 prevented the analysis of data at this pH. The PGE_2 concentration had been chosen in pilot experiments. Previously, data acquired by me as well as several colleagues had revealed a similar pH effect on forskolin-stimulated cAMP levels. Low cAMP levels might have been caused by enhanced, opioid-independent Gαi activity at acidic pH, as observed in [^{35}S]-GTPγS binding experiments. Yet, PTX did not block the pH-dependent reduction in PGE_2-induced cAMP levels. Previously,

experiments performed in our group had revealed PTX treatment similarly did not affect forskolin-induced cAMP levels. Furthermore, basal cAMP levels at pH 7.4 and 6.0 showed no difference between pH 7.4 and pH 6.0. Accordingly, $G\alpha_i$ did not mediate the reduction. pH-dependent alterations in AC activity are the likely cause of reduced cAMP levels at acidic extracellular pH (J. Q. Wang et al., 2004).

4.4.2 Fentanyl and NLX modulation of AC at acidic pH

Fentanyl-induced cAMP reductions were not altered at acidic pH, mirroring the pH-independent G-protein activation observed via [^{35}S]-GTPγS binding. As NLX binding to MOR was impaired at acidic pH, I analyzed NLX antagonism of fentanyl-induced cAMP reduction. Acidic pH impaired NLX antagonism, shifting both the EC_{50} and maximum effect. These findings were in good agreement with reduced NLX binding at acidic pH. While the pharmacological parameters of the dose-response curve at pH 6.0 could not be interpreted due to the baseline effect, NLX antagonism was clearly detectable. This effect apparently contrasted with the results discussed in 4.2: at the receptor binding level, NLX binding appeared fully abolished at pH 6.0. However, affinities in the nM range are required to produce stable signal in radioligand binding assays, and the failure do detect specific binding in such assays does not exclude the possibility of medium to low affinity binding (Hulme & Trevethick, 2010). Alternatively, .it is reasonable to assume that the low number of receptors capable of NLX binding at pH 6.0 (9 % of the total receptor population, according to the Henderson-Hasselbalch equation) is insufficient to yield stable signals as the signal to noise ratio deteriorates (Bylund & Murrin, 2000). The observed differences in apparent pH sensitivity at different stages of the opioid signaling cascade could be explained by differences in "tightness of coupling" to the ligand binding step (Costa, Klinz, Vachon, & Herz, 1988). Full-scale opioid reduction of cAMP levels requires less available MOR binding sites than does full G-protein activation, as Costa et al. (1988) demonstrated by progressive chemical elimination of opioid receptor binding sites.

The data distribution of the NLX dose-response curve at pH 7.4 unexpectedly seemed to follow a biphasic rather than a classical dose-response curve. Opioids typically display bell-shaped dose-response curves under conditions of strong receptor-G-protein coupling (Heusler et al., 2016). The observed inflection of the dose-response curve might therefore be due to the high concentration of competing fentanyl used in the experiment. The fentanyl dose was chosen to match that used in single-dose experiments within our group. Similar experiments had previously shown full NLX antagonism regardless of pH (Spahn

et al., 2017, Supplementary Figure 3). In those previous experiments, the loss of NLX antagonism was unintentionally masked by normalization, as the pH-dependent baseline effects were more pronounced when using forskolin to stimulate the AC. This discrepancy of findings demonstrates the necessity for careful consideration of baseline effects

In cells expressing MOR-H297$^{6.52}$A, the fentanyl cAMP dose-response relationship was partly impaired compared to MOR-WT. The reduction in fentanyl efficacy in AC inhibition might be caused by the loss of a non-essential, yet not irrelevant, interaction between ligand and receptor. This result is in slight contrast with the results of [^{35}S]-GTPγS binding experiments, where fentanyl-induced MOR activation appeared to be independent of H297$^{6.52}$. However, a small, statistically insignificant increase in the EC_{50} had been observed at the level of G-protein activation as well. Amplification of the signal downstream of G-protein activation might lead to a stronger manifestation of the effect. Notably, fentanyl-induced cAMP reduction via MOR-H297$^{6.52}$A was assessed at physiological pH only, because G-protein activation at the mutant receptor was previously found pH-independent. Despite the partial effect the mutation had on fentanyl modulation of cAMP values, the data clearly demonstrated that substitution of H297$^{6.52}$ does not hinder fentanyl-induced activation of MOR.

4.5 Technical strengths and limitations of the study

The pH has a multifaceted and complex role in biological and biochemical processes (see chapter 1.6.2). Accordingly, *in vitro* methods are usually performed at a defined pH (or pH range) to ensure full functionality of all assay components and prevent that changes in pH cause off-target effects. In the present study, established assays were subjected to a wide pH range. Not surprisingly, interpretation of the data presented in this study was complicated by the recurring pH-effects on assay baselines. Crucially, the pH generally affects the function of enzymes (Nelson et al., 2017).The pivotal enzymes contributing to the findings of the present work are the GTPase of G-proteins and the AC, and acidification manifested in pH-dependent baseline shifts where either of these was involved. To enable comparison of the opioid-induced effects between pH values, the affected assay baselines were normalized by pH. Data transformation generally carries the risk of data distortion, therefore the method of normalization should correspond to the mechanism that caused the baseline shifts in the first place (see e.g. Hugel, Kadiri, Rodeau,

Gaillard, & Schlichter, 2012). In the present work, pH-dependent assay baselines were therefore thoroughly examined to provide data transparency.

Another limitation of the present study is the use of an immortalized cell line. To test the effects of single amino acid exchanges and acidic extracellular pH *in vitro*, I used HEK 293 cells, because they are easy to transfect, do not express endogenous MOR and exhibit some neuronal markers (Stepanenko & Dmitrenko, 2015). HEK 293 cells are of human origin and were initially identified as kidney cells. After decades of in vitro culture, they do not resemble any cell type found in humans, and until verified in neurons, it may therefore not be assumed that the signaling events described here will not differ in *vivo* (Stepanenko & Dmitrenko, 2015). However, the use of the robust HEK 293 cell line enabled studying receptor behavior and intracellular signaling under the harsh conditions of a severely acidified extracellular milieu.

Finally, membrane expression opioid receptors could not be quantified. The specificity of antibodies targeting opioid receptors has repeatedly been questioned, and radioligand binding is not suitable for quantification of receptors mutants with expected alterations in ligand binding (Niwa, Rowbotham, & Lambert, 2012; Scherrer et al., 2009). For this reason, quantitative comparisons of absolute values between cell types were circumvented throughout the work.

4.6 Broader context and relevance of the study

As detailed in the introduction, novel pH-dependent analgesics that selectively activate peripheral opioid receptors in injured tissue represent a promising strategy to circumvent opioid-induced adverse effects while providing efficient analgesia. The present study provides crucial mechanistic detail for the design of pH-selective peripheral opioids. In the broader context of opioid analgesia, several aspects need to be given further consideration.

As many studies have hitherto demo pH-sensing is not the main function of MOR-H297$^{6.52}$. A central role in the binding of a wide range of ligands has been demonstrated by *in vitro* and *in silico* studies, and it was suggested that H297$^{7.65}$ functionally contributes to MOR activation (Cong et al., 2015; Spivak et al., 1997). Accordingly, formation of a pH-independent interaction between receptor and ligand, as e.g. fentanyl appears to engage in, might be a prerequisite for optimal MOR binding and activation at acidic pH.

Moreover, the residue H297$^{7.65}$ differentiates between ligands of the classic opioid receptors (MOR, KOR, DOR) versus ORL1 (Mollereau, Moisand, Butour, Parmentier, & Meunier, 1996; Toll, Bruchas, Calo, Cox, & Zaveri, 2016). Ligands that bind largely independent of MOR H297$^{6.52}$ should be checked carefully for off-target effects on ORL1. Tellingly, several fentanyl derivates display considerable affinities at the ORL1 (Hawkinson, Acosta-Burruel, & Espitia, 2000).

Intriguingly, all known endogenous opioid peptides harbor an N-terminal tyrosine, and so does the synthetic peptide agonist DAMGO (Pasternak & Pan, 2013; Toll et al., 2016). Previous to the discovery of high-resolution opioid receptor structures, Barnard (1993) observed that the N-terminal tyrosine of enkephalin contains a chemical motif that can be found in many opioid agonists, namely the phenolic group that forms the water-mediated hydrogen bond to H297$^{6.52}$. Accordingly, endogenous opioid peptides are likely to be affected by the pH-sensing mechanism demonstrated in this study, but I did not investigate this further.

Peripheralization of opioid compounds, typically achieved by topical application of systemically inactive concentrations or by preventing passage of the blood-brain barrier, is a well-established practice in pain research (DeHaven-Hudkins & Dolle, 2004). It has repeatedly been noted that concentration-dependent permeation of the blood-brain barrier of such substances must be avoided (Gupta et al., 2001; Tegeder et al., 2003). Likewise, absolute restriction pH-selective opioids to injured tissue will be required to ensure patient safety. A possible caveat to the approach, activity-dependent intracellular acidification has been observed in neurons (Boffi, Knabbe, Kaiser, & Kuner, 2018). Intracellular opioid receptors, e.g. expressed in ER membranes, have been shown to contribute to signaling by exogenous opioids in cultured neurons, and it appears reasonable to assume that similar effects could be produced *in vivo* (Stoeber et al., 2018). Additional safety measures, such as acidic pH release from larger prodrugs that cannot cross the blood-brain barrier, might be considered (Gonzalez-Rodriguez et al., 2017).

The importance of preventing residual activity in the CNS is further stressed by the high abuse potential of fentanyl, the parent compound of the first pH-selective analgesics developed in our group. Overdose deaths from fentanyl and a growing variety of derivatives are on the increase in Europe as well as the USA (Ellis et al., 2018; EMCDDA, 2018; Karila et al., 2018). Alternative parent compounds with a safer profile might be

considered for the development of pH-selective opioids should the first generation of fentanyl-derived analgesics reveal unexpected side effects in future studies.

4.7 Conclusion and outlook

The present study presents a detailed investigation of opioid ligand binding and signaling at acidic pH. With the help of my colleagues, I could demonstrate that acidic pH selectively impairs the binding and signaling of NLX and DAMGO, but not of fentanyl. I demonstrated that this ligand selectivity is likely to be caused by protonation of MOR residue H297$^{6.52}$.

The mechanism was initially proposed based on structural information provided by high-resolution crystal structures of opioid receptors in complex with morphinan-based ligands and brought together several seemingly contradictory findings on opioid binding, among them some of the earliest studies on opioid binding and signaling (Childers, 1988; Childers & LaRiviere, 1984; Huang et al., 2015; Lambert & Childers, 1984; Manglik et al., 2012; Rasenick & Childers, 1989; Selley et al., 1993; Spahn et al., 2017). When the first high-resolution structure of MOR in complex with a peptide ligand was published in 2018, the concept proved transferable to ligands of an entirely different chemical class (Koehl et al., 2018).

The novelty of the present findings lies in combining findings from previously unrelated publications in a common, patho-physiologically relevant mechanism and examining the synergistic effects of ligand recognition and receptor protonation at physiological and acidic pH. To directly prove that protonation of H297$^{6.52}$ mediates the pH-dependent reductions in ligand binding, the abolition of a pH-dependent signal in MOR-H297$^{6.52}$A would have to be demonstrated.

However, as a strong dependence on H297$^{6.52}$ for ligand binding appeared to be the predictor for a ligand's pH-dependent binding, the affected ligands did not yield sufficient signal at MOR-H297$^{6.52}$A to test this. An important step to further validate that protonation of H297$^{6.52}$ impairs opioid binding would therefore be to assess further compounds regarding their dependency on both pH and H297$^{6.52}$. A screening of opioids from all chemically distinct groups would allow to determine the reliability of structural features as predictors of pH-sensitivity. In addition, the pharmacological parameters of endogenous

opioid peptide signaling at acidic pH could reveal whether and how acidosis is likely to interfere with endogenous opioid signaling.

In addition, a deeper understanding of MOR function might be gained by studying the pH-dependent role of histidine H319$^{7.36}$. H$^{7.36}$ contributes to pH sensing in the proton-activated GPCRs OGR1 and GPR4 (Liu et al., 2010; Ludwig et al., 2003). In high-resolution structures of MOR, H$^{7.36}$ is situated close to the entrance of the binding pocket that is wide open to the extracellular space (PDB entries 4DKL,6DDF, 5C1M; Huang et al., 2015; Koehl et al., 2018; Manglik et al., 2012). Of note, an interaction between H$^{7.36}$ and MOR ligands has not been shown in these structures. Nonetheless, the residue was suggested to be involved in ligand binding based on experimental evidence that preceded the solvation of high-resolution opioid receptor structures, where amino acid exchange H319$^{7.36}$A impaired binding of several agonists, including DAMGO and the fentanyl derivative ohmfentanyl, but not NLX (Xu et al., 1999).

In conclusion, as the mechanism proposed in the present work offers a clear rationale how to predict low pH impairment of opioid ligands based on their chemical structure, probing these predictions offers a straightforward tool for verification. Once the mechanism is thus verified, it can - and should - be leveraged in targeted drug design to further the development of pH-selective opioids.

5 References

Abram, S. E., Yi, J., Fuchs, A., & Hogan, Q. H. (2006). Permeability of injured and intact peripheral nerves and dorsal root ganglia. *Anesthesiology, 105*(1), 146-153.

Arnis, S., Fahmy, K., Hofmann, K. P., & Sakmar, T. P. (1994). A conserved carboxylic acid group mediates light-dependent proton uptake and signaling by rhodopsin. *J Biol Chem, 269*(39), 23879-23881.

Atwood, B. K., Lopez, J., Wager-Miller, J., Mackie, K., & Straiker, A. (2011). Expression of G protein-coupled receptors and related proteins in HEK293, AtT20, BV2, and N18 cell lines as revealed by microarray analysis. *BMC Genomics, 12*, 14. doi:10.1186/1471-2164-12-14

Ballesteros, J. A., & Weinstein, H. (1995). Integrated Methods for the Construction of Three-Dimensional Probing of Structure-Function Relations in G Protein-Coupled Receptors. *Methods in Neurosciences, 25*, 366-428.

Barnard, E. A. (1993). Opioid receptors: pipe dreams realized. *Curr Biol, 3*(4), 211-214.

Berg, J. M., Gatto, G. J., Stryer, L., & Tymoczko, J. L. (2003). *Biochemistry* (Eighth edition ed.).

Berg, K. A., Patwardhan, A. M., Sanchez, T. A., Silva, Y. M., Hargreaves, K. M., & Clarke, W. P. (2007). Rapid modulation of micro-opioid receptor signaling in primary sensory neurons. *J Pharmacol Exp Ther, 321*(3), 839-847. doi:10.1124/jpet.106.116681

Berman, H. M., Westbrook, J., Feng, Z., Gilliland, G., Bhat, T. N., Weissig, H., . . . Bourne, P. E. (2000). The Protein Data Bank. *Nucleic Acids Res, 28*(1), 235-242.

Boffi, J. C., Knabbe, J., Kaiser, M., & Kuner, T. (2018). KCC2-dependent Steady-state Intracellular Chloride Concentration and pH in Cortical Layer 2/3 Neurons of Anesthetized and Awake Mice. *Front Cell Neurosci, 12*, 7. doi:10.3389/fncel.2018.00007

Bradford, M. M. (1976). A rapid and sensitive method for the quantitation of microgram quantities of protein utilizing the principle of protein-dye binding. *Anal Biochem, 72*, 248-254.

Brownstein, M. J. (1993). A brief history of opiates, opioid peptides, and opioid receptors. *Proc Natl Acad Sci U S A, 90*(12), 5391-5393.

Burgess, P. R., & Perl, E. R. (1967). Myelinated afferent fibres responding specifically to noxious stimulation of the skin. *J Physiol, 190*(3), 541-562.

Bylund, D. B., & Murrin, L. C. (2000). Radioligand saturation binding experiments over large concentration ranges. *Life Sci, 67*(24), 2897-2911. doi:10.1016/s0024-3205(00)00877-8

Cai, Q., Qiu, C. Y., Qiu, F., Liu, T. T., Qu, Z. W., Liu, Y. M., & Hu, W. P. (2014). Morphine inhibits acid-sensing ion channel currents in rat dorsal root ganglion neurons. *Brain Res, 1554*, 12-20. doi:10.1016/j.brainres.2014.01.042

Capasso, M. (2014). Regulation of immune responses by proton channels. *Immunology, 143*(2), 131-137. doi:10.1111/imm.12326

Chavan, S. S., Pavlov, V. A., & Tracey, K. J. (2017). Mechanisms and Therapeutic Relevance of Neuro-immune Communication. *Immunity, 46*(6), 927-942. doi:10.1016/j.immuni.2017.06.008

Childers, S. R. (1988). Opiate-inhibited adenylate cyclase in rat brain membranes depleted of Gs-stimulated adenylate cyclase. *J Neurochem, 50*(2), 543-553.

Childers, S. R., & LaRiviere, G. (1984). Modification of guanine nucleotide-regulatory components in brain membranes. II. Relationship of guanosine 5'-triphosphate effects on opiate receptor binding and coupling receptors with adenylate cyclase. *J Neurosci, 4*(11), 2764-2771.

Chovatiya, R., & Medzhitov, R. (2014). Stress, inflammation, and defense of homeostasis. *Mol Cell, 54*(2), 281-288. doi:10.1016/j.molcel.2014.03.030

Cockerill, G., & Reed, S. (2011). *Essential fluid, electrolyte and pH homeostasis*.

Cong, X., Campomanes, P., Kless, A., Schapitz, I., Wagener, M., Koch, T., & Carloni, P. (2015). Structural Determinants for the Binding of Morphinan Agonists to the mu-Opioid Receptor. *PLoS One, 10*(8), e0135998. doi:10.1371/journal.pone.0135998

Costa, T., Klinz, F. J., Vachon, L., & Herz, A. (1988). Opioid receptors are coupled tightly to G proteins but loosely to adenylate cyclase in NG108-15 cell membranes. *Mol Pharmacol, 34*(6), 744-754.

Cunningham, B. C., & Wells, J. A. (1989). High-resolution epitope mapping of hGH-receptor interactions by alanine-scanning mutagenesis. *Science, 244*(4908), 1081-1085.

Dai, S. P., Huang, Y. H., Chang, C. J., Huang, Y. F., Hsieh, W. S., Tabata, Y., . . . Sun, W. H. (2017). TDAG8 involved in initiating inflammatory hyperalgesia and establishing hyperalgesic priming in mice. *Sci Rep, 7*, 41415. doi:10.1038/srep41415

Davis, M. P., LeGrand, S. B., & Lagman, R. (2005). Look before leaping: combined opioids may not be the rave. *Support Care Cancer, 13*(10), 769-774. doi:10.1007/s00520-005-0839-y

De Lean, A., Stadel, J. M., & Lefkowitz, R. J. (1980). A ternary complex model explains the agonist-specific binding properties of the adenylate cyclase-coupled beta-adrenergic receptor. *J Biol Chem, 255*(15), 7108-7117.

Deetjen, P., Speckmann, E.-J., Benndorf, K., & Alzheimer, C. (2005). *Physiologie* (4., vollst. überarb. Aufl. ed.).

DeHaven-Hudkins, D. L., & Dolle, R. E. (2004). Peripherally restricted opioid agonists as novel analgesic agents. *Curr Pharm Des, 10*(7), 743-757.

Dembla, S., Behrendt, M., Mohr, F., Goecke, C., Sondermann, J., Schneider, F. M., . . . Oberwinkler, J. (2017). Anti-nociceptive action of peripheral mu-opioid receptors by G-beta-gamma protein-mediated inhibition of TRPM3 channels. *Elife, 6*. doi:10.7554/eLife.26280

DeWire, S. M., Yamashita, D. S., Rominger, D. H., Liu, G., Cowan, C. L., Graczyk, T. M., . . . Violin, J. D. (2013). A G protein-biased ligand at the mu-opioid receptor is potently analgesic with reduced gastrointestinal and respiratory dysfunction compared with morphine. *J Pharmacol Exp Ther, 344*(3), 708-717. doi:10.1124/jpet.112.201616

Dhawan, B. N., Cesselin, F., Raghubir, R., Reisine, T., Bradley, P. B., Portoghese, P. S., & Hamon, M. (1996). International Union of Pharmacology. XII. Classification of opioid receptors. *Pharmacol Rev, 48*(4), 567-592.

Di Cera, E. (2000). *Thermodynamics in biology*. Oxford ; New York: Oxford University Press.

Divin, M. F., Bradbury, F. A., Carroll, F. I., & Traynor, J. R. (2009). Neutral antagonist activity of naltrexone and 6beta-naltrexol in naive and opioid-dependent C6 cells expressing a mu-opioid receptor. *Br J Pharmacol, 156*(7), 1044-1053. doi:10.1111/j.1476-5381.2008.00035.x

Dosen-Micovic, L., Ivanovic, M., & Micovic, V. (2006). Steric interactions and the activity of fentanyl analogs at the mu-opioid receptor. *Bioorg Med Chem, 14*(9), 2887-2895. doi:10.1016/j.bmc.2005.12.010

Dreborg, S., Sundstrom, G., Larsson, T. A., & Larhammar, D. (2008). Evolution of vertebrate opioid receptors. *Proc Natl Acad Sci U S A, 105*(40), 15487-15492. doi:10.1073/pnas.0805590105

Ellis, C. R., Kruhlak, N. L., Kim, M. T., Hawkins, E. G., & Stavitskaya, L. (2018). Predicting opioid receptor binding affinity of pharmacologically unclassified designer substances using molecular docking. *PLoS One, 13*(5), e0197734. doi:10.1371/journal.pone.0197734

EMCDDA. (2018, June 2018). European Drug Report 2018: Trends and Developments. Retrieved from http://www.emcdda.europa.eu/publications/edr/trends-developments/2018

Emmerson, P. J., Liu, M. R., Woods, J. H., & Medzihradsky, F. (1994). Binding affinity and selectivity of opioids at mu, delta and kappa receptors in monkey brain membranes. *J Pharmacol Exp Ther, 271*(3), 1630-1637.

Erra Diaz, F., Dantas, E., & Geffner, J. (2018). Unravelling the Interplay between Extracellular Acidosis and Immune Cells. *Mediators Inflamm, 2018*, 1218297. doi:10.1155/2018/1218297

Freissmuth, M., Offermanns, S., & Böhm, S. (2016). *Pharmakologie und Toxikologie: von den molekularen Grundlagen zur Pharmakotherapie* (2., aktualisierte und erweiterte Auflage ed.).

Ghanouni, P., Schambye, H., Seifert, R., Lee, T. W., Rasmussen, S. G., Gether, U., & Kobilka, B. K. (2000). The effect of pH on beta(2) adrenoceptor function. Evidence for protonation-dependent activation. *J Biol Chem, 275*(5), 3121-3127.

Gonzalez-Rodriguez, S., Quadir, M. A., Gupta, S., Walker, K. A., Zhang, X., Spahn, V., . . . Stein, C. (2017). Polyglycerol-opioid conjugate produces analgesia devoid of side effects. *Elife, 6*. doi:10.7554/eLife.27081

Granier, S., Manglik, A., Kruse, A. C., Kobilka, T. S., Thian, F. S., Weis, W. I., & Kobilka, B. K. (2012). Structure of the delta-opioid receptor bound to naltrindole. *Nature, 485*(7398), 400-404. doi:10.1038/nature11111

Grimsley, G. R., Scholtz, J. M., & Pace, C. N. (2009). A summary of the measured pK values of the ionizable groups in folded proteins. *Protein Sci, 18*(1), 247-251. doi:10.1002/pro.19

Groh, A., Krieger, P., Mease, R. A., & Henderson, L. (2018). Acute and Chronic Pain Processing in the Thalamocortical System of Humans and Animal Models. *Neuroscience, 387*, 58-71. doi:10.1016/j.neuroscience.2017.09.042

Gupta, A., Bodin, L., Holmstrom, B., & Berggren, L. (2001). A systematic review of the peripheral analgesic effects of intraarticular morphine. *Anesth Analg, 93*(3), 761-770.

Han, J. C., & Han, G. Y. (1994). A procedure for quantitative determination of tris(2-carboxyethyl)phosphine, an odorless reducing agent more stable and effective than dithiothreitol. *Anal Biochem, 220*(1), 5-10. doi:10.1006/abio.1994.1290

Happe, H. K., Bylund, D. B., & Murrin, L. C. (2001). Agonist-stimulated [35S]GTPgammaS autoradiography: optimization for high sensitivity. *Eur J Pharmacol, 422*(1-3), 1-13.

Hassan, A. H., Ableitner, A., Stein, C., & Herz, A. (1993). Inflammation of the rat paw enhances axonal transport of opioid receptors in the sciatic nerve and increases their density in the inflamed tissue. *Neuroscience, 55*(1), 185-195. doi:10.1016/0306-4522(93)90465-r

Hawkinson, J. E., Acosta-Burruel, M., & Espitia, S. A. (2000). Opioid activity profiles indicate similarities between the nociceptin/orphanin FQ and opioid receptors. *Eur J Pharmacol, 389*(2-3), 107-114. doi:10.1016/s0014-2999(99)00904-8

Heinricher, M. M., Tavares, I., Leith, J. L., & Lumb, B. M. (2009). Descending control of nociception: Specificity, recruitment and plasticity. *Brain Res Rev, 60*(1), 214-225. doi:10.1016/j.brainresrev.2008.12.009

Heusler, P., Tardif, S., & Cussac, D. (2016). Agonist stimulation at human mu opioid receptors in a [(35)S]GTPgammaS incorporation assay: observation of "bell-shaped" concentration-response relationships under conditions of strong receptor G protein coupling. *J Recept Signal Transduct Res, 36*(2), 158-166. doi:10.3109/10799893.2015.1069845

Hill, R., Disney, A., Conibear, A., Sutcliffe, K., Dewey, W., Husbands, S., . . . Henderson, G. (2018). The novel mu-opioid receptor agonist PZM21 depresses respiration and induces tolerance to antinociception. *Br J Pharmacol*. doi:10.1111/bph.14224

Huang, W., Manglik, A., Venkatakrishnan, A. J., Laeremans, T., Feinberg, E. N., Sanborn, A. L., . . . Kobilka, B. K. (2015). Structural insights into micro-opioid receptor activation. *Nature*. doi:10.1038/nature14886

Hugel, S., Kadiri, N., Rodeau, J. L., Gaillard, S., & Schlichter, R. (2012). pH-dependent inhibition of native GABA(A) receptors by HEPES. *Br J Pharmacol, 166*(8), 2402-2416. doi:10.1111/j.1476-5381.2012.01956.x

Hulme, E. C., & Trevethick, M. A. (2010). Ligand binding assays at equilibrium: validation and interpretation. *Br J Pharmacol, 161*(6), 1219-1237. doi:10.1111/j.1476-5381.2009.00604.x

Ikeda, K., Kobayashi, T., Kumanishi, T., Niki, H., & Yano, R. (2000). Involvement of G-protein-activated inwardly rectifying K (GIRK) channels in opioid-induced analgesia. *Neurosci Res, 38*(1), 113-116.

Ingram, S. L., & Williams, J. T. (1994). Opioid inhibition of Ih via adenylyl cyclase. *Neuron, 13*(1), 179-186.

Isom, D. G., Sridharan, V., Baker, R., Clement, S. T., Smalley, D. M., & Dohlman, H. G. (2013). Protons as second messenger regulators of G protein signaling. *Mol Cell, 51*(4), 531-538. doi:10.1016/j.molcel.2013.07.012

Jagla, C., Martus, P., & Stein, C. (2014). Peripheral opioid receptor blockade increases postoperative morphine demands--a randomized, double-blind, placebo-controlled trial. *Pain, 155*(10), 2056-2062. doi:10.1016/j.pain.2014.07.011

Jarpe, M. B., Knall, C., Mitchell, F. M., Buhl, A. M., Duzic, E., & Johnson, G. L. (1998). [D-Arg1,D-Phe5,D-Trp7,9,Leu11]Substance P acts as a biased agonist toward neuropeptide and chemokine receptors. *J Biol Chem, 273*(5), 3097-3104. doi:10.1074/jbc.273.5.3097

Julius, D., & Basbaum, A. I. (2001). Molecular mechanisms of nociception. *Nature, 413*(6852), 203-210. doi:10.1038/35093019

Karhausen, J., Haase, V. H., & Colgan, S. P. (2005). Inflammatory hypoxia: role of hypoxia-inducible factor. *Cell Cycle, 4*(2), 256-258.

Karila, L., Marillier, M., Chaumette, B., Billieux, J., Franchitto, N., & Benyamina, A. (2018). New synthetic opioids: Part of a new addiction landscape. *Neurosci Biobehav Rev*. doi:10.1016/j.neubiorev.2018.06.010

Katritch, V., Fenalti, G., Abola, E. E., Roth, B. L., Cherezov, V., & Stevens, R. C. (2014). Allosteric sodium in class A GPCR signaling. *Trends Biochem Sci, 39*(5), 233-244. doi:10.1016/j.tibs.2014.03.002

Kawabata, A. (2011). Prostaglandin E2 and pain--an update. *Biol Pharm Bull, 34*(8), 1170-1173.

Kayser, V., & Guilbaud, G. (1983). The analgesic effects of morphine, but not those of the enkephalinase inhibitor thiorphan, are enhanced in arthritic rats. *Brain Res, 267*(1), 131-138.

Kenakin, T. (1995). Agonist-receptor efficacy. II. Agonist trafficking of receptor signals. *Trends Pharmacol Sci, 16*(7), 232-238.

Kimergard, A., Foley, M., Davey, Z., Dunne, J., Drummond, C., & Deluca, P. (2017). Codeine use, dependence and help-seeking behaviour in the UK and Ireland: an online cross-sectional survey. *QJM, 110*(9), 559-564. doi:10.1093/qjmed/hcx076

Koehl, A., Hu, H., Maeda, S., Zhang, Y., Qu, Q., Paggi, J. M., . . . Kobilka, B. K. (2018). Structure of the micro-opioid receptor-Gi protein complex. *Nature*. doi:10.1038/s41586-018-0219-7

Labuz, D., & Machelska, H. (2013). Stronger antinociceptive efficacy of opioids at the injured nerve trunk than at its peripheral terminals in neuropathic pain. *J Pharmacol Exp Ther, 346*(3), 535-544. doi:10.1124/jpet.113.205344

Lambert, S. M., & Childers, S. R. (1984). Modification of guanine nucleotide-regulatory components in brain membranes. I. Changes in guanosine 5'-triphosphate regulation of opiate receptor-binding sites. *J Neurosci, 4*(11), 2755-2763.

Lans, I., Dalton, J. A., & Giraldo, J. (2015a). Selective Protonation of Acidic Residues Triggers Opsin Activation. *J Phys Chem B, 119*(30), 9510-9519. doi:10.1021/acs.jpcb.5b01908

Lans, I., Dalton, J. A., & Giraldo, J. (2015b). Selective Protonation of Acidic Residues Triggers Opsin Activation. *J Phys Chem B*. doi:10.1021/acs.jpcb.5b01908

Le Merrer, J., Becker, J. A., Befort, K., & Kieffer, B. L. (2009). Reward processing by the opioid system in the brain. *Physiol Rev, 89*(4), 1379-1412. doi:10.1152/physrev.00005.2009

Li, J. G., Chen, C., Yin, J., Rice, K., Zhang, Y., Matecka, D., . . . Liu-Chen, L. Y. (1999). ASP147 in the third transmembrane helix of the rat mu opioid receptor forms ion-pairing with morphine and naltrexone. *Life Sci, 65*(2), 175-185.

Li, S., & Hong, M. (2011). Protonation, tautomerization, and rotameric structure of histidine: a comprehensive study by magic-angle-spinning solid-state NMR. *J Am Chem Soc, 133*(5), 1534-1544. doi:10.1021/ja108943n

Li, Y., & van den Pol, A. N. (2008). Mu-opioid receptor-mediated depression of the hypothalamic hypocretin/orexin arousal system. *J Neurosci, 28*(11), 2814-2819. doi:10.1523/JNEUROSCI.5447-07.2008

Liu, J. P., Nakakura, T., Tomura, H., Tobo, M., Mogi, C., Wang, J. Q., . . . Okajima, F. (2010). Each one of certain histidine residues in G-protein-coupled receptor GPR4 is critical for extracellular proton-induced stimulation of multiple G-protein-signaling pathways. *Pharmacol Res, 61*(6), 499-505. doi:10.1016/j.phrs.2010.02.013

Lodish, H. F. (2013). *Molecular cell biology* (7th ed.). New York: W.H. Freeman and Co.

Logothetis, D. E., Kurachi, Y., Galper, J., Neer, E. J., & Clapham, D. E. (1987). The beta gamma subunits of GTP-binding proteins activate the muscarinic K+ channel in heart. *Nature, 325*(6102), 321-326. doi:10.1038/325321a0

Ludwig, M. G., Vanek, M., Guerini, D., Gasser, J. A., Jones, C. E., Junker, U., . . . Seuwen, K. (2003). Proton-sensing G-protein-coupled receptors. *Nature, 425*(6953), 93-98. doi:10.1038/nature01905

Machelska, H. (2007). Targeting of opioid-producing leukocytes for pain control. *Neuropeptides, 41*(6), 355-363. doi:10.1016/j.npep.2007.06.001

Maguire, P., Tsai, N., Kamal, J., Cometta-Morini, C., Upton, C., & Loew, G. (1992). Pharmacological profiles of fentanyl analogs at mu, delta and kappa opiate receptors. *Eur J Pharmacol, 213*(2), 219-225.

Manglik, A., Kruse, A. C., Kobilka, T. S., Thian, F. S., Mathiesen, J. M., Sunahara, R. K., . . . Granier, S. (2012). Crystal structure of the micro-opioid receptor bound to a morphinan antagonist. *Nature, 485*(7398), 321-326. doi:10.1038/nature10954

Manglik, A., Lin, H., Aryal, D. K., McCorvy, J. D., Dengler, D., Corder, G., . . . Shoichet, B. K. (2016). Structure-based discovery of opioid analgesics with reduced side effects. *Nature, 537*(7619), 185-190. doi:10.1038/nature19112

Mangmool, S., & Kurose, H. (2011). G(i/o) protein-dependent and -independent actions of Pertussis Toxin (PTX). *Toxins (Basel), 3*(7), 884-899. doi:10.3390/toxins3070884

Mason, P. (2011). *Medical neurobiology*. New York: Oxford University Press.

Masuho, I., Ostrovskaya, O., Kramer, G. M., Jones, C. D., Xie, K., & Martemyanov, K. A. (2015). Distinct profiles of functional discrimination among G proteins determine the actions of G protein-coupled receptors. *Sci Signal, 8*(405), ra123. doi:10.1126/scisignal.aab4068

Matus-Ortega, M. E., Leff Gelman, P., Calva-Nieves, J. C., Flores-Zamora, A., Salazar-Juarez, A., Torner-Aguilar, C. A., . . . Anton-Palma, B. (2017). Mexneurin is a novel precursor of peptides in the central nervous system of rodents. *FEBS Lett, 591*(12), 1627-1636. doi:10.1002/1873-3468.12679

Mazak, K., Hosztafi, S., & Noszal, B. (2015). Species-specific lipophilicity of morphine antagonists. *Eur J Pharm Sci, 78*, 1-7. doi:10.1016/j.ejps.2015.06.026

McMahon, S. B. (2013). *Wall and Melzack's textbook of pain* (6th ed.). Philadelphia, PA: Elsevier/Saunders.

Mendieta, J., Rico, A. I., Lopez-Vinas, E., Vicente, M., Mingorance, J., & Gomez-Puertas, P. (2009). Structural and functional model for ionic (K(+)/Na(+)) and pH dependence of GTPase activity and polymerization of FtsZ, the prokaryotic ortholog of tubulin. *J Mol Biol, 390*(1), 17-25. doi:10.1016/j.jmb.2009.05.018

Merskey, H., Bogduk, N., & International Association for the Study of Pain. Task Force on Taxonomy. (1994). *Classification of chronic pain : descriptions of chronic pain syndromes and definitions of pain terms* (2nd ed.). Seattle: IASP Press.

Milligan, G. (2003). Principles: extending the utility of [35S]GTP gamma S binding assays. *Trends Pharmacol Sci, 24*(2), 87-90.

Mirzadegan, T., Benko, G., Filipek, S., & Palczewski, K. (2003). Sequence analyses of G-protein-coupled receptors: similarities to rhodopsin. *Biochemistry, 42*(10), 2759-2767. doi:10.1021/bi027224+

Mollereau, C., Moisand, C., Butour, J. L., Parmentier, M., & Meunier, J. C. (1996). Replacement of Gln280 by His in TM6 of the human ORL1 receptor increases affinity but reduces intrinsic activity of opioids. *FEBS Lett, 395*(1), 17-21.

Mousa, S. A., Cheppudira, B. P., Shaqura, M., Fischer, O., Hofmann, J., Hellweg, R., & Schafer, M. (2007). Nerve growth factor governs the enhanced ability of opioids to suppress inflammatory pain. *Brain, 130*(Pt 2), 502-513. doi:10.1093/brain/awl330

Mousa, S. A., Shaqura, M., Al-Madol, M., Tafelski, S., Khalefa, B. I., Shakibaei, M., & Schafer, M. (2017). Accessibility of axonal G protein coupled mu-opioid receptors requires conceptual changes of axonal membrane targeting for pain modulation. *J Control Release, 268*, 352-363. doi:10.1016/j.jconrel.2017.10.016

Mullis, K. B., & Faloona, F. A. (1987). Specific synthesis of DNA in vitro via a polymerase-catalyzed chain reaction. *Methods Enzymol, 155*, 335-350.

Munk, C., Harpsoe, K., Hauser, A. S., Isberg, V., & Gloriam, D. E. (2016). Integrating structural and mutagenesis data to elucidate GPCR ligand binding. *Curr Opin Pharmacol, 30*, 51-58. doi:10.1016/j.coph.2016.07.003

Murakami, N., Yokomizo, T., Okuno, T., & Shimizu, T. (2004). G2A is a proton-sensing G-protein-coupled receptor antagonized by lysophosphatidylcholine. *J Biol Chem, 279*(41), 42484-42491. doi:10.1074/jbc.M406561200

Nelson, D. L., Cox, M. M., & Lehninger, A. L. (2017). *Lehninger principles of biochemistry* (Seventh edition. ed.). New York, NY

Houndmills, Basingstoke: W.H. Freeman and Company ;

Macmillan Higher Education.

NIDA. (2007). The Neurobiology of Drug Addiction. Retrieved from https://www.drugabuse.gov/neurobiology-drug-addiction

NIDA. (2018). Drugs, brains, and behavior : the science of addiction. *NIH publication.* Revised edition. Retrieved from https://www.drugabuse.gov/publications/drugs-brains-behavior-science-addiction

Ninkovic, J., & Roy, S. (2013). Role of the mu-opioid receptor in opioid modulation of immune function. *Amino Acids, 45*(1), 9-24. doi:10.1007/s00726-011-1163-0

Niwa, H., Rowbotham, D. J., & Lambert, D. G. (2012). Evaluation of primary opioid receptor antibodies for use in western blotting. *Br J Anaesth, 108*(3), 530-532. doi:10.1093/bja/aes015

Nummenmaa, L., & Tuominen, L. (2018). Opioid system and human emotions. *Br J Pharmacol, 175*(14), 2737-2749. doi:10.1111/bph.13812

Ott, S., & Costa, T. (1989). Enzymatic degradation of GTP and its "stable" analogues produce apparent isomerization of opioid receptors. *J Recept Res, 9*(1), 43-64.

Pandy-Szekeres, G., Munk, C., Tsonkov, T. M., Mordalski, S., Harpsoe, K., Hauser, A. S., . . . Gloriam, D. E. (2018). GPCRdb in 2018: adding GPCR structure models and ligands. *Nucleic Acids Res, 46*(D1), D440-D446. doi:10.1093/nar/gkx1109

Pasternak, G. W., & Pan, Y. X. (2013). Mu opioids and their receptors: evolution of a concept. *Pharmacol Rev, 65*(4), 1257-1317. doi:10.1124/pr.112.007138

Pattinson, K. T. (2008). Opioids and the control of respiration. *Br J Anaesth, 100*(6), 747-758. doi:10.1093/bja/aen094

Patwardhan, A. M., Berg, K. A., Akopain, A. N., Jeske, N. A., Gamper, N., Clarke, W. P., & Hargreaves, K. M. (2005). Bradykinin-induced functional competence and trafficking of the delta-opioid receptor in trigeminal nociceptors. *J Neurosci, 25*(39), 8825-8832. doi:10.1523/JNEUROSCI.0160-05.2005

Pert, C. B., Pasternak, G., & Snyder, S. H. (1973). Opiate agonists and antagonists discriminated by receptor binding in brain. *Science, 182*(4119), 1359-1361.

Pert, C. B., & Snyder, S. H. (1973a). Opiate receptor: demonstration in nervous tissue. *Science, 179*(4077), 1011-1014.

Pert, C. B., & Snyder, S. H. (1973b). Properties of opiate-receptor binding in rat brain. *Proc Natl Acad Sci U S A, 70*(8), 2243-2247.

Pettersen, E. F., Goddard, T. D., Huang, C. C., Couch, G. S., Greenblatt, D. M., Meng, E. C., & Ferrin, T. E. (2004). UCSF Chimera--a visualization system for exploratory research and analysis. *J Comput Chem, 25*(13), 1605-1612. doi:10.1002/jcc.20084

Pocock, G., Richards, C. D., & Richards, D. A. (2017). *Human physiology* (Fifth edition. ed.). Oxford: Oxford University Press.

Raehal, K. M., & Bohn, L. M. (2014). beta-arrestins: regulatory role and therapeutic potential in opioid and cannabinoid receptor-mediated analgesia. *Handb Exp Pharmacol, 219*, 427-443. doi:10.1007/978-3-642-41199-1_22

Ranganathan, A., Dror, R. O., & Carlsson, J. (2014). Insights into the role of Asp79(2.50) in beta2 adrenergic receptor activation from molecular dynamics simulations. *Biochemistry, 53*(46), 7283-7296. doi:10.1021/bi5008723

Rasenick, M. M., & Childers, S. R. (1989). Modification of Gs-stimulated adenylate cyclase in brain membranes by low pH pretreatment: correlation with altered guanine nucleotide exchange. *J Neurochem, 53*(1), 219-225.

Regan, P. M., Langford, D., & Khalili, K. (2016). Regulation and Functional Implications of Opioid Receptor Splicing in Opioid Pharmacology and HIV Pathogenesis. *J Cell Physiol, 231*(5), 976-985. doi:10.1002/jcp.25237

Rodriguez-Gaztelumendi, A., Spahn, V., Labuz, D., Machelska, H., & Stein, C. (2018). Analgesic effects of a novel pH-dependent mu-opioid receptor agonist in models of neuropathic and abdominal pain. *Pain, 159*(11), 2277-2284. doi:10.1097/j.pain.0000000000001328

Schafer, M., Imai, Y., Uhl, G. R., & Stein, C. (1995). Inflammation enhances peripheral mu-opioid receptor-mediated analgesia, but not mu-opioid receptor transcription in dorsal root ganglia. *Eur J Pharmacol, 279*(2-3), 165-169.

Scheer, A., Fanelli, F., Costa, T., De Benedetti, P. G., & Cotecchia, S. (1996). Constitutively active mutants of the alpha 1B-adrenergic receptor: role of highly conserved polar amino acids in receptor activation. *EMBO J, 15*(14), 3566-3578.

Scherrer, G., Imamachi, N., Cao, Y. Q., Contet, C., Mennicken, F., O'Donnell, D., . . . Basbaum, A. I. (2009). Dissociation of the opioid receptor mechanisms that control mechanical and heat pain. *Cell, 137*(6), 1148-1159. doi:10.1016/j.cell.2009.04.019

Selley, D. E., Breivogel, C. S., & Childers, S. R. (1993). Modification of G protein-coupled functions by low-pH pretreatment of membranes from NG108-15 cells: increase in opioid agonist efficacy by decreased inactivation of G proteins. *Mol Pharmacol, 44*(4), 731-741.

Shaqura, M. A., Zollner, C., Mousa, S. A., Stein, C., & Schafer, M. (2004). Characterization of mu opioid receptor binding and G protein coupling in rat hypothalamus, spinal cord, and primary afferent neurons during inflammatory pain. *J Pharmacol Exp Ther, 308*(2), 712-718. doi:10.1124/jpet.103.057257

Sherrington, C. S. (1903). Qualitative difference of spinal reflex corresponding with qualitative difference of cutaneous stimulus. *J Physiol, 30*(1), 39-46.

Sievers, F., Wilm, A., Dineen, D., Gibson, T. J., Karplus, K., Li, W., . . . Higgins, D. G. (2011). Fast, scalable generation of high-quality protein multiple sequence alignments using Clustal Omega. *Mol Syst Biol, 7*, 539. doi:10.1038/msb.2011.75

Simon, E. J., Hiller, J. M., & Edelman, I. (1973). Stereospecific binding of the potent narcotic analgesic (3H) Etorphine to rat-brain homogenate. *Proc Natl Acad Sci U S A, 70*(7), 1947-1949. doi:10.1073/pnas.70.7.1947

Sirohi, S., Dighe, S. V., Madia, P. A., & Yoburn, B. C. (2009). The relative potency of inverse opioid agonists and a neutral opioid antagonist in precipitated withdrawal and antagonism of analgesia and toxicity. *J Pharmacol Exp Ther, 330*(2), 513-519. doi:10.1124/jpet.109.152678

Smith, A. P. (1977). The effect of pH on stereospecific opiate binding to mouse brain membranes. *Res Commun Chem Pathol Pharmacol, 17*(3), 375-398.

Sobczak, M., Salaga, M., Storr, M. A., & Fichna, J. (2014). Physiology, signaling, and pharmacology of opioid receptors and their ligands in the gastrointestinal tract: current concepts and future perspectives. *J Gastroenterol, 49*(1), 24-45. doi:10.1007/s00535-013-0753-x

Spahn, V., Del Vecchio, G., Labuz, D., Rodriguez-Gaztelumendi, A., Massaly, N., Temp, J., . . . Stein, C. (2017). A nontoxic pain killer designed by modeling of pathological receptor conformations. *Science, 355*(6328), 966-969. doi:10.1126/science.aai8636

Spahn, V., Del Vecchio, G., Rodriguez-Gaztelumendi, A., Temp, J., Labuz, D., Kloner, M., . . . Stein, C. (2018). Opioid receptor signaling, analgesic and side effects induced by a computationally designed pH-dependent agonist. *Sci Rep, 8*(1), 8965. doi:10.1038/s41598-018-27313-4

Spivak, C. E., Beglan, C. L., Seidleck, B. K., Hirshbein, L. D., Blaschak, C. J., Uhl, G. R., & Surratt, C. K. (1997). Naloxone activation of mu-opioid receptors mutated at a histidine residue lining the opioid binding cavity. *Mol Pharmacol, 52*(6), 983-992.

Stein, C. (2018). New concepts in opioid analgesia. *Expert Opin Investig Drugs*, 1-11. doi:10.1080/13543784.2018.1516204

Stein, C., & Machelska, H. (2011). Modulation of peripheral sensory neurons by the immune system: implications for pain therapy. *Pharmacol Rev, 63*(4), 860-881. doi:10.1124/pr.110.003145

Stein, C., Millan, M. J., Shippenberg, T. S., Peter, K., & Herz, A. (1989). Peripheral opioid receptors mediating antinociception in inflammation. Evidence for involvement of mu, delta and kappa receptors. *J Pharmacol Exp Ther, 248*(3), 1269-1275.

Stein, C., Millan, M. J., Yassouridis, A., & Herz, A. (1988). Antinociceptive effects of mu- and kappa-agonists in inflammation are enhanced by a peripheral opioid receptor-specific mechanism. *Eur J Pharmacol, 155*(3), 255-264.

Stepanenko, A. A., & Dmitrenko, V. V. (2015). HEK293 in cell biology and cancer research: phenotype, karyotype, tumorigenicity, and stress-induced genome-phenotype evolution. *Gene, 569*(2), 182-190. doi:10.1016/j.gene.2015.05.065

Stoeber, M., Jullie, D., Lobingier, B. T., Laeremans, T., Steyaert, J., Schiller, P. W., . . . von Zastrow, M. (2018). A Genetically Encoded Biosensor Reveals Location Bias of Opioid Drug Action. *Neuron, 98*(5), 963-976 e965. doi:10.1016/j.neuron.2018.04.021

Strange, P. G. (2010). Use of the GTPgammaS ([35S]GTPgammaS and Eu-GTPgammaS) binding assay for analysis of ligand potency and efficacy at G protein-coupled receptors. *Br J Pharmacol, 161*(6), 1238-1249. doi:10.1111/j.1476-5381.2010.00963.x

Sullivan, L. C., Chavera, T. S., Jamshidi, R. J., Berg, K. A., & Clarke, W. P. (2016). Constitutive Desensitization of Opioid Receptors in Peripheral Sensory Neurons. *J Pharmacol Exp Ther, 359*(3), 411-419. doi:10.1124/jpet.116.232835

Sun, J., Chen, S. R., Chen, H., & Pan, H. L. (2019). mu-Opioid receptors in primary sensory neurons are essential for opioid analgesic effect on acute and inflammatory pain and opioid-induced hyperalgesia. *J Physiol, 597*(6), 1661-1675. doi:10.1113/JP277428

Syrovatkina, V., Alegre, K. O., Dey, R., & Huang, X. Y. (2016). Regulation, Signaling, and Physiological Functions of G-Proteins. *J Mol Biol, 428*(19), 3850-3868. doi:10.1016/j.jmb.2016.08.002

Tegeder, I., Meier, S., Burian, M., Schmidt, H., Geisslinger, G., & Lotsch, J. (2003). Peripheral opioid analgesia in experimental human pain models. *Brain, 126*(Pt 5), 1092-1102. doi:10.1093/brain/awg115

Terenius, L. (1973). Stereospecific interaction between narcotic analgesics and a synaptic plasm a membrane fraction of rat cerebral cortex. *Acta Pharmacol Toxicol (Copenh), 32*(3), 317-320.

Terskiy, A., Wannemacher, K. M., Yadav, P. N., Tsai, M., Tian, B., & Howells, R. D. (2007). Search of the human proteome for endomorphin-1 and endomorphin-2 precursor proteins. *Life Sci, 81*(23-24), 1593-1601. doi:10.1016/j.lfs.2007.09.025

Thompson, A. A., Liu, W., Chun, E., Katritch, V., Wu, H., Vardy, E., . . . Stevens, R. C. (2012). Structure of the nociceptin/orphanin FQ receptor in complex with a peptide mimetic. *Nature, 485*(7398), 395-399. doi:10.1038/nature11085

Tiwari, V., Yang, F., He, S. Q., Shechter, R., Zhang, C., Shu, B., . . . Raja, S. N. (2016). Activation of Peripheral mu-opioid Receptors by Dermorphin [D-Arg2, Lys4] (1-4) Amide Leads to Modality-preferred Inhibition of Neuropathic Pain. *Anesthesiology, 124*(3), 706-720. doi:10.1097/ALN.0000000000000993

Toll, L., Bruchas, M. R., Calo, G., Cox, B. M., & Zaveri, N. T. (2016). Nociceptin/Orphanin FQ Receptor Structure, Signaling, Ligands, Functions, and Interactions with Opioid Systems. *Pharmacol Rev, 68*(2), 419-457. doi:10.1124/pr.114.009209

UniProt Consortium, T. (2018). UniProt: the universal protein knowledgebase. *Nucleic Acids Res, 46*(5), 2699. doi:10.1093/nar/gky092

Valentino, R. J., & Volkow, N. D. (2018). Untangling the complexity of opioid receptor function. *Neuropsychopharmacology, 43*(13), 2514-2520. doi:10.1038/s41386-018-0225-3

Vanderah, T. W., Schteingart, C. D., Trojnar, J., Junien, J. L., Lai, J., & Riviere, P. J. (2004). FE200041 (D-Phe-D-Phe-D-Nle-D-Arg-NH2): A peripheral efficacious kappa opioid agonist with unprecedented selectivity. *J Pharmacol Exp Ther, 310*(1), 326-333. doi:10.1124/jpet.104.065391

Vetter, I., Kapitzke, D., Hermanussen, S., Monteith, G. R., & Cabot, P. J. (2006). The effects of pH on beta-endorphin and morphine inhibition of calcium transients in dorsal root ganglion neurons. *J Pain, 7*(7), 488-499. doi:10.1016/j.jpain.2006.01.456

Vetter, I., Wyse, B. D., Monteith, G. R., Roberts-Thomson, S. J., & Cabot, P. J. (2006). The mu opioid agonist morphine modulates potentiation of capsaicin-evoked TRPV1 responses through a cyclic AMP-dependent protein kinase A pathway. *Mol Pain, 2*, 22. doi:10.1186/1744-8069-2-22

Viscusi, E. R., Skobieranda, F., Soergel, D. G., Cook, E., Burt, D. A., & Singla, N. (2019). APOLLO-1: a randomized placebo and active-controlled phase III study investigating oliceridine (TRV130), a G protein-biased ligand at the micro-opioid receptor, for management of moderate-to-severe acute pain following bunionectomy. *J Pain Res, 12*, 927-943. doi:10.2147/JPR.S171013

Wacker, D., Stevens, R. C., & Roth, B. L. (2017). How Ligands Illuminate GPCR Molecular Pharmacology. *Cell, 170*(3), 414-427. doi:10.1016/j.cell.2017.07.009

Wang, D., Raehal, K. M., Bilsky, E. J., & Sadee, W. (2001). Inverse agonists and neutral antagonists at mu opioid receptor (MOR): possible role of basal receptor signaling in narcotic dependence. *J Neurochem, 77*(6), 1590-1600.

Wang, J. Q., Kon, J., Mogi, C., Tobo, M., Damirin, A., Sato, K., . . . Okajima, F. (2004). TDAG8 is a proton-sensing and psychosine-sensitive G-protein-coupled receptor. *J Biol Chem, 279*(44), 45626-45633. doi:10.1074/jbc.M406966200

Wang, Y. L., Zeng, C., Xie, D. X., Yang, Y., Wei, J., Yang, T., . . . Lei, G. H. (2015). Single-dose intra-articular bupivacaine plus morphine after knee arthroscopic surgery: a meta-analysis of randomised placebo-controlled studies. *BMJ Open, 5*(6), e006815. doi:10.1136/bmjopen-2014-006815

Warne, T., Edwards, P. C., Dore, A. S., Leslie, A. G. W., & Tate, C. G. (2019). Molecular basis for high-affinity agonist binding in GPCRs. *Science, 364*(6442), 775-778. doi:10.1126/science.aau5595

Weibel, R., Reiss, D., Karchewski, L., Gardon, O., Matifas, A., Filliol, D., . . . Gaveriaux-Ruff, C. (2013). Mu opioid receptors on primary afferent nav1.8 neurons contribute to opiate-induced analgesia: insight from conditional knockout mice. *PLoS One, 8*(9), e74706. doi:10.1371/journal.pone.0074706

Willis, W. D., & Westlund, K. N. (1997). Neuroanatomy of the pain system and of the pathways that modulate pain. *J Clin Neurophysiol, 14*(1), 2-31.

Wimpey, T. L., & Chavkin, C. (1992). 8-Bromo-cAMP blocks opioid activation of a voltage-gated potassium current in isolated hippocampal neurons. *Neurosci Lett, 137*(1), 137-140.

World Health Organization. (2017, August 2017). WHO Model List of Essential Medicines. Retrieved from http://apps.who.int/iris/bitstream/handle/10665/273826/EML-20-eng.pdf

Wu, H., Wacker, D., Mileni, M., Katritch, V., Han, G. W., Vardy, E., . . . Stevens, R. C. (2012). Structure of the human kappa-opioid receptor in complex with JDTic. *Nature, 485*(7398), 327-332. doi:10.1038/nature10939

Xu, H., Lu, Y. F., Partilla, J. S., Zheng, Q. X., Wang, J. B., Brine, G. A., . . . Rothman, R. B. (1999). Opioid peptide receptor studies, 11: involvement of Tyr148, Trp318 and His319 of the rat mu-opioid receptor in binding of mu-selective ligands. *Synapse, 32*(1), 23-28. doi:10.1002/(SICI)1098-2396(199904)32:1<23::AID-SYN3>3.0.CO;2-N

Zeng, C., Gao, S. G., Cheng, L., Luo, W., Li, Y. S., Tu, M., . . . Lei, G. H. (2013). Single-dose intra-articular morphine after arthroscopic knee surgery: a meta-analysis of randomized placebo-controlled studies. *Arthroscopy, 29*(8), 1450-1458 e1452. doi:10.1016/j.arthro.2013.04.005

Zollner, C., Shaqura, M. A., Bopaiah, C. P., Mousa, S., Stein, C., & Schafer, M. (2003). Painful inflammation-induced increase in mu-opioid receptor binding and G-protein coupling in primary afferent neurons. *Mol Pharmacol, 64*(2), 202-210. doi:10.1124/mol.64.2.202

6 Appendix

6.1 Summary (English)

Opioid analgesics constitute the most effective treatment of severe pain, but they also cause adverse and often fatal side effects. Selective targeting of peripheral opioid receptors in injured tissue is a promising strategy to convey analgesia devoid of severe adverse effects. Drug targeting to injured tissue can be achieved by exploiting the acidic pH associated with inflammation. Yet, little is known on ligand recognition and signaling of opioid receptors at acidic pH.

In the present study, I demonstrate that at acidic pH, μ-opioid receptor (MOR) responses are modulated depending on a specific structural property of bound ligands. In radioligand binding experiments, acidic pH reduced binding of naloxone (NLX) and [D-Ala2,N-Me-Phe4,Gly5-ol]-enkephalin (DAMGO), ligands that form hydrogen bond networks to histidine residue $H297^{6.52}$ within the receptor binding pocket. Furthermore, I observed impaired DAMGO-induced G-protein activation (as assessed by [^{35}S]-GTPγS binding) and naloxone modulation of cAMP levels at acidic pH. In contrast, acidic pH did not alter G-protein activation and cAMP responses induced by fentanyl, a ligand that is unable to form hydrogen bonds to MOR residue $H297^{6.52}$. The exchange of residue $H297^{6.52}$ by alanine (A) abolished high-affinity binding of [^{3}H]-NLX and [^{3}H]-DAMGO, as well as DAMGO-induced G-protein activation. This mutation did not significantly alter fentanyl-induced G-protein activation, but reduced cAMP responses to fentanyl. I conclude that $H297^{6.52}$A is crucial to effective binding of DAMGO and NLX to the MOR, while this residue contributes less to the binding of fentanyl. Overall, these findings indicate that acidic pH selectively impairs binding and consequent signaling of ligands that strongly depend on hydrogen bond formation to $H297^{6.52}$. To ensure maximum MOR binding and signaling in inflamed tissue, I suggest that opioid ligands should bind largely independent of $H297^{6.52}$.

6.2 Zusammenfassung (Deutsch)

Opioid-Analgetika stellen die wirksamste Behandlung von starken Schmerzen dar, verursachen jedoch auch nachteilige und häufig tödliche Nebenwirkungen. Die selektive Aktivierung von peripheren Opioidrezeptoren in verletztem Gewebe ist eine vielversprechende Strategie, Analgesie ohne schwerwiegende Nebenwirkungen zu bewirken. Eine selektive Wirkung von Arzneimitteln ausschließlich in verletztem Gewebe kann unter Ausnutzung des mit Entzündung verbundenen sauren pH-Werts erreicht werden. Die zugrundeliegenden Mechanismen der Ligandenerkennung und Signalübertragung von Opioidrezeptoren bei sauren pH-Werten sind jedoch bisher weitgehend unbekannt. In der vorliegenden Studie demonstriere ich, dass ein saures Milieu Reaktionen des μ-Opioidrezeptors (MOR) ligandenabhängig verändert.

In Radioligandenbindungsexperimenten verringerte der saure pH die Bindung von Naloxon und DAMGO, welche bei Bindung Wassserstroffbrücken zur Seitenkette des Histidins $H297^{6.52}$ in der Bindungstasche des MOR ausbilden. Darüber hinaus verringerten saure pH-Werte die DAMGO-induzierte G-Protein-Aktivierung (ermittelt über die [^{35}S]-GTPγS-Bindung) und die Modulation der cAMP-Spiegel durch Naloxon. Im Gegensatz dazu waren G-Protein-Aktivierung durch und cAMP-Reaktionen auf Fentanyl, einen Liganden der keine Wasserstoffbrückenbindungen zu $H297^{6.52}$ ausbildet, bei saurem pH-Wert nicht verändert. Am MOR hob der Austausch der Aminosäure $H297^{6.52}$ durch A die hochaffine Bindung von [^{3}H]-NLX und [^{3}H]-DAMGO sowie die DAMGO-induzierte G-Protein-Aktivierung auf. Diese Mutation veränderte die Fentanyl-induzierte G-Protein-Aktivierung nicht signifikant, reduzierte jedoch die cAMP-Reaktionen auf Fentanyl. Folglich war $H297^{6.52}$A für die effektive Bindung von DAMGO und NLX an den MOR von entscheidender Bedeutung, während diese Aminosäure zur Bindung von Fentanyl weniger beitrug. Insgesamt beeinträchtigte der saure pH-Wert die Bindung und Signalübertragung von Liganden, deren Bindung an den Rezeptor stark von Wasserbrückenbindungen zu $H297^{6.52}$ abhängt. Um eine maximale MOR-Bindung und Signalübertragung in entzündetem Gewebe zu gewährleisten erscheint es somit ratsam, Opioid-Analgetika zu entwickeln welche weitgehend unabhängig von $H297^{6.52}$ binden.

6.3 Statement of Contribution

Several persons contributed experimental work that was included in the present thesis.
Dr. Viola Seitz (née Spahn) designed, performed and analyzed the experiments depicted in Figure 12 and Figure 15 B. In addition, when my contract expired and I was no longer admitted to the isotope lab, she performed the experiments depicted in A and B that were designed and analyzed by me.
Dr. Giovanna Del Vecchio designed and performed the experiments depicted in Figure 23 B.
Nicole Vogel assisted me in performing the experiments depicted in Figure 15 A.
Dr. Nicolas Massaly designed and performed the experiments depicted in Figure 23 C.

When the respective work was undertaken, all the persons mentioned above were employed at the research group of Prof. Dr. C. Stein at the Department of Experimental Anesthesiology of the Charité - Universitätsmedizin Berlin, Campus Benjamin Franklin.

6.4 Declaration of Authorship

I hereby certify that this thesis has been composed by me and is based on my own work, unless stated otherwise. No other person's work has been used without due acknowledgment. All references and verbatim extracts have been quoted, and all sources of information, including figures and data sets, have been specifically acknowledged.

This thesis, in same or similar form, has not been submitted to any other institution.

6.5 Publications

The main findings presented in the present work are summarized in an article published as online pre-print version on July 29th, 2019:

Meyer, J., Del Vecchio, G., Seitz, V., Massaly, N., & Stein, C. (2019). Modulation of mu-opioid receptor activation by acidic pH is dependent on ligand structure and an ionizable amino acid residue. Br J Pharmacol. doi:10.1111/bph.14810.

6.6 Technical controls

6.6.1 Pharmacological parameters derived from buffer optimization experiments

Table S1. Pharmacological parameters derived from [3H]-NLX saturation binding curves in Figure 11 A. Data acquired in HEM are duplicates of data depicted and analyzed in Figure 13 A.

	Tris	HEM
K_d [nM]	2,5	2,0
B_{max} [fmol/mg protein]	206.1	158,3

Table S2. Pharmacological parameters derived from [^{35}S]-GTPγS binding experiments depicted in Figure 11 B. n = 2, no statistical analysis was performed

	Tris	HEM
Log EC_{50}	-7.42	-7,03
EC_{50}	38,3 nM	93,7 nM
span	474.8 cpm	564,7 cpm

6.6.2 Pharmacological parameters derived from low pH pre-incubation experiments

Table S3. Pharmacological parameters derived from data depicted in Figure 12. Maximum [^{35}S]-GTPγS binding was analyzed by measuring the span (top minus bottom value) of the curves to demonstrate that baselines were independent of pH.

		pH 7.4	**pH 6.5**	**pH 5.5**
[^{3}H]-DAMGO binding	K_d [nM]	1.4 ± 0.7	1.0 ± 0.4	1.6 ± 0.4
	B_{max} [fmol / mg protein]	198.6 ± 25.6	195.5 ± 16.9	235.8 ± 17.4
DAMGO-induced [^{35}S]-GTPγS binding	EC_{50} (95% CI)	26.8 nM (6.0 pM – 0.1 mM)	92.3 nM (0.2 nM – 71 µM)	31.4 nM (1.5 pM – 0.7 µM)
	log (EC_{50})	-7.57 ± 1.82	-7.04 ± 1.44	-7.50 ± 2.15
	Span [cpm]	695.5 ± 453.5	686.5 ± 393.9	565.1 ± 437.4
Fentanyl-induced [^{35}S]-GTPγS binding	EC_{50} (95% CI)	19.4 nM (0.2 nM – 2.6 µM)	23.6 nM (80.4 nM – 1.5 µM)	20.6 nM (0.03 nM – 12.4 µM)
	log (EC_{50})	-7.71 ± 1.05	-7.63 ± 0.89	-7.69 ± 1.38
	Span [cpm]	701.2 ± 269.0	712.3 ± 229.0	644.7 ± 322.1
Fentanyl-induced **[^{35}S]-GTPγS saturation binding**	K_d [nM]	0.5 ± 0.3	0.2 ± 0.1	0.3 ± 0.2
	B_{max} [fmol / mg protein]	53.2 ± 11.6	45.8 ± 7.5	39.5 ± 6.7

K_d and B_{max} or logEC_{50} and span were each compared by one-way ANOVA, no significant differences were found, $n = 6$ per experiment.